UCRL-53868-00
Volume 2
September
2001

Engineering Technology Reports

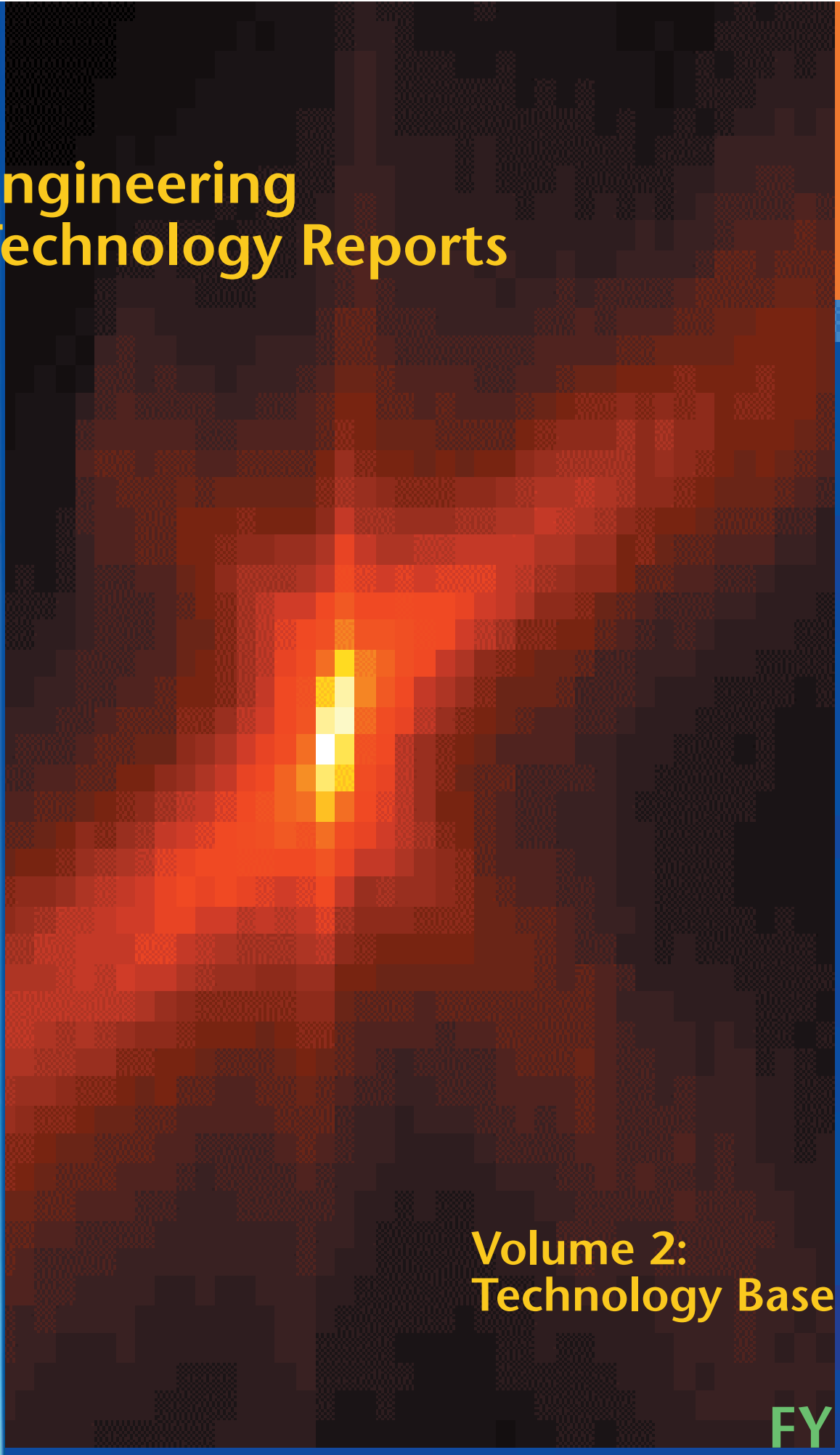

Volume 2: Technology Base

FY 00

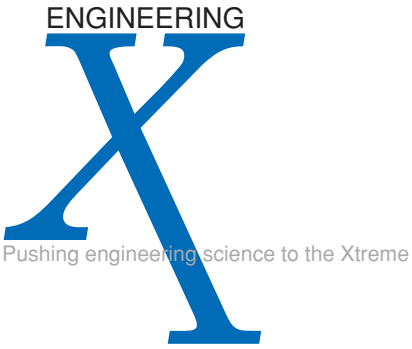

Acknowledgments

Scientific Editing
Andrea L. Baron
Robert T. Langland
Camille Minichino

Graphic Design
Irene J. Chan

Art Production/Layout
Pamela A. Allen
Irene J. Chan
Lucy C. Dobson

Composition
Andrea L. Baron

Document Approval and Report Services
Cynthia Tinoco

Cover:
Stylized graphic of an image from a CCD camera.

UCRL-53868-00
Volume 2
September
2001

Engineering Technology Reports

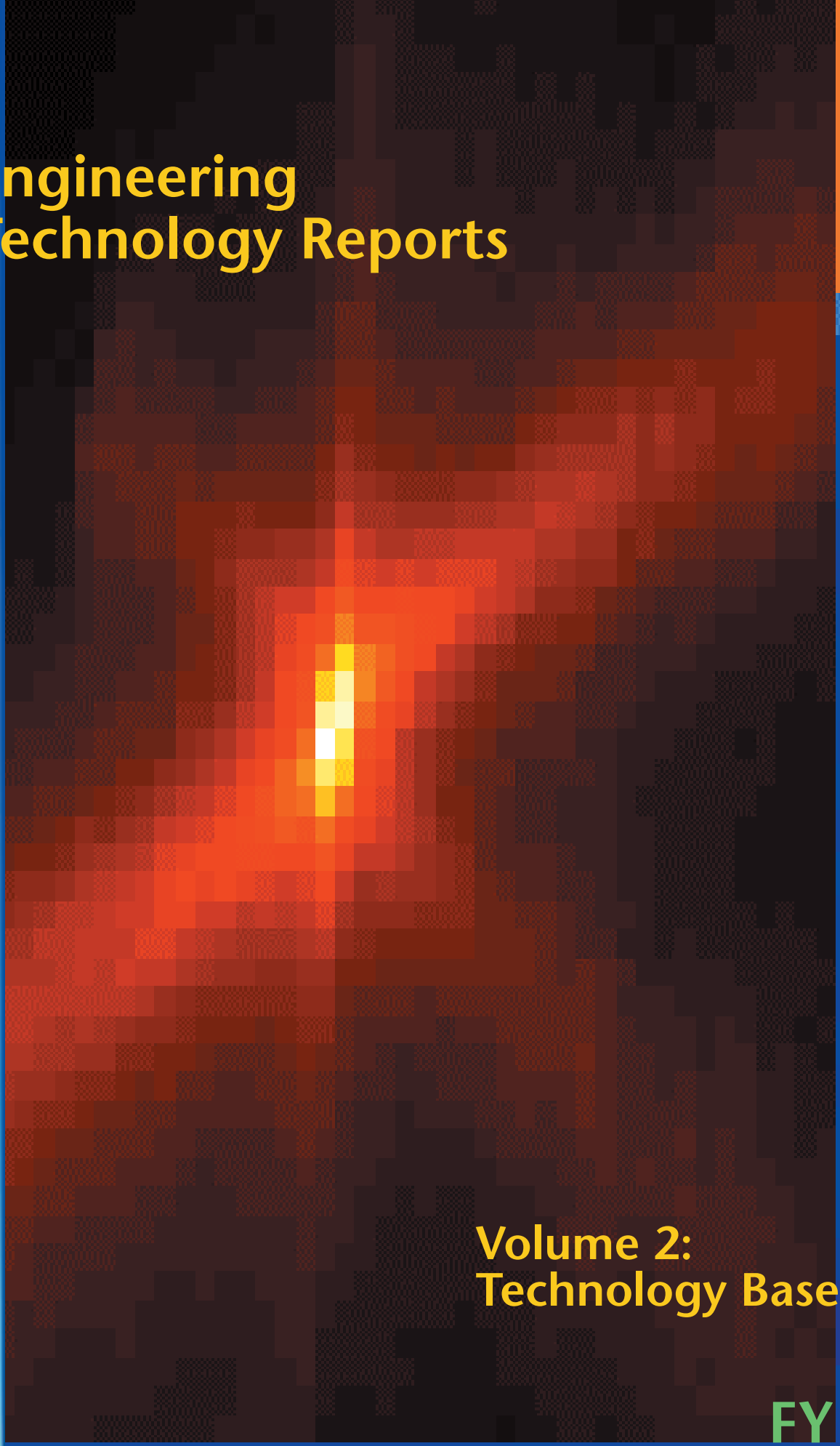

Volume 2: Technology Base

FY 00

Introduction

1. Communication Technology

2. Precision Engineering

3. Accelerators and High-Energy Physics

4. Computations and Numerical Simulation

5. Complex Systems and Information Technology

6. Microtechnology and Microdevices

7. Nondestructive Characterization

Selected Engineering Publications

Author Index

Introduction

Spiros Dimolitsas, Associate Director for Engineering

In FY-2000, Engineering at Lawrence Livermore National Laboratory faced significant pressures to meet critical project milestones, and immediate demands to facilitate the reassignment of employees as the National Ignition Facility (the 600-TW laser facility being designed and built at Livermore, and one of the largest R&D construction projects in the world) was in the process of re-baselining its plan while executing full-speed its technology development efforts. This drive for change occurred as an unprecedented level of management and program changes were occurring within LLNL. I am pleased to report that we met many key milestones and achieved numerous technological breakthroughs.

This report summarizes our efforts to perform feasibility and reduce-to-practice studies, demonstrations, and/or techniques—as structured through our technology centers.

Whether using computational engineering to predict how giant structures like suspension bridges will respond to massive earthquakes or devising a suitcase-sized microtool to detect chemical and biological agents used by terrorists, we have made solid technical progress.

Five Centers focus and guide longer-term investments within Engineering, as well as impact all of LLNL. Each Center is responsible for the vitality and growth of the core technologies it represents. My goal is that each Center will be recognized on an international scale for solving compelling national problems requiring breakthrough innovation. The Centers and their leaders are as follows:

- Center for Complex Distributed Systems: David B. McCallen
- Center for Computational Engineering: Kyran D. Mish
- Center for Microtechnology: Raymond P. Mariella, Jr.
- Center for Nondestructive Characterization: Harry E. Martz, Jr.
- Center for Precision Engineering: Keith Carlisle

FY-2000 highlights

The **Center for Complex Distributed Systems** exploits emerging information technologies to develop integrated systems for data gathering, processing, and communication, and new methodologies for assimilating measured data with computational models in data-driven simulations. Effective combination of data and simulation leads to enhanced understanding and characterization of complex systems ranging from large applied physics experiments to complex, highly heterogeneous geologic systems associated with underground defense facilities and nuclear materials geologic repositories. The Center's Tech-Base activities include the construction of an experimental testbed for evaluating the performance of small inertial sensors. This includes development of a library of measured vibration waveforms of interest, such as vehicle motions and optical system vibrations, that can be called upon, on demand, to evaluate prototype sensor packages. The Center also investigated the feasibility of updating atmospheric dispersion models with real-time atmospheric data.

The **Center for Computational Engineering** provides for the development and deployment of software tools that aid in the LLNL engineering mission. Highlights of the Center's Tech-Base projects include 1) enhancement of the usability of the EIGER electromagnetics framework to permit its application to a broader range of national security programs; 2) a demonstration project to promote lower-cost software development via code reuse and extensibility; and 3) extension of the ALE3D code, funded by the Accelerated Strategic Computing Initiative (ASCI), to permit analyses of incompressible fluids. This project permitted the LLNL ASCI program to provide support for other programs at LLNL and within DOE, including energy programs oriented toward the design of more fuel-efficient vehicles. We have added a real-world computing capability that opens the door to solving a wide variety of fluid/solid interaction problems in transportation, aerospace, and infrastucture settings.

The mission of the **Center for Microtechnology** is to invent, develop, and apply microtechnologies for LLNL programs in global security, global ecology, and bioscience. Its capabilities cover materials, fabrication,

devices, instruments, or systems that require microfabricated components, including microelectromechanical systems (MEMS), electronics, photonics, microstructures, and microactuators. Center staff have achieved considerable national recognition for the successes demonstrated in Chem-Bio National Security Program instrumentation, supported by the DOE and the Defense Intelligence Agency. Over the last year, nine prototypes of the handheld nucleic acid analyzer, the HANAA, were provided for beta testing by evaluators with a variety of applications, generally focused on bioterrorism response. The majority of the Center's Tech-Base projects support defense programs and nonproliferation. These include the development of high-voltage photovoltaics, microaccelerometers, and fabrication techniques for physics experiments that support Stockpile Stewardship. Also, the Center continues to develop techniques to fabricate fluidics that enable the miniaturization of bioassays.

The **Center for Nondestructive Characterization** advances, develops and applies nondestructive characterization (NDC) measurement technology to significantly impact the manner in which LLNL inspects, and through this, designs and refurbishes systems and components. The Center plays a strategic and vital role in the reduction-to-practice of scientific and engineering NDC technologies, such as acoustic, infrared, microwave, ultrasonic, visible and x-ray imaging, to allow Engineering in the near term to incorporate these technologies in LLNL and DOE programs. This year's technology projects include methods for improved 3-D signal and image processing; area-array ultrasonics measurements; light intensity detection and ranging; and x-ray digital radiography and computed tomography. We can now process data sets in all three dimensions, as opposed to only two dimensions; and a novel sensor for area-array ultrasonics imaging has been reduced-to-practice.

The **Center for Precision Engineering** is dedicated to the advancement of high accuracy engineering, metrology and manufacturing. The scope of work includes precision-engineered systems supporting metrology over the full range of length scale, from atom-based nanotechnology and advanced lithographic technology to large-scale systems, including optical telescopes and high energy laser systems. A new focus is the manufacturing and characterization of "meso-scale devices" for LLNL's NIF. Millimeter-scale physics experiments will provide data about shock physics, equation of state, opacity, and other essential measurements of weapons physics. This year's highlights include a project whose goal is to advance our precision manufacturing capability in both accuracy and scale. This is a three-year project that has already raised outside interest from NASA, DoD and the Air Force Spaced-Based Laser program for the fabrication of optics.

Leveraging our work

In a sense, our Centers serve as the internal venture capitalists for our programs. They provide the mechanism by which Engineering can help LLNL's programs attract funding, while pioneering the technologies that will sustain long-term investment.

Engineering must continually work to build LLNL's competitive advantage; we must continue to create things that are technically one-of-a-kind. Our Centers do this by fusing the best of mechanical and electronics engineering, creating a synergy that most organizations cannot. Our future depends on how we find innovative but cost-effective engineering solutions to emerging technical problems that lead to solutions on a national scale.

Communication Technology

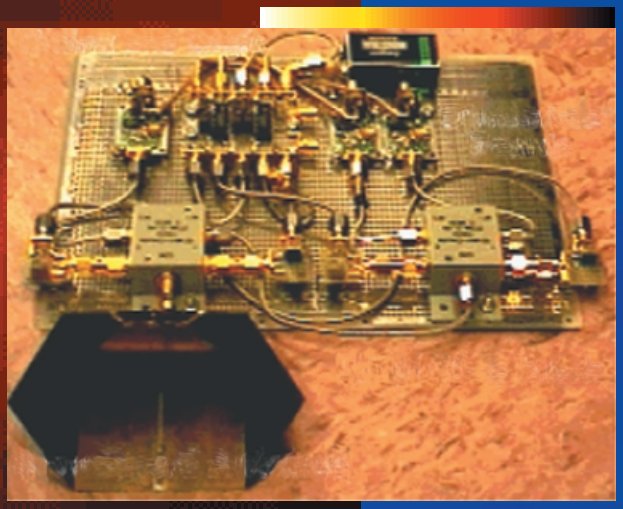

1

Digital/Software Radio

H.-Y. Pao, A. Meyer, T. Story

The software radio is a "next generation" technology that is already seeing limited use, enabled by recent advances in the computational power and/or power consumption of digital signal processing (DSP) devices. The value of software radio is that it can be reconfigured at any time to match the transmission standards of any communication system. Software radio is the ultimate in flexibility, allowing access to multiple standards. For example, it may be implemented in a wireless handset that can operate with any cellular standard. With this technology, true nationwide or worldwide coverage is possible. Improvements and upgrades can also be accommodated by simple software changes that can be automatically downloaded via the service network whenever necessary.

Software radio is the quintessential, albeit unachievable, expression of radio signal processing. Conceptually, the software is implemented in a processor attached directly to an antenna. The RF signal is downconverted to an intermediate frequency (IF) signal before conversion of the analog signal to the digital signal by an analog-to-digital converter (ADC). After ADC, all remaining signal processing functionality is rendered in software by a digital signal processor (DSP), which extracts the original baseband information. This concept is unattainable with current technology. This project, therefore, defines a hybrid radio that uses both analog and digital signal processing.

Our original proposal was to construct a radio receiver by using commercially available RF module, ADC and DSP technology (Fig. 1). The received weak RF signal is coupled to a generic analog RF front-end, which filters unwanted noise, amplifies the signal to the proper level, and downconverts the signal to an IF signal that is sampled and converted to a digital IF signal. This digital IF signal is processed in a DSP for implementing various standards and protocols, and performing the necessary functions to convert the digital IF to a baseband signal.

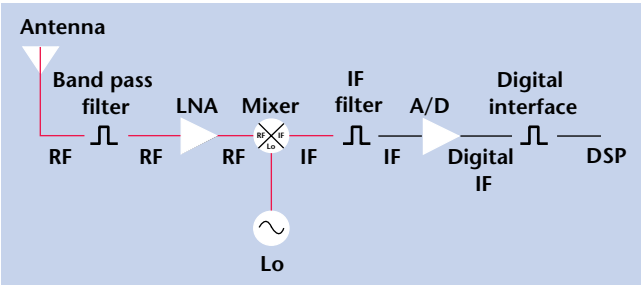

Figure 1. Block diagram of the proposed wireless digital software radio.

We proposed to implement both the ADC and the frequency downconversion by the undersampling method to: 1) eliminate the additional digital frequency downconverter stage; and 2) reduce the raw data size to be processed via DSP.

Due to unexpected budget difficulties, we changed the scope of this project. In the past year we finished the design and development of the analog RF front-end (Fig. 2), consisting of four major blocks: a downconverter, an upconverter, control circuitry, and a power supply. The final design was fabricated on a three-layer PC board with 50-Ω transmission lines where necessary.

Future plans are to: 1) design and develop the A/D converter and associated interface circuits; 2) design and develop the DSP test board; 3) develop the software architecture and algorithm for implementation of the sampling at IF frequency, the QPSK modulation and demodulation scheme, and the direct conversion of the RF signal to the digital signal by the undersampling method. We believe that reducing the above to practice will result in a revolutionary milestone for digital communications.

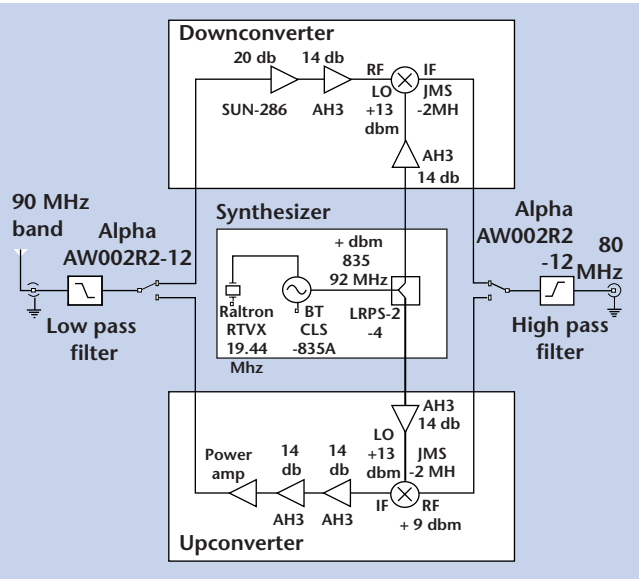

Figure 2. RF front-end block diagram.

Communications and Networking Initiative

R. Bryant, S. Azevedo

Emerging communications and networking (C&N) technologies are key drivers in the major programs at LLNL, supporting the national security mission. The ability to collect and move information in a secure and reliable manner between sensors, data acquisition and control systems, and high-performance computers and storage systems is of strategic importance to stockpile stewardship, nonproliferation and arms control, and environmental, energy, and biomedical programs. Access to and fusion of real-time information provides situational awareness and information dominance, allowing immediate and better decisions to be made regarding actions to take.

The goal of the Communications and Networking Initiative is to leverage LLNL's current C&N strengths in addressing future programmatic needs and to establish a state-of-the art C&N Facility. A centralized C&N Facility within the Engineering Directorate will pull together distributed C&N capabilities, create a state-of-the-art facility for developing, integrating, and demonstrating LLNL's capabilities, provide an internal and external focal point for LLNL C&N R&D, and for setting directions for technology R&D and equipment needs.

The C&N Facility will provide facilities and equipment to support development in areas such as wireless sensor networking, ultra-capacity optical networks, control and diagnostic networks, free-space optical communications, adaptive optics, information operations and security.

In FY00 we evaluated Facility needs, developed plans for siting and design, and supported the development of C&N-related projects and C&N-related Institutional General Purpose Equipment.

Three proposals were funded in FY00: Ultra-Wideband Communications, Cooperative Mobile Sensing Networks, and Secure Communications in High-Speed Fiber Optical Networks using Code Division Multiple Access Transmission.

State-of-the-art equipment is required to enable the development and testing of advanced C&N technology and systems. With input from the C&N working group, a prioritized equipment list was generated. This included a high-speed bit-error rate tester, deep-memory and real-time oscilloscopes, optical and RF spectrum analyzers, adaptive optics communications link hardware, anechoic chamber staging hardware, and ultra-wideband test equipment.

Phased plans were developed to upgrade an existing LLNL building to house the C&N Facility. This building has available space and has areas that are secured for classified work and areas for unclassified projects, allowing a mix of C&N projects. It also contains the microwave test laboratory and anechoic chamber for controlled EM testing.

In FY01, the plans are to build the first phase of the C&N Facility, and to move equipment and personnel into it. Initial plans are to move our National Transparent Optical Network equipment into the Facility and to provide connectivity to the Power Wall for graphics display and remote collaboration. Plans for the follow-on phases of the C&N Facility will be developed, including projects and personnel that will use the C&N Facility resources.

NTON High-Bandwidth-Enabled Medical Informatics

W. J. Lennon

Future scientific, engineering, and particularly medical research and operations will be conducted under a distributed information model. Computing and storage resources will themselves be distributed and will generally be remote from the researchers. Collaborative work models exacerbate this problem by making it even more likely that we will have to support a distributed environment. The current Internet has given us an introduction to solving problems independent of location, but leaves much to be desired in terms of capacity and dependability.

This project sought to prototype approaches to these problems in the medical research and operations domain by leveraging and extending the reach of the Department of Defense Advanced Research Projects Agency (DARPA) Supernet, an extreme bandwidth, core research testbed. The West Coast segment of the Supernet project is the National Transparent Optical Network (NTON) led by Nortel, LLNL, GST Telecommunications, Sprint, and BART. In addition to Supernet networks, NTON is linked to other, slower research networks that span the United States at data rates still substantially faster than routine Internet connections.

Three collaborations have been pursued: LLNL's Advanced Telecommunications Program with the National Museum of Health and Medicine; LLNL's cancer treatment planning project, Peregrine, with the National Institutes of Health/National Cancer Institute (NCI); and LLNL's Medical Technologies Program (MTP) with the UC Davis Medical Center (UCDMC). Non-medical collaborations likely to reduce costs to "Sacramento" participants were pursued with the UC Davis School of Engineering and several California State Departments.

In FY00, we successfully spawned an externally funded project, The Visible Embryo, to begin a national collaboration centered around the capture, identification, and management of the Carnegie Collection of fetal pathology. The collection is being digitized at the Human Development Anatomy Center within the National Museum of Health and Medicine.

Following a successful demonstration of Peregrine over the lower speed Internet between the NCI and Ireland, the NCI Radiation Oncology workstation was moved to LLNL, installed, and interfaced to NTON. This project provided an interim videophone to support collaboration while developing the link between LLNL and the NCI over five research networks (two local area networks and three Supernet networks).

The major project effort was designing NTON access to Sacramento for a direct, high-speed connection between LLNL's Peregrine and MTP, and UCDMC. We have identified sufficient fiber and conduit to connect UCDMC to an NTON repeater/amplifier node in Sacramento. We identified the expenditures needed to upgrade the Sacramento node from bypassed city status to net access status. These efforts helped to effect a recent Memorandum of Understanding between LLNL/MTP and UCDMC.

In addition to UCDMC, we worked with the UC/Davis School of Engineering to identify a direct fiber connection between LLNL, UCDMC and the Davis campus. This link would be used as an alternate route and as an optical network research facility. We also identified potential Sacramento collaborations with the State of California's Department of Information Technology (DOIT) and Department of Transportation (CalTrans). One study grant was spawned and another was indicated by year end.

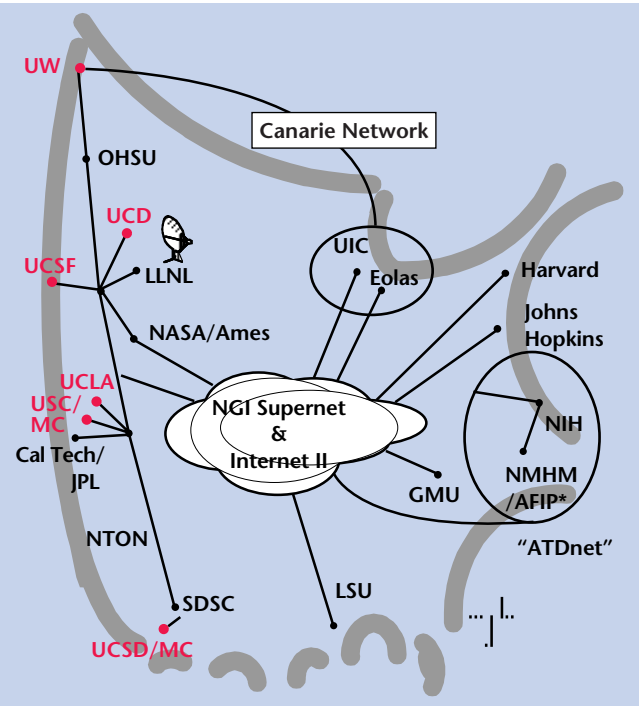

DARPA-funded NTON and other research networks linking medical resources and researchers throughout the country.

Ultra-Wideband Communications

F. Dowla, A. Spiridon, T. Rosenbury, D. Benzel, S. Azevedo

Radio frequency (RF) communication with sub-nanosecond duration ultra-wideband (UWB) pulses, without the use of a carrier frequency, is a new concept in covert and secure wireless communications. UWB radios provide LLNL with a unique technology that is in high demand in many national security problems. Last year we developed an approach to UWB radios to address three critical problems: rapid synchronization, channel equalization, and sampling. We established the basic design philosophy for UWB radios to optimize radio transceiver designs. In the current project we studied the possibility of using LLNL's expertise in short-pulse radars to address problems in short-range covert communications.

The objective of this project was not only to develop UWB radios that addressed the difficult problems of fast synchronization, multipath distortion, and fast sampling, but also to develop a signal processing and modeling approach to UWB systems. We have worked out the basic designs of a new generation LLNL short-pulse (200 ps)-based UWB radio, and are in a unique position to solve important programmatic problems in this area.

In urban warfare or intelligence operations, covert RF communication is essential. However, with conventional technologies becoming easily accessible to adversarial parties, radio communication devices are susceptible to detection and possibly to decoding and interception. For modern defense, intelligence and law-enforcement applications, U. S. personnel require advanced communications strategies that will rapidly send voice, data, and video information among the sensors and participants. The most vulnerable and dangerous scenario for troops is when their operations take them near the enemy (within a kilometer). Short-range (< 1 km) communication systems are crucial for future DOD and other agency missions. Many types of systems are being developed for short-range communications, however most have short falls in many of these critical areas: power consumption, cost, size, data capacity, and most importantly covertness.

Our new UWB system will meet military requirements, as well as maintain low probability of detection and low probability of intercept that is crucial for clandestine operation. Our communication system uses low-power, small-size sensor communication hardware, and is able to operate in a mobile environment.

Next year we plan to further develop the important issues in UWB radios and also apply UWB radios to LLNL programmatic problems. The main issues are: 1) the ability to generate very short duration large amplitude pulses at very high pulse repetition frequency; 2) the ability to compensate and correct for the multipath effects; and 3) rapid synchronization of multiple receivers and transmitters.

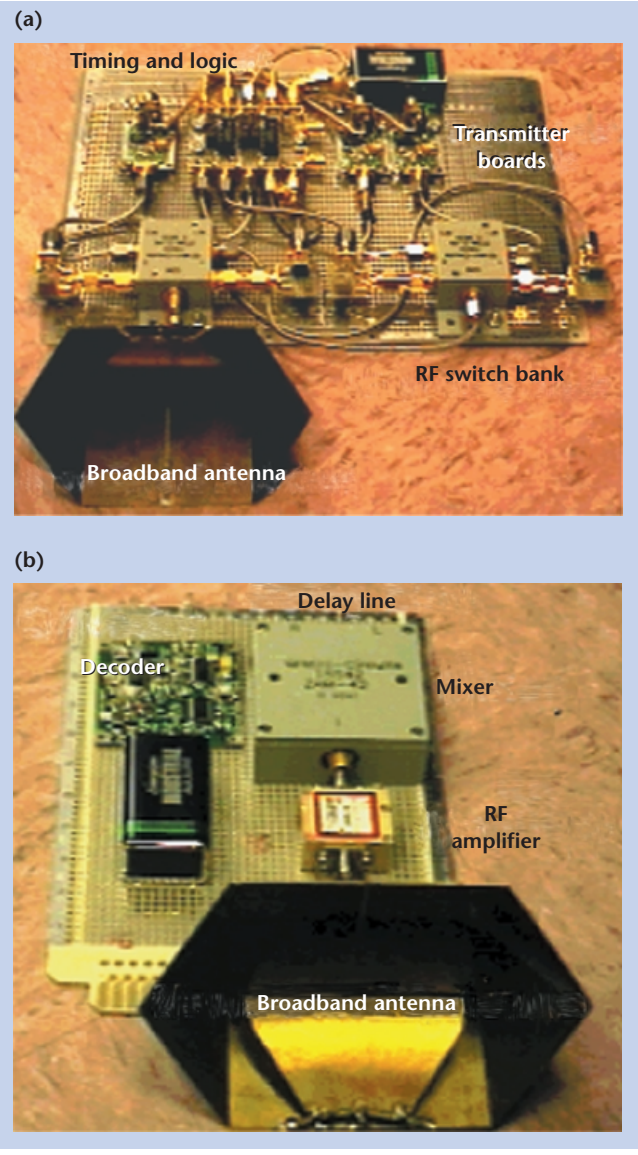

Photographs showing UWB radio components.

Low-Cost Security Sensors Using RFID Communication

A. Spiridon, R. Bryant, F. Dowla

Radio Frequency Identification Devices (RFID) technology has matured to a level that provides relatively inexpensive wireless access to sensors deployed to monitor security. Our effort started with defining an RFID system to report which repositories were open, and later explored applying RFID to vault security. The system study of vault security focused on the use of passive RF tags to monitor and control portal access to the vault. A key issue with passive RFID is the limited link coverage from the system's interrogating node to the individual tags. All commercial systems use relatively narrow bandwidth, which suffers from fades. Adapting ultra-wide bandwidth (UWB) communication technology to RFID becomes attractive.

The objective of this effort is to enhance security operation at the national laboratories by providing continuous monitoring of the status of sensitive assets while keeping the cost of the system at an affordable level. The wireless communication links of RFID systems are used to collect the information from dispersed RFID tags. The advantage of the wireless links is two-fold: it allows mobility (*e.g.*, tags on hard disk drives), and it reduces the cost of wiring when tags are deployed on fixed points such as repositories.

Our emphasis was on integrating a commercial RFID system into the security system design, more than on developing the technology of RFID. The maturity of the commercial system provided a relatively quick assessment of nominal designs in meeting Laboratory security needs and in identifying technology thrusts for future needs.

Repository monitoring was one of the applications addressed. The WhereNet was identified as the lead system meeting the requirements. It is an active RFID, where the tag is battery-powered. As shown in Fig. 1, the tag mounted on the repository is attached to a sensor, and every few seconds transmits an identifying packet, reporting as to whether the repository is open. A sensor, developed by the Safeguards and Security Department of LLNL supplies the tag with the repository information. The WhereNet system has a 200-ft range from the tags to the antennas. It would have been desirable to evaluate and demonstrate the system at the Laboratory, but no funds were available. A key step in using the system at the Laboratory is checking that the transmitted signals comply with security regulations.

The second application addressed was control of classified access, to a meeting or a vault, by interrogation of tags as they pass by a portal (Fig. 2). The tags give the IDs of the people carrying them and are passive; their power source is the interrogation signal. Checkpoint has a system that can read multiple tags as they pass by a portal, with tags costing less than a dollar. The tag's range is limited to a few feet from the portal. The challenge is to improve the range while keeping the cost low, an issue that UWB might solve. Technology insertion will also address allowing the mounting of tags on restricted environments, *e.g.*, hard disk drives, and assuring security integrity of the tags system.

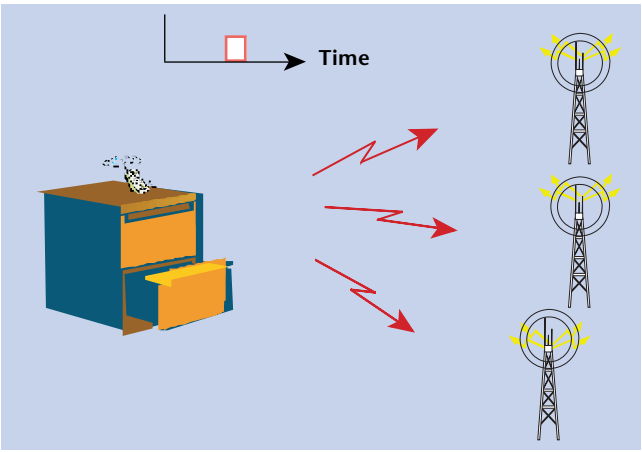

Figure 1. WhereNet tag pulses with ID and sensor information, and intercepts at three antennas for position fix.

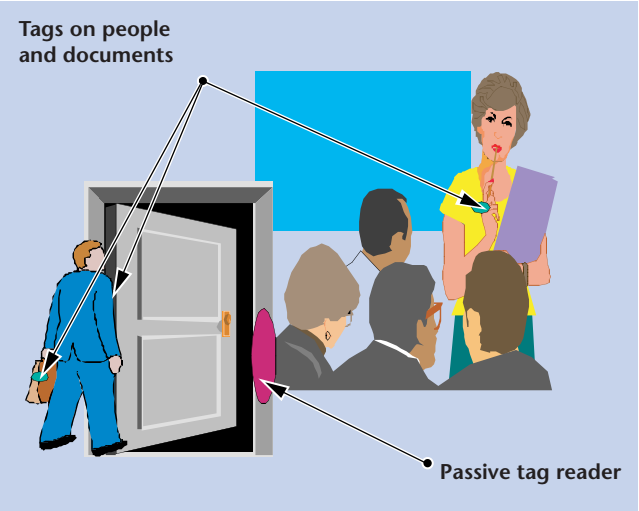

Figure 2. Control of classified access using passive tags.

Precision Engineering

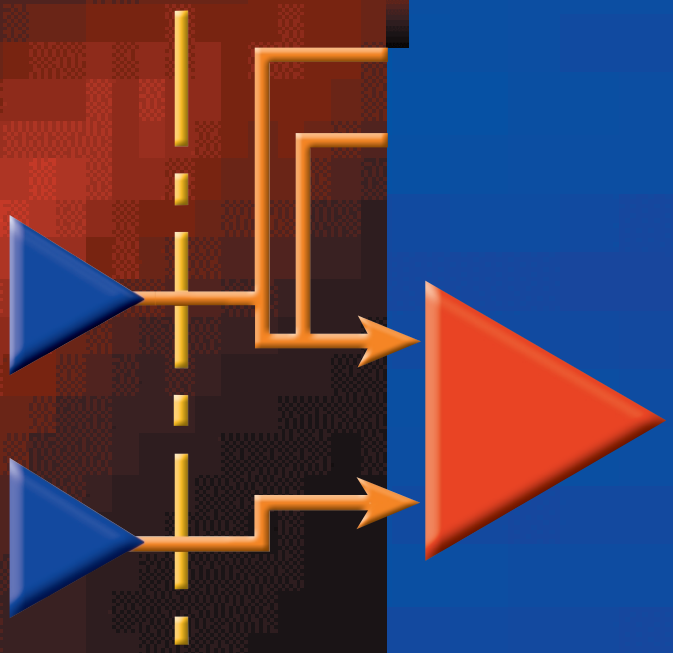

Lawrence Livermore National Laboratory ULTRA-350 Test Bed

D. J. Hopkins, T. A. Wulff, K. Carlisle

LLNL in-house-designed high precision diamond turning machines have used capstan drive technology, laser interferometer position feedback, tachometer velocity loop feedback, permanent magnet (PM) brush motors and analog velocity and position loop servo compensation. A new LLNL diamond turning machine is planned that will use brushless linear motors, high precision linear scales, machine controller motor commutation and digital servo compensation for the velocity and position loops. To minimize the risks of these technologies in the new machine design, LLNL has established a test bed to evaluate these technologies for application in high precision diamond turning. As of this writing, the linear scales are still under investigation for positioning accuracy, however our test bed has demonstrated these technologies will perform as required to meet the new diamond turning machine design goals.

The figure shown is an abbreviated block diagram of the major components of the ULTRA 350 test bed. The test bed is primarily composed of commercially available components, including a slide with opposed hydrostatic bearings, the oil bearing pump system, the PM brushless linear motor, a three-phase output, two-phase input linear motor amplifier, and the controller.

The controller is the heart of the servo system, providing the encoder resolution extension algorithm, the commutation algorithm, and all the tuning parameters. Additional analog inputs and outputs have been activated as shown on the diagram. These inputs and outputs, when properly scaled can be used with a dynamic signal analyzer (DSA) for the purpose of setting and verifying the servo system compensation.

Setup consisted of the necessary mechanical and electrical connections as well as the development of an E-Stop system to protect the operator and equipment of the test bed. A brake can be actuated to hold the slide in position in the event of an E-Stop. In addition, the encoder resolution extension and commutation algorithms and controller variables were set up and initialized.

The approach to servo compensation was to evaluate and tune the current, velocity, and position loops individually. A DSA was used to accurately measure transfer functions (output/input) of the system loops. The analyzer provides a Bode plot of gain and phase versus frequency.

The ultimate goal of this control system is to precisely control the position of the slide, reject slide disturbance forces and provide the highest static and dynamic machine stiffness.

After tuning and evaluating the system, we are able to report two important measurements taken from the test bed: 1) clearly definable 10 nm step slide moves as measured with a LVDT gauge and 2) a displacement curve showing smooth slide reversal at rates less than 100 nm/min.

Our results show that the dynamics of the linear motor test bed system are much easier to compensate than the capstan drive systems of older machines. It also appears that bandwidth for a given system can be much higher with a linear motor drive system than a capstan drive system.

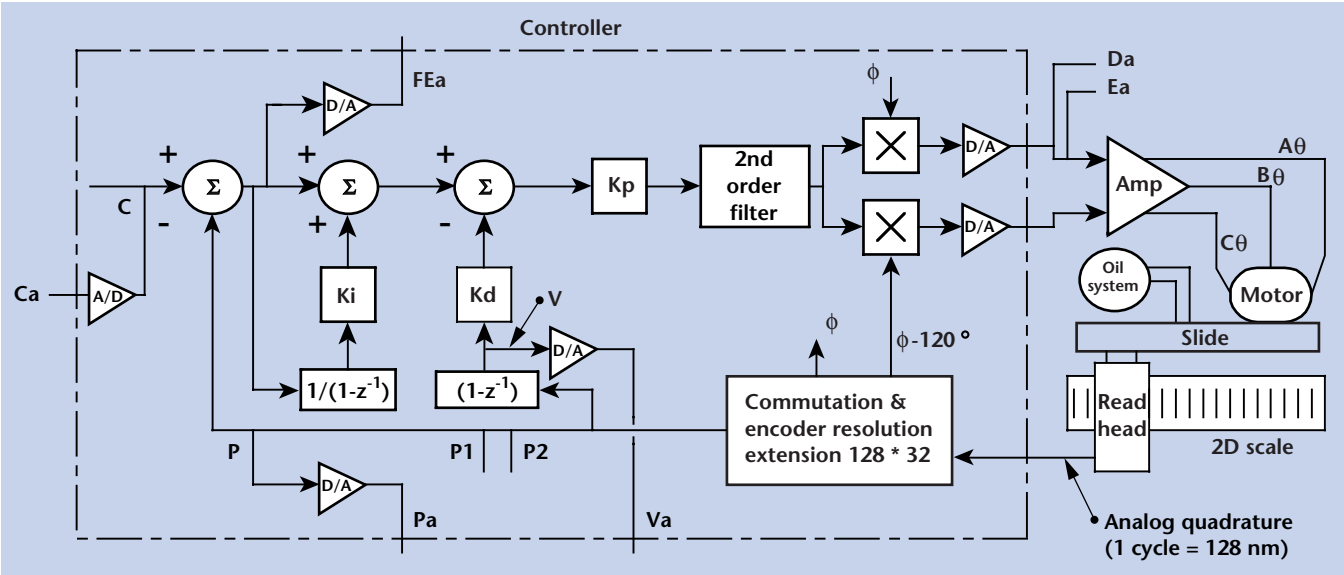

Abbreviated block diagram of the ULTRA-350 test bed.

Manufacture of Meso-Scale Devices for Studying High-Energy-Density Weapons Physics

K. Blaedel, R. P. Mariella, Jr., H. E. Martz, Jr., H. Louis, P. Davis

A manufacturing capability, comprising a facility, machine-tools, and people, is a critical and necessary ingredient of the Stockpile Stewardship Program (SSP). We have proposed a set of development activities that will lead to a succession of improvements to LLNL's current capabilities in five areas: material removal, material deposition, component dimensional metrology, machine-assisted assembly, and dimensional characterization of the assembly. The facility will be capable of providing high-quality High-Energy-Density Experimental Science Program (HEDES) target assemblies, for fielding on the NIF or elsewhere. These targets comprise an assembly of mm-size components with sub-μm features, and are made from a variety of materials.

Small target assemblies for the Defense and Nuclear Technology program that are fabricated within the Engineering Directorate are used for experimental studies on fundamental physics important to the design of nuclear weapons. Current experiments use target assemblies that are often a compromise between what the experimentalist desires and what the manufacturing engineer can fabricate. We have narrowed this gap by defining the long-term requirements for manufacturing "meso-scale" target assemblies for HEDES support of the SSP and by a proposal path for a manufacturing capability for these devices that includes both fabrication and characterization.

The experiments in a modern facility will be quite *new* and different from those of the past. New target assemblies are required that derive from the desire to model 3-D events and to incorporate more and more of the physics understanding into the experiments. The experiments will also need to become more *quantitative, i.e.*, more precise in fabrication and characterization than is currently possible.

The best way to define the requirements of a manufacturing facility would be to have a complete specification for the product to be manufactured. However, the requirements of the physics experiments to be conducted more than five years in the future are difficult to predict. Therefore, we postulate a difficult-to-manufacture assembly that "represents" what the experimental physicists might want to field in the year 2006.

Engineering can attend to how we might manufacture such a target assembly. The dream is to bring modern manufacturing to bear on the fabrication of meso-scale physics experiments. While the end goal is defined in terms of a capability that will come to exist in the year 2006, the path to that end goal requires intermediate steps. This provides us with improved capability that we desperately need before 2006 and with milestones against which to measure our progress toward the end goal.

In FY00 we made some progress along the general direction prescribed by our roadmap: 1) we tested a fixturing concept that embodies the datum/reference surfaces for assembly and alignment within a fixture that is married to the component until its assembly; 2) we fabricated and characterized surfaces in materials of interest to test commercially available probes that might be used as the sensor in a coordinate measuring machine; 3) we contracted commercial vendors of micromachining to produce targets of the future; and 4) we purchased commercial vision systems to understand the current state-of-the-art machine-assisted assembly and to gain experience in this arena.

For FY01, we identified a possible area of research leading to an LDRD project: to develop tele-operated manipulation on a small scale, oriented specifically toward microsurgery, but developing sensors, feedback, and control that is generally applicable to small-scale assembly. A project on microtomography and one on micro-stereo-lithography will also be funded.

Accelerators and High-Energy Physics

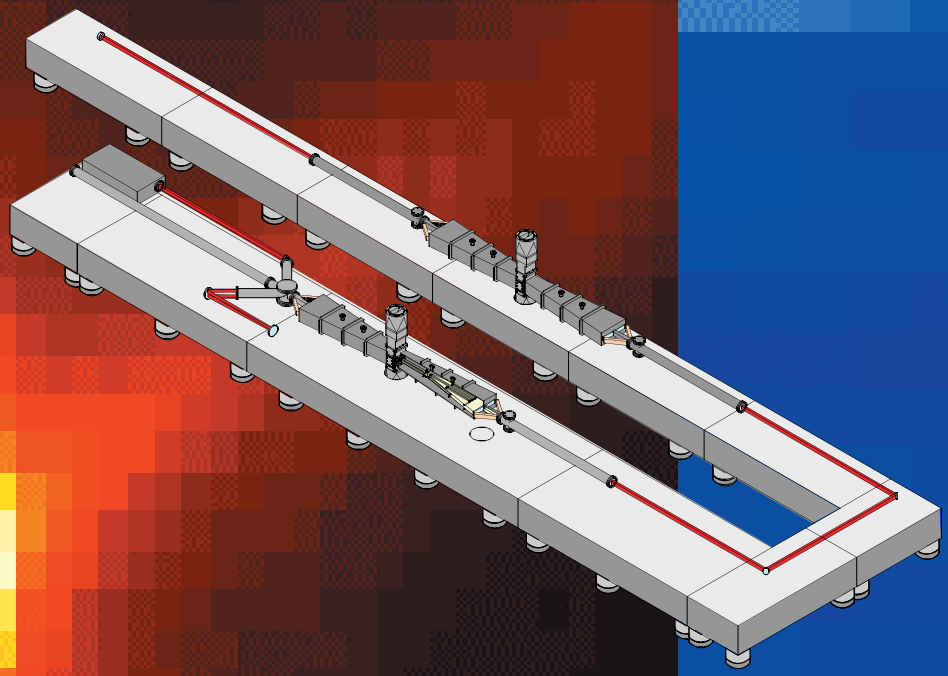

3

Preliminary Design for a Photon Collider

K. van Bibber

We have generated a preliminary design of a photon collider and conclude that a gamma-gamma collider is feasible within present technology.

The next major DOE facility acquisition in high energy physics is expected to be an electron-positron linear collider, with a center-of-mass energy on the order of 1 TeV. For this Next Linear Collider or NLC, an option is also under study to produce gamma-gamma collisions at a center-of-mass energy of several hundred GeV, yielding new and complementary physics to e^+e^- collisions.

The principal challenges of the photon collider are the simultaneous high peak power (TW) and high average power (10 kW) required, and the optical transport needed to bring the laser and electron beams into collision with micron-level tolerances. Furthermore the laser optics must be integrated into the highly constricted accelerator final focus region without increasing backgrounds in the high energy physics detector.

We have identified a suitable laser technology and architecture, the Mercury laser (Yb:S-FAP) being developed for inertial fusion energy, which appears ideal to adapt to our application (see figure). A key demonstration was successfully carried out, necessary for the pulses—normally a few ns long—to be compressed to the required few ps. An optical system and four-mirror telescope were designed to transport the laser light into the center of the detector and bring it into collision with the electron beams. Initial engineering was carried out incorporating the optical elements, supports, and movers within the beam vacuum pipe.

We also began accelerator physics studies that showed how to modify the electron beam's final focus to optimize the gamma-gamma luminosity by as much as a factor of two.

Based on the success of this preliminary study, a crash-program was launched to develop a complete design for a photon collider in FY01.

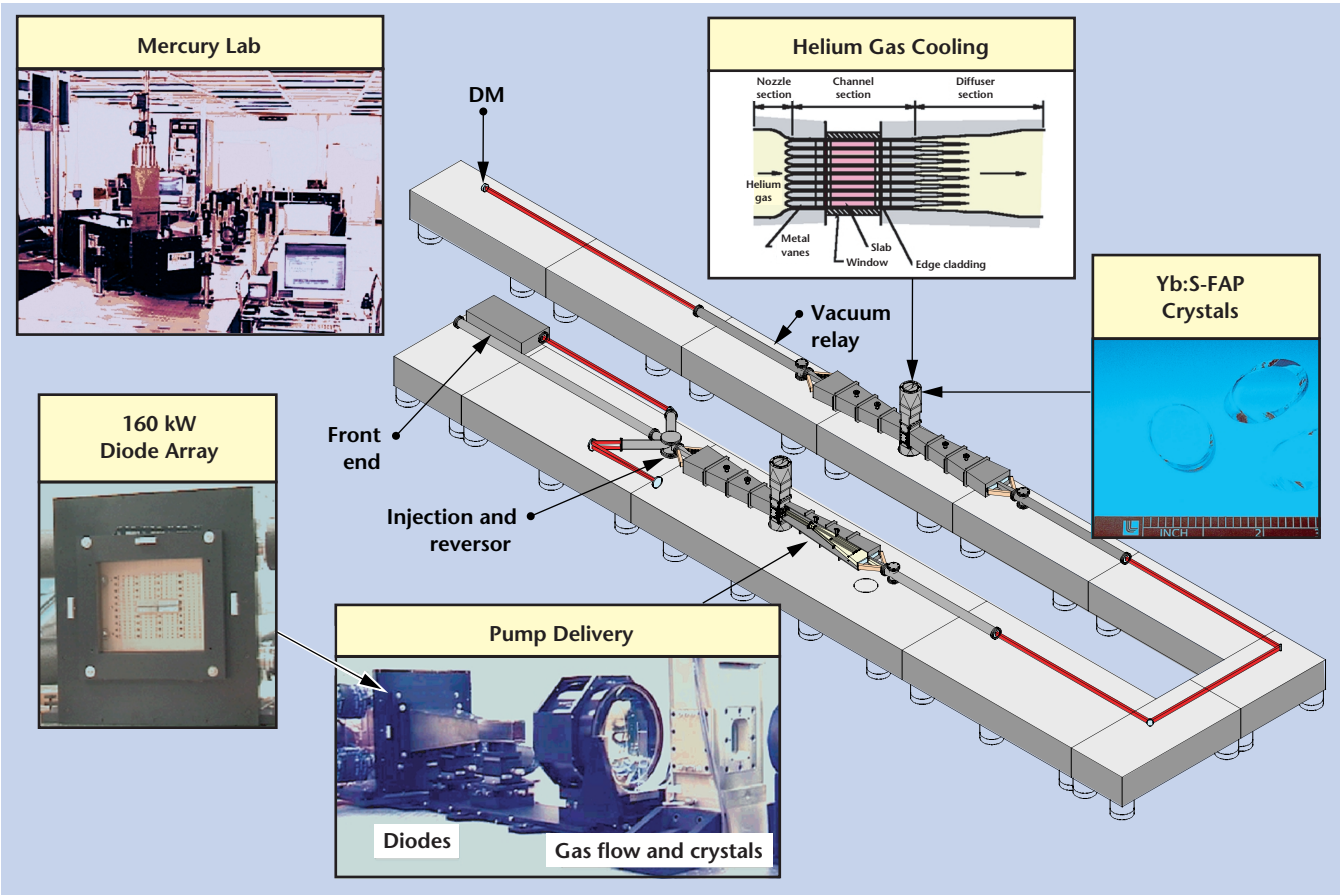

The Mercury laser, using three key technologies: gas cooling, diode-laser pumping, and Yb:S-FAP crystals.

Electron Beam Divergence Measurement at FXR Using Optical Transition Radiation

G. LeSage, S. D. Nelson, J. Zentler, M. Ong, G. Earley, S. Hibbs, P. Tirapelle, M. McGregor, G. DeWolf, L. Seppala

In support of diagnostics development for particle beam accelerators of interest to DOE (such as the new DARHT-II accelerator complex), we successfully demonstrated the use of optical transition radiation (OTR) on the Flash X-Ray accelerator (FXR) at LLNL's Site 300. These experiments demonstrated the ability to measure electron beam emittance for a 18-MeV, 3.2-kA, 60-ns (192 μC) electron beam.

The theory of OTR is based on charged particles radiating as they cross a boundary between two dielectric media. A metal or dielectric foil is used to produce an OTR pattern as the electron beam passes from vacuum to bulk media. An angular pattern peaked at $+/- 1/\gamma$ is centered about the specular direction. The pattern produced by the whole beam has lobe widths characteristic of the divergence, spot size, and energy spread. A theoretical distribution of electrons can be used to fit the OTR pattern to given values of emittance and energy spread.

The repetition rate of FXR is one pulse every few minutes, but with these beam parameters foil heating was a concern. However, for single shot (instant) heating, the final temperature is independent of foil thickness since both volume and energy absorption scale linearly. We must ignore radiative and conduction cooling since deposited power is orders of magnitude greater than power dissipation. Calculations show that 2–3 $\mu C/mm^2$ can be tolerated by thin dielectric and metallic foils. For an FXR spot radius of 5 mm, single shot charge fluence is 2.45 $\mu C/mm^2$ and efforts must be taken to ensure that the spot size is not reduced below this. With a normalized emittance of 3000 π mm-mrad, the beam divergence at this waist is 16.6 mrad at 18 MeV. So this divergence is well suited to measurement with a single OTR foil. The transfer matrix for a 4-lens system shows that spatial offset is 58.88 μm/mrad on input to the fiber bundle. The fiber bundle and optics package give 54.4 μm/pixel so the total system has a resolution of 1.08 pixel/mrad. For a $+/- 4/\gamma$ field of view for an 18-MeV beam, $\gamma = 36.2$ requiring a capture of 16.6° divergence cone angle requiring the use of very large (8–n.) lenses.

Good OTR data was collected at FXR which demonstrates an excellent alignment procedure. A linear polarizer verifies the radial polarization inherent in OTR light with the two-lobe pattern. The solenoid magnetic settings were adjusted to visually determine when the beam was collimated. This provides the first single-shot operator feedback of this nature at FXR. For a beam radius of 5mm and a divergence of 16 mrad, the resulting emittance corresponds to $\varepsilon = 3300\ \pi$ mm-mrad.

The ability to obtain beam emittance measurements for high-current high-energy electron beams has been demonstrated at FXR. Future work using a modified form of the existing system will allow for additional beam diagnostics.

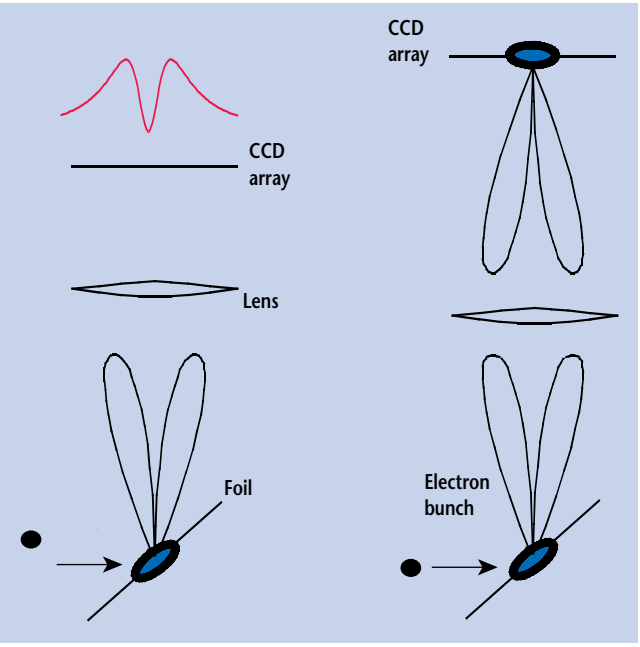

An angular spread of OTR light is produced when the electron beam strikes the foil material. The Charged Coupled Device (CCD) array records the light.

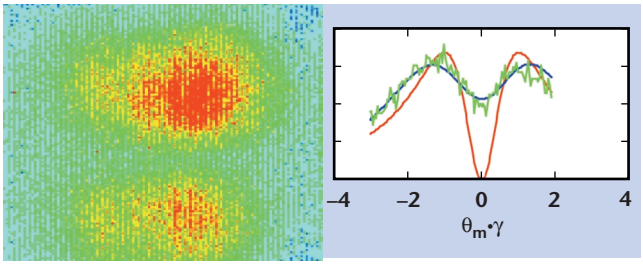

The two lobes of the OTR light are clearly visible in this false-color CCD image [left]. The full beam spears the single electron "perfect" OTR distribution. Lineouts [right] show the data for a cold beam (deep null), the measured data (noisy), and the underlying smooth curve shows the expected angular distribution for 16 mrad.

Computations and Numerical Simulation

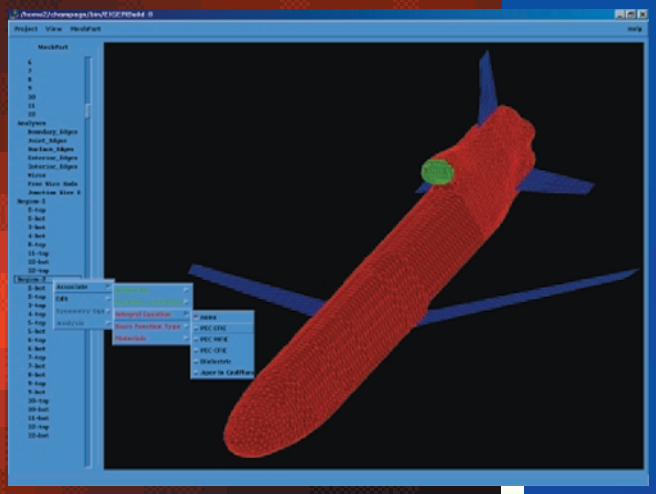

4

Graphical User Interfaces for Frequency-Domain EM Software Tools

R. M. Sharpe, N. J. Champagne

The graphical user interface (GUI) is often deemed *the* most important feature of modern software tools since it either facilitates advanced analysis and design or restricts features from use by individuals with limited knowledge of the underlying theory. The GUI must provide visual mesh diagnostics required for model validation before performing EM analysis (which is fundamentally different from the diagnostics used in most mechanical engineering based tools where the mesh is typically generated). In addition, the GUI must assist with the problem setup by identifying regions where objects interact and by specifying the boundary conditions to be applied. Also, the exact formulation and numerical solution must be specified along with desired output of EM quantities such as currents, far fields, and impedance. The goal of this project is to develop an advanced preprocessor and user interface to fulfill all of these needs for frequency domain EM codes.

The basic algorithms used in frequency domain solutions are boundary element methods (BEM). These solutions are typically applied to surface and wire discretizations of the desired geometry. Continuity of the geometry must be verified before the underlying numerical details (elements and basis functions) are confirmed and specified. During this effort, appropriate diagnostics were added to complete this verification. Also, features were added to automatically determine mathematical regions where similar interactions may be applied. This augments the functionality of the tools since many mesh generation packages are unable to group geometry and apply labels that can be used for this same purpose.

A key extension added to the GUI is the incorporation of volumetric elements used with finite element methods (FEM) to solve the wave equation. In addition, a combination of treatments (hybrid BEM/FEM) may now be applied to a given problem. This enables an optimized solution where the best solution method can be applied to the appropriate portion of a geometry to yield a completely self-consistent hybrid result. Output quantities may also be specified in the GUI so that exact current plots, near- and far-field patterns, and input impedances may be obtained.

Next year's effort will focus on extending the hybrid pre-processing capabilities to include higher-order methods in both geometry (elements) and numerical procedure (basis functions). This will enable improved convergence of the solution with minimal computational resources. In addition, the GUI will be ported to Windows platforms as well as the Unix platforms that are currently supported.

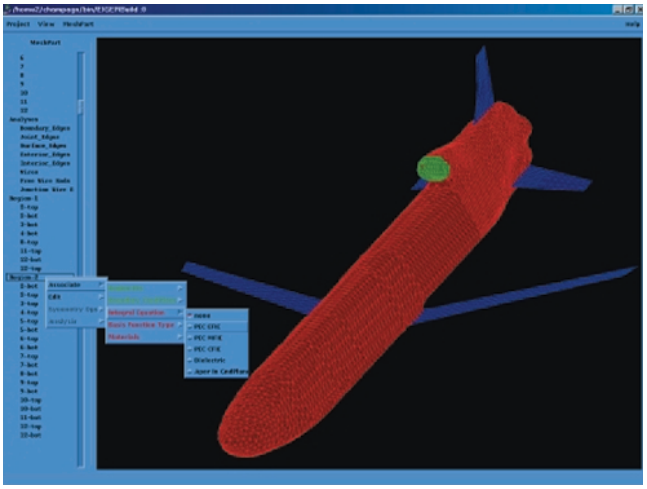

Current GUI applied to a complex airframe to prepare for EM analysis. In this step, the boundary conditions are being applied to the problem.

The Engineering Common Code Base Project

K. Mish

Software development within the Engineering Directorate at LLNL has traditionally been subdivided into two thrust areas: computational mechanics and computational electromagnetics. Although these disparate physical cases are governed by similar mathematical principles, little effort has been expended on the goal of sharing software between these two subdisciplines. This project's motivation was to begin the process of developing core software components that could be deployed in both mechanics and electromagnetics applications. The initial effort was concentrated on developing common tools for implicit finite-element analysis, since this mathematical capability is readily adapted to both mechanics and electromagnetics.

Engineering simulations generally tend to use unstructured finite-element approximations, since this is the only general method capable of handling the complexities commonly found in engineering applications. For example, while finite-difference and other common numerical techniques are widely used to solve partial differential equations in scientific fields, these discretization techniques have substantial limitations in dealing with such engineering complexities as heterogenous materials, complex geometries, and strongly nonlinear material or geometric response. Finite-element models readily model such complexities, and this robust generality is one of the main reasons why finite-element models are so common in engineering practice.

The best-known example of a finite-element application developed at LLNL is the DYNA3D code, which performs nonlinear dynamic simulations of deformable solids. DYNA3D is carefully optimized for solving such problems, which precludes use of much of the DYNA3D code base in other fields, such as computational electromagnetics. In particular, DYNA3D is an explicit finite-element stress-analysis code (which implies that it avoids solving the system of finite-element equations that correspond to Newton's laws of motion) that uses low-order hexahedral finite elements (a necessary choice of elements which limits the rate of convergence of the finite-element approximation). These limitations of DYNA3D cause little practical concern for the sort of transient mechanics simulations that DYNA3D is designed to solve, but for more general analysis cases, such as those found in electromagnetics or in mechanical manufacturing processes, these optimizations limit the utility of the DYNA3D code.

The Engineering Common Code Base project provides a means for a wide variety of LLNL engineers, mathematicians, and physicists to work together to identify common features of finite-element technology that could be written once, and then deployed across multiple engineering analysis codes towards the goal of extending the range of LLNL analysis tools beyond the explicit mechanics domain. Some of the results represent near-term benefits for LLNL codes such as ALE3D, while others provide longer-term payoffs in improved understanding of finite-element theory. Representative results of this Engineering-led collaboration include:

1) Development and deployment of a multi-physics-aware solver architecture for LLNL's ALE3D ASCI engineering code, specifically designed to take advantage of the hybrid shared/distributed-memory architecture of LLNL ASCI supercomputers. This work was deployed via the DOE-standard FEI 2.0 specification in conjunction with staff from LLNL's DNT and Computation directorates, working collaboratively with Sandia engineers (see figure).

2) Development of a unified mathematical model for high-order finite-element approximation that can be used in both mechanics and electromagnetics simulations. This collaborative effort across three LLNL directorates resulted in the identification of an area of research for an FY01 LDRD project. The LLNL Center for Applied Scientific Computing (CASC) is now developing the theory for long-sought convergence improvements for finite-element simulation techniques.

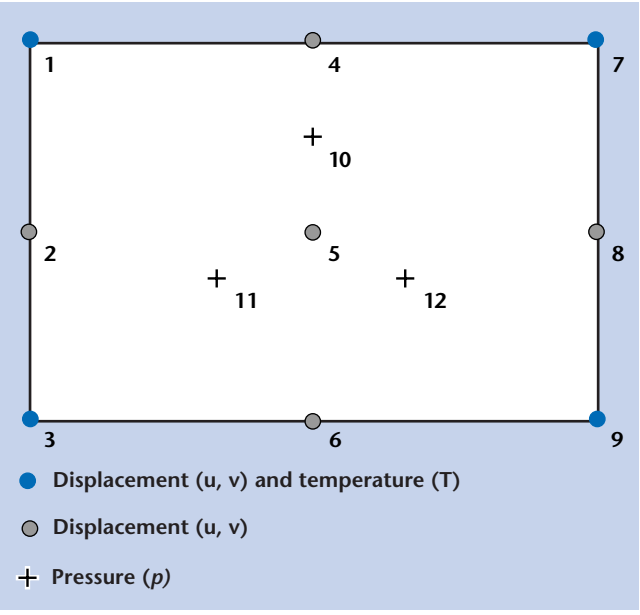

Typical multi-physics element used in DOE engineering simulations.

Object-Oriented Bookkeeping Library Documentation

D. Steich, T. Brugger

The focus of our techbase activities for FY00 was to edit and document C++ object-oriented libraries. One project involved exploration of object-oriented technologies to abstract the physics from the bookkeeping. The other project involved exploration into automated all-hex volumetric partitioning of 2-D surface descriptions. During the course of these projects, a set of three libraries—Utilities, Entity-Attribute, and Mesh—were developed. These libraries were in a constant state of flux with varying degrees of documentation.

Our accomplishments in FY00 included first pass documentation of the source code. This documentation included both the class descriptions and the functionality in the code. The source code documentation included details associated with the object-oriented implementation of the libraries. Class descriptions and functionality were documented using Doc++, including an HTML description. We use the phrase "first pass" documentation to mean that the documentation is far from polished or complete. Full documentation including a user's manual was beyond the scope of this project. The partial documentation added in this project included tens of thousands of lines of text.

As we were documenting, we cleaned up the code by removing obsolete and/or defeatured portions, and enhancing the consistency of the library's class member functions. For example, the Utilities library includes a set of container classes designed for quick automated insertion and removal of objects. There are fixed sized, adjustable, sorted, non-contiguous, and stack-based containers, each specialized for specific tasks. Code clean-up tasks involved adding uniform, transparent copy, comparison, read/write, and other operators for each and between each of the container types.

Finally, we worked on some software Pthread issues associated with the libraries. Some of the library tools replicate data structures on multiple processor environments. The implementation involves many lightweight threads simultaneously running on each processor, with each thread handling communication requests for objects of a given type. Currently, when running many threads per processor on more than eight processors our Pthreads implementation often creates excessive thread-to-thread contention. The problem is system-dependent and appears to have more to do with the total number of threads than the number of processors.

When two or more threads on the same processor want to access the same resource, all but one of the threads must wait. The waiting threads would go to sleep and the first thread to wake after the resource was free would be the next to lock it down. The above scenario is typical and in itself poses no difficulties, as long as it happens infrequently.

However, when we had a dozen or more threads per processor, for still unknown reasons *all* waiting threads would get a busy signal and go through tens of thousands of wait cycles before any one of the threads would gain access to the idle resource. This race condition would occur only when there were many threads running. When using only a few threads on a few processors, one thread was almost always successful in locking down the resource after each wait cycle.

Overall the bottleneck is exponential. Doubling the total number of threads often leads to n^2-like slow downs, although results varied on different platforms. The problem can be greatly alleviated by using randomized sleep times for each thread, but no general solution has been found.

It is hoped that tools found in these libraries will be useful in future code development efforts.

Electromagnetic Propagation and Imaging in Dense Media

H. M. Buettner

We investigated the feasibility of using electromagnetic (EM) induction techniques for detecting and characterizing deeply buried facilities. EM modeling with the finite difference frequency domain code fdfd was used to predict the responses of a tunnel with and without associated electrical conductors. This modeling indicated that the EM response from the electrical conductors in the tunnel was sufficient to detect the tunnel from surface magnetic field measurements. A simple experiment conducted at LLNL verified the effect, but it was much smaller than predicted. The difference was thought to be the result of a mismatch between the experiment and the modeling.

EM methods show promise for detecting underground facilities because of the EM responses from the various conductors, which are part of such a facility: signal cables, wiring, ducting, reinforcing bars, structural steel, and other components. One geophysical method, ground-penetrating radar (GPR), has good spatial resolution, but is limited to shallow applications because the skin depth at GPR frequencies is typically only a few meters. By contrast, EM induction methods, which operate at frequencies from a few hundred Hz to a few kHz, have skin depths of tens to hundreds of meters. Thus deep probing is possible with EM induction.

The computer code fdfd, developed at LLNL for computing the EM response to conducting plumes during environmental remediation, was used for underground facility problems by requiring that the tangential electric fields vanish along any conductors like wires or meshes.

The computer modeling was done for the "realistic"case of a tunnel with a 4-m-x-4-m cross-section, buried at a depth of 20 m in an earth with a conductivity of 0.01 s/m. The EM source was a magnetic dipole located 12.5 m from the tunnel axis, and the frequency was 1 kHz. The received magnetic fields were computed along survey lines that traversed the tunnel perpendicular to its axis. The figure shows the phase response of the magnetic field versus distance along a survey line passing through the source. Three cases are shown: the bare tunnel (void), the tunnel with a single wire along the roof (wire), and the tunnel with a mesh on the roof (mesh). The wire and mesh responses are clearly different from the void response.

This optimistic result prompted a simple field experiment at LLNL in the buffer zone near the northwest corner. We used a sewer line buried at a depth of about 3.5 m as the tunnel, and ran a wire inside it as the conductor. We ran a survey across the tunnel as described in the paragraph above with the wire open-circuited at both ends, and then with the wire electrically connected to the surrounding soil. We found a measurable difference in both the magnitude and phase responses for the two cases. However, this difference was much smaller than the modeling had predicted, and not large enough to be of practical value.

We believe the reason for the discrepancy is that the experiment and the modeling did not match. Specifically, the modeling assumed a wire in contact with the soil along its entire length, but the wire in the experiment was insulated along its length and was connected only at its ends. To match the modeling, a bare wire in contact with the soil along its entire length is needed. This situation is not easy to create in a simple, inexpensive experiment.

To conclude, the modeling shows that tunnels with conductors can probably be detected from surface measurements, but we were unable to confirm this experimentally.

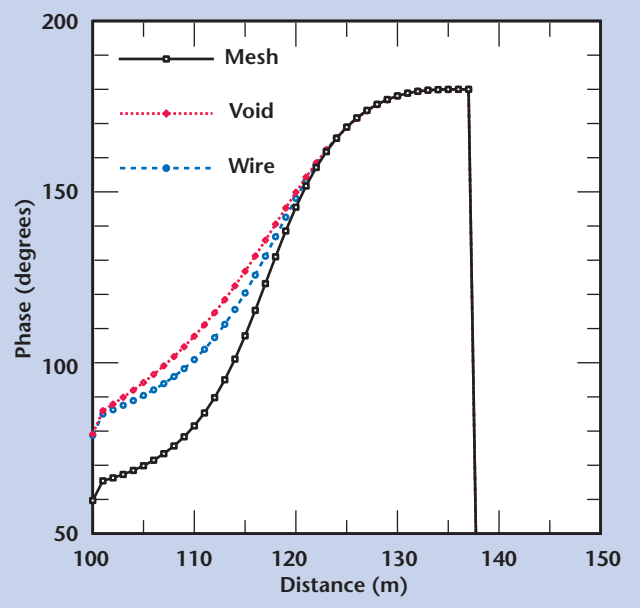

Phase response of the magnetic field for a bare tunnel, a tunnel with a wire, and a tunnel with a mesh.

Beowulf Cluster for Imaging and EM Modeling Applications

H. Jones

In the early to mid-nineties, the computing landscape witnessed the confluence of low-cost commodity computing hardware, including network components, with that of Open Source software such as the Linux operating system, the GNU compilers and programming tools, and MPI and PVM message-passing libraries. The Accelerated Strategic Computing Initiative (ASCI), chartered with developing the next generation tera-flop capable platforms, also recognized that the highest performance computational components arrived in PCs first. So, in addition to the compute engines for ASCI's progression of world's fastest computers, individual PCs also were capable of breathtaking performance increases. This in turn drove many to look at networked PCs as a solution class to problems that were computationally intensive or communications tolerant. A prototype cluster, Beowulf, was developed in 1994 and demonstrated for communications-tolerant applications such as the gravitational N-body problem, that supercomputer-style performance could be had at low cost.

With the computation model independent of specific hardware, a Beowulf cluster has a natural built-in upgrade path. Unlike the popular Network-of-Workstations compute model, a Beowulf typically contains one master node, and dedicated slave nodes on an interconnection network isolated from the external institutional LAN. Beowulfs are typically seen on the Top 500 Supercomputer list.

Recognizing that we could demonstrate low-cost high-performance computing for specific classes of applications important to Engineering and LLNL, the two year tech-base proposal had the following goals for the first year: 1) set up 32-node prototype using Fast Ethernet interconnection network; 2) demonstrate base performance and scaling for EUV defect scattering, pulse-echo radar EM modeling, and image reconstruction for radar applications (space-wavelength domain decomposition); and 3) enhance parallel computing culture/talent base. With slight modification of the targeted applications, we easily demonstrated the efficacy of the Beowulf cluster.

Our goals for the second year were: 1) apply cluster to communications-tolerant applications, typically using MPI; 2) investigate efficacy of Open Source job-scheduling middleware such as DQS, Mosix, PBS, Condor; 3) investigate commercial signal- and image-processing package framework as cluster front-end (IDL); 4) demonstrate cluster-aware back-end processing within signal- and image-processing framework; and 5) transfer technology.

Project Status

The cluster is used for production work by IS&T. Other groups within Engineering also express interest.

Mosix, BProc, DQS, PBS, Condor, and other job-scheduling middleware are being investigated. None up to this point has general acceptance within the community, and this subject continues to be the focal point of discussion.

In keeping with our transfer of technology goals, the FY01 NDE tech base will focus on NDE cluster-based image reconstruction algorithms, including cone beam tomography. IDL as cluster front-end, and additionally as a cluster-aware back-end compute engine will be used.

This project has been successful in demonstrating the efficacy of low-cost high-performance computing using the Beowulf model. Although middleware applications, which support transparent cluster usage via process scheduling mechanisms, resist standardization, it was found that many applications can nonetheless be used effectively without such support, requiring only minor alterations to fit the new compute model.

Ground Effects in Counterterrorism and Ballistic Missile Defense

R. Couch, T. Dunn

An act of terrorism, a ballistic missile attack, or a counter-proliferation interdiction can lead to the dispersal of nuclear materials, chemicals, or biological agents into the atmosphere. Once dispersed, they are highly likely to reach the ground, possibly in or near centers of population. The real-time recognition, identification, tracking, and neutralization of such dispersed materials, *i.e.*, the problem of ground effects, is a national strategic problem to be solved.

Agent dispersion models are essential to the counter-proliferation, counterterrorism, and ballistic missile defense programs. Agent dispersion scenarios for missile defense may occur at altitudes ranging from sea level (cruise missiles) to very high altitudes (long range ballistic missiles). Ambient conditions for agent dispersion events overlap for lower altitude missile intercepts and counter proliferation /terrorism scenarios. Increased interest in the application of modeling capabilities for ballistic missile defense and counter-proliferation requires that current agent dispersion models be maintained and enhanced. Currently, an operational capability does not exist to recognize, characterize the nature of, and track a dispersing cloud as it moves through the atmosphere.

This activity supports an NAI-sponsored project that is focused on providing experimental data related to the dispersal of chemical agents. The focus of this project is the enhancement of a simulation capability for scenarios involving the deposition by thermal, impact, or blast loading of sufficient energy to cause multiphase regions in chemical/biological agents with the goal of predicting the dispersion of the agents.

Modeling the complex scenarios associated with ballistic missile attack, or a counter-proliferation interdiction can involve many complex physical processes. The goal of this project is to support a code that provides the basic framework for modeling these highly dynamic and transient effects. ALE3D was used as the vehicle for the model development because of its existing multi-physics capabilities and its current usage for simulations of similar events. ALE3D provides coupled fluid and structural modeling that can be combined with the effects of thermal transport and chemical reaction.

The major features required to provide the relevant modeling capabilities are: 1) particle transport; 2) non-ideal gas representation; 3) surface tension; and 4) mixed phase, liquid-vapor-droplet model.

These features require model enhancement followed by model verification and validation. Since the surface tension model is intended for use in droplet breakup simulations, it is also necessary to validate ALE3D as a tool for predicting drag coefficients on deformable bodies.

The current year's activities produced a particle transport model and a non-ideal gas model. Both were verified and validated by comparisons with known solutions. The accuracy of ALE3D in modeling the drag on rigid structures was also assessed. It was observed that ALE3D produced results of similar accuracy to well known CFD codes, and thus would be applicable to the class of problems of interest.

The remaining models are expected to be available during the second year of the project.

*Note: Our work is part of a general tech-base effort to maintain and continue the enhancement of LLNL codes.

Enhanced Fluid Dynamics Capability and Multidisciplinary Coupling in ALE3D

R. McCallen, T. Dunn, G. Laskowski, K. Westerberg

The need for robust multi-disciplinary modeling tools is increasing. ALE3D, a multi-physics hydrocode developed at LLNL, provides many of the physics options required, but not all. Low Mach number flows is one area where model enhancements are needed. To address this, an incompressible flow model has been implemented to handle cases where compressible flow modeling is inefficient. With this capability and additional improvements in ALE3D algorithms, many programmatic modeling problems of immediate and future concern can be solved, *e.g.*, vehicle aerodynamics and under-hood thermal transport for reducing energy consumption; near-field biological or chemical dispersion for counter-proliferation and missile defense projects; arterial hemodynamics for medical applications; micro-fluidics; and thermal convection in storage facilities for the defense programs. Thermal recovery time for the beam tubes and amplifiers on the National Ignition Facility can also be evaluated.

The ALE3D code is at the forefront of multi-physics modeling. Its unique capabilities and demonstrated applications in massively parallel computing are unmatched by currently available commercial and non-commercial software. The flow, thermal, and structural phenomena have different stability and accuracy criteria that direct the numerical solution approach, grid resolution, and time step.

We have provided an improved modeling capability by incorporating an incompressible flow module in ALE3D. This addition, coupled to its structural, heat transfer, and chemistry models, will push us into previously unattainable areas of computational modeling. The implementation was completed in FY99. Moving towards the goal of multi-physics modeling, the heat transfer model was coupled to the flow during FY00. Simulating thermal-advection problems is necessary for applications involving the heating of an air filled room by machinery or other heat sources.

The flow was solved using an Eulerian formulation of the time-dependent incompressible Navier-Stokes equations. Coupling of the heat transfer model required the addition of an advection term to the thermal transport equation and a Boussinesq term to the flow momentum equation representing the buoyancy force. The temperature was solved independent of the flow equations.

The resulting matrices for the flow and heat transfer equations were assembled using the Finite Element Interface developed by Sandia National Laboratories in collaboration with LLNL. The system of equations was solved using the HYPRE parallel solver package developed at LLNL's Center for Advanced Scientific Computing. The library packages allow the use of many advanced iterative linear solvers and preconditioners designed for efficient matrix solutions on massively parallel computer systems.

The new capability was validated by simulating the flow and temperature in an enclosed cavity: a differentially-heated, tall (8:1 height-to-width ratio) rectangular cavity with a Rayleigh number (measure of buoyancy) of 3.4×10^5 and Prandtl number (measure of viscous dissipation to heat conduction) of 0.71. The figure shows the geometry and calculated temperature fluctuations for a series of snapshots in time. Pockets of warmer (red) and colder (blue) fluid relative to the mean flow move from the hot wall on the right towards the cold wall to the left in a counterclockwise flow. It was found that the average temperature and velocity values were captured with a relatively coarse mesh, although capturing the unsteady temperature fluctuations required a finer grid.

The goal for FY01 is the coupling of the flow and structural models, using simple grid re-mapping techniques for the fluid/structure interface. Additional work will include improvements to the turbulence modeling capability, model accuracy, and solution speed. We will also continue our verification and validation study of the incompressible flow model and the fluid heat transfer coupling for a variety of applications.

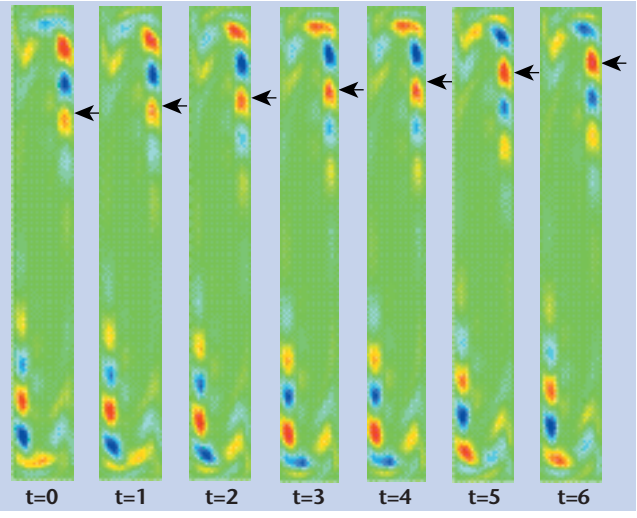

Contours of the calculated temperature fluctuations (instantaneous minus the mean or time-averaged temperature) in the enclosed cavity. Snapshots in advancing time are shown from left to right. The arrows point out the position of a single warmer region that is moving upward along the hot wall.

*Note: Our work is part of a general tech-base effort to maintain and continue the enhancement of LLNL codes.

Feature Enhancements in DYNA3D for Weapons, Defense, and Earthquake Simulations

J. Lin

In addition to the ongoing tasks of DYNA3D code and manual maintenance, user support and the Collaborator Program administration, our work in FY00 included new features added in DYNA3D: the enhanced Deformable-Rigid Material Switching, the latest PENCRV3D modules with cratering algorithms, Los Alamos National Laboratory's (LANL) Visco-SCRAM and Hyperfoam materials, and failure mechanisms for the Defense Threat Reduction Agency (DTRA) Concrete Material.

The Deformable-Rigid Material Switching feature in DYNA3D allows parts of the finite-element model to be treated as rigid bodies at any time during a simulation. The goal is to speed up the analysis turnaround time. The method originally targeted component-drop tests and vehicle impact simulations as the most promising applications. In the future, engineering analysts will use material switching to model the manufacturing process of weapons system components. This technique allows the repeated analyses of a specific component under a variety of manufacturing boundary conditions, such as thermal and shear, while the remainder of the model is treated as a set of rigid body groups.

The important advantage of this method is that it avoids the very difficult mesh-merging task needed in the standard series of simulations to model manufacturing processes. We have added user-defined boundary conditions and integration time step limits, multiple on/off operations for a large number of material-switching groups, and damping applied to rigid bodies to complement the previously existing capabilities.

Another feature added to DYNA3D was PENCRV3D, a target resistance-predicting module. In conventional penetration simulations, detailed modeling of target structures is required to properly represent the target resistance. PENCRV3D uses instead a series of mathematical formulas to achieve this purpose. The penetration resistance of individual material layers is represented by pressure equations developed by fitting dynamic cavity expansion equations to experimental penetration data. PENCRV3D is capable of modeling targets composed of materials such as rock, soil, and concrete. PENCRV3D had been successfully integrated into DYNA3D as a load-generating module. In the latest version, cratering algorithms, which render more accurate assessment of penetration depth and penetrator orientation, along with other user-friendly features such as automatic searching for penetrator nose/tail, material grouping, and penetrator nose area calculation were added. The DYNA3D-PENCRV3D link has proved a useful tool for the weapons program.

Engineers at LANL have developed sophisticated material models to meet their needs in modeling components in weapons systems. They have provided two of these models for inclusion in our DYNA3D source. The Visco-SCRAM and Hyperfoam are materials designed for modeling polymer-bonded explosives and temperature-dependent orthotropic foam, respectively. They are available as materials for continuum elements.

LLNL engineers have been developing techniques to simulate the coupled fluid-structure interaction of dams under earthquake or blast conditions. The modeling of cracks and failure in their simulations necessitates the inclusion of failure mechanisms in a concrete material model. The author has added this feature to the DTRA Concrete Material, their concrete material model of choice. A procedure for eliminating unrealistic external forces associated with the erroneous deformation of failed elements has also been added to accommodate the failure mechanism.

In FY00, the author served as publication referee for the *ASCE Journal of Structural Engineering* and the *International Journal of Numerical Methods in Engineering*, and co-authored *DYNA3D Code Practices and Development* (UCRL-ID-138654). The report describes our ongoing effort in maintaining and distributing DYNA3D through the Collaborator Program and DOE's Energy Science and Technology Software Center. It also highlights the enhancements and modifications in DYNA3D during the past eight years.

Next year, we plan to investigate and implement segment-to-segment contact algorithms.

*Note: Our work is part of a general tech-base effort to maintain and continue the enhancement of LLNL codes.

Advances in GRIZ, TOPAZ, and NIKE3D Code Development

D. Speck, A. Shapiro, M. Puso

Advances in codes for graphics and data management have been made in FY00. Accomplishments encompass improvements in GRIZ, TOPAZ, and NIKE3D.

Mili/GRIZ

Significant breakthroughs have been achieved in this last year to integrate the flexibility provided by the new Mesh I/O LIbrary (Mili) with the GRIZ visualization software and augment the state plotting capability with a full time history plotting capability.

Mili enhancements were developed to support new functionality needed for the analysis programs. These included routines for correctly locating and writing new states after a restart of the analysis programs and for overwriting the initial nodal coordinates when DYNA3D detects initial slide surface penetration.

A major new addition in GRIZ Version 4 provides a time-series plotting capability that is equal in scope to the state plotting capability. It includes desirable plot design features such as legend, background grid, curve glyphs, and dynamic cursor coordinate display. A user setable min-state/max-state constraint limits both the display and data reads.

Other advances include: 1) a batch mode capability to provide offscreen rendering; 2) a comprehensive "tell" command to report data fields and other statistics in the database; 3) JPEG format image output that makes movie generation with standard tools easy, fast, and convenient for the analyst; 4) support for particle databases such as those generated for smooth particle or molecular dynamics simulations; 5) support for handling material superclass data to allow more visualization options; and 6) improvements to the internal self-timing routine to support up to ten simultaneous timers for more flexible performance monitoring.

Heat Transfer Codes

New code features and algorithms were added to LLNL's heat transfer codes to support NIF and weapons activities: 1) modifications to the REMAP software, to accept I8 formatted input for input meshes with more than 100,000 elements and nodes; 2) 3-D beam and beam fluid element for NIF applications; 3) four non-symmetric iterative solvers in TOPAZ3D for modeling advection-diffusion; and 4) a new TOPAZ3D manual, available electronically.

NIKE3D

The most important new advances in NIKE3D code development include the following: 1) a nonsymmetric stiffness matrix and assembly, along with a parallel solver; 2) improvements in the automatic contact algorithm needed for the implicit methodology; 3) better search algorithms for Type 3 contact to overcome local search anomalies; 4) a transverse isotropy capability for cyclic plasticity for sheet forming problems; 5) an input interface for user-developed material models similar to the ABAQUS method; 6) an upgraded NIKE-DYNA link to hand off hourglass forces, fully integrated brick element data, and friction forces at slide surfaces; 7) collaboration on the development of a Cosserat brick element; 8) added capability to interpolate the eight Gauss point stresses to the nodes; 9) new segment "freeze" techniques for contact algorithms, plus further changes to improve the robustness of the search algorithms; and 10) new intelligent schemes to achieve equilibrium convergence when the applied loads approach zero. The new schemes allow analysts to simulate actual loading situations and still achieve convergence.

*Note: Our work is part of a general tech-base effort to maintain and continue the enhancement of LLNL codes.

Fractography of Flexure Tested Structural Ceramics

R. A. Riddle, C. Syn

Structural ceramic specimens previously tested for their flexural strength by four-point bending were provided for SEM fractography. The ceramics comprised 34 "machined" and 35 "lapped," ASTM Standard C 1161, size B specimens. The Weibull statistics of the measured flexural strengths are shown below. SEM fractography was performed to characterize the fracture behavior of the material by locating and identifying the fracture-initiating flaws. From the results of the SEM fractography, fracture toughness of the specimens was evaluated.

From SEM fractographs, we determined the nature, shape, dimensions and location of the fracture-initiating flaw in each specimen. From the dimensions and location or from the "mirror" size of the fracture-initiating flaw, the fracture stress intensity factor, K_1 was calculated. Defects of round or square shapes were regarded as circular defects and others were taken as elliptic defects with their long and short dimensions on the fracture surface as the major and minor axes of an equivalent ellipse. Depending whether a given fracture origin was located on the initial "tension" surface or in the interior, an appropriate geometrical factor was calculated by comparing the equivalent geometry of origin with the list of the factors given by standards. Fracture stress intensity factors were evaluated using the calculated origin sizes.

Typical examples of different defects located at the fracture origins are shown in the figure for the "lapped"and "machined" sets of flexure specimens.

Except in the cases of large over-sized grains, it was difficult or impossible to clearly locate and identify the fracture originating defects. In several cases, an aggregate of grain-boundary porosity open to the surface or clusters of small oversized grains and grain-boundary porosity seemed to have initiated the fracture. In such cases, the determination of defect size could be subjective. In a few cases, there seemed to be a missing chunk between the two fracture surfaces making the identification of fracture origin impossible. In several cases, it was not possible simply because the specimens were severely contaminated or damaged by inappropriate handling and storage practice. The identification of fracture initiating defects was much easier in the "lapped" specimens since the boundary between the fracture surface and the "tension" surface was clearly visible in them.

The calculated values of the fracture stress intensity factor, K_1, are substantially smaller than a fracture toughness value, K_{1c}= 3.68 MPa·$m^{1/2}$ reported in the literature. The difference is especially large, almost by an order of magnitude in some cases, where an oversized grain was identified as the fracture source. This means that the fracture originating crack size, especially the crack depth, should be substantially larger than the size of the over-sized grain identified as the fracture origin. Since the specimens contain a rather high porosity of about 14%, it seems reasonable to assume that almost all grains, especially large over-sized grains, were linked to the grain-boundary voids, increasing the effective crack size. Thus it may be necessary to find a way to measure the size of grain-boundary voids. The difference is smaller in cases where a "mirror" pattern was observed, probably because a "mirror" pattern can be generated only when the origin size is very large.

Recommendations for future tech-base work include: 1) characterization of the base microstructural features; 2) measurements of long-, short-range, and microscopic residual stresses in the original part, slugs, and test specimens by NDE, x-ray and neutron diffraction techniques; 3) introduction of indentation-induced pre-cracks or machined notches; and 4) flexure tests of larger specimens for size effect on the Weibull statistics.

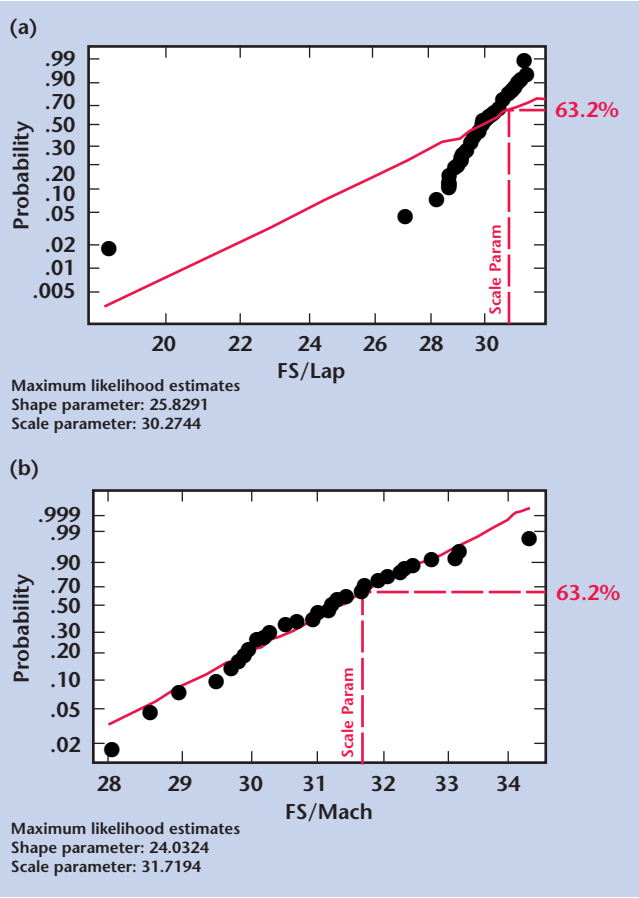

Weibull plots of measured flexural strengths for (a) lapped and (b) machined specimens.

EM Effects Induced by Gamma Radiation in Cables and Transmission Lines

D. Mayhall, M. Bland

When x-ray or gamma photons penetrate an electrical cable, energetic electrons and holes (also known as primary charge carriers or carriers) are created in the constituent metals and dielectrics of the cable by material and energy-dependent photoelectric, Compton scattering, and particle-antiparticle pair production processes. These energetic charge carriers, in turn, create many low-energy secondary charge carriers through avalanche ionization processes. The primary and secondary charge carriers generate electrical currents as they move through and along the cable materials. These photon-induced currents can generate EM waves that can propagate along the cable and into connected electric circuits. With their accompanying currents and voltages, the EM waves can cause undesired and catastrophic upset, unintended and potentially disastrous operation, and temporary or permanent failure in connected and even unconnected electronic systems.

Energetic photon radiation problems have interested LLNL for many decades and still remain essentially unsolved. Presently, no computer model exists for prediction of these effects in electronic systems of interest. Using existing equations and algorithms, we built a computer model for energetic photon effects in cables and their associated electronic systems. Although this effort has been small, we have made substantial progress toward the creation of a time-dependent, nonlinear computer code to numerically treat these types of photon-induced problems.

We have worked with a set of physical equations that describe the interaction of energetic photon radiation with the dielectric materials in electrical cables. These time-dependent, nonlinear differential equations include the effect of material impurities on the dynamic behavior of charge carriers in the component dielectrics. Primary and secondary carrier generation, carrier trapping, and recombination processes are included. These carrier equations, combined with Maxwell's complete equations, allow the prediction of EM waves and their associated currents and voltages in electrical cables and connected and nearby electronic systems.

We have modified a previously very successful, time-dependent, 2-D, rectangular coordinate, EM, electron fluid computer code to include primary and secondary charge carrier generation, free and trapped electron populations, and photon-induced material conductivity. We have applied this code for transverse magnetic modes to demonstrate the generation and propagation of a predominantly transverse EM mode wave in a section of a parallel plate cable, containing one model polymeric dielectric between two perfectly electrically conducting metal plates. The inclusion of the spatially-dependent photon attenuation in the dielectric allows the time- and spatially-dependent carrier dynamics to be calculated self-consistently in each computational cell. The effect of local electric and magnetic field levels on the charge carrier properties can thus be included in this code.

In the future, we will make our computational model more realistic to allow the prediction of energetic photon effects in real cables in underground tests.

Complex Systems and Information Technology

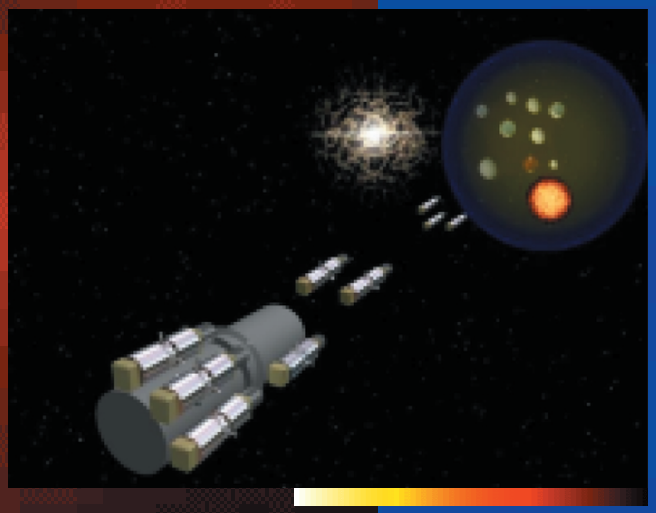

5

Extreme Bandwidth Security Tools

G. Pavel, W. J. Lennon, C. Dunlap, D. Colon

While intrusion detection and firewall protection are available at multi-megabit per second data rates, cost effective analysis and management of these data streams is currently beyond the state of the art. Organizations like LLNL will be depending on very high-speed networks for a variety of collaborations in the near future, but can no longer deploy networks for regular business without being able to manage their security. We are leveraging our role in high-bandwidth networking to strengthen our collaboration between nationally recognized experts in different aspects of high-performance network analysis and security management. The goal is to jump start the commercial development of security tools so that they are readily available when LLNL and other organizations require multi-gigabit per second networks for normal production activities.

Engineering's participation in the National Transparent Optical Network (NTON) Consortium provides contact with experts in networks operating above 1 Gb/s. NTON is the West Coast member of Supernet, a cross-country network funded by DARPA's NGI (Next Generation Internet) Program, comprising several interconnected and inter-operating testbeds. The NTON backbone runs at 10 Gb/s (OC-192) with 2.5 Gb/s (OC-48) and 622 Mb/s (OC-12) links to sites such as LLNL, LBNL, Sandia, NASA, SLAC, Caltech, and UC Berkeley. This provides an excellent platform for experimenting with extreme bandwidth security tools.

We believe it is feasible to create a network intrusion detector (NID) that operates at OC-48. Experiments and demonstrations at OC-12 will prove feasibility and establish credibility to pursue upgrading the design to the higher rate. LLNL has expertise in NIDs, having developed the software used at DOE sites. Currently the software can perform on the existing 100 Mb/s networks, but scaling the performance to high-bandwidth networks is not as simple as running on faster processors. Some hardware assistance is necessary.

We felt that collaboration between a vendor of a programmable network protocol analyzer and NID software developers could produce a prototype of a high-bandwidth intrusion detector.

In FY00, we acquired Boeing's FPGA-based AS4950 network protocol analyzer, and began collaborating with Boeing to combine their hardware with NAI's NID software to produce an intrusion detector operating at OC-12. Boeing will modify the firmware and software in the Generic Processing Engine (GPE) in the AS4950 to support sophisticated pattern matching that will filter out packets that are not of interest. LLNL will modify NID to communicate with the hardware, sending patterns and receiving filtered packets (see figure). The collaboration has produced a design specification for the Boeing modifications that is currently proprietary to Boeing. It is also the basis for a Cooperative Research and Development Agreement (CRADA) that is being negotiated with Boeing. The company has begun implementation of the design and we have started modifications to NID.

We investigated other intrusion detection software that is available publicly, with the intent of comparing performance in combination with the Boeing hardware with that of NID. We selected NTop, an open source package similar in function to Coral Reef, which had already been used to create a lightweight intrusion detector. This package is being modified to work with Boeing's specification.

In FY01, we expect to complete the modifications and demonstrate an intrusion detector operating on an OC-12 link at a highly visible venue such as the annual Supercomputing and Communications Conference. Initial capability may not have all the features necessary for production use, such as packet fragment reassembly, but will clearly show the feasibility of the approach. The lessons learned from designing this system will also help develop an architectural approach that can scale to OC-48 speeds and higher.

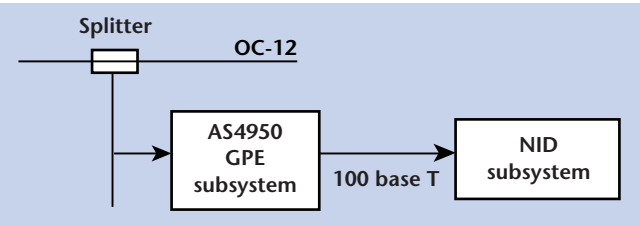

System Block Diagram for network intrusion detector.

Small Munition Fuzing with Time-Of-Flight Radar

T. Rosenbury

Micropower impulse radar (MIR) was tested as a prototype proximity fuze sensor for possible use in XM-80 submunitions. LLNL was asked to develop a circuit board sensor to evaluate the possibility that MIR could provide a height-of-burst signal. Neither ECCM (anti-jamming) nor antenna development was required. During testing, the MIR sensor met or exceeded all requirements.

As currently designed, the MIR is a miniaturized, low-power, broadband, pulsed radar that uses time-of-flight measurement to determine range to objects. In normal applications a short (sub-ns) pulse is transmitted. After a fixed time (range) the receiver is turned on and the reflected energy is measured. A second pulse is transmitted, and after a slightly longer delay the reflected energy is measured. The delay is increased successively after each pulse/reflected pulse (energy) is stored. After a range of 50 ft, the receiver time delay is set to zero and the process is repeated. The MIR was capable of detecting quasi-static targets (velocities <5ft/s).

The MIR used for proximity detection is a modification of the existing concept (see Fig. 1). The transmitter/receiver electronics are basically the same; however, the "range gate" is opened after a short delay, after transmit pulse, and detects objects in close range to the desired fuzing range. The return pulses are integrated until a threshold value has been exceeded. Fast closure rates could be achieved by altering the MIR pulse rate and range cell resolution. By filtering the integrator detector pulses, it is possible to set a closure rate. The closure rate was designed to ignore a slow moving/stationary target and detect targets with velocities of 15 ft/s to 260 ft/s.

Drop tests were conducted by the Army Research Laboratory. LLNL conducted independent drop tests, using multiple fuzes over both sand and a 4-ft-x-4-ft aluminum plate.

The MIR met and exceeded the requirement and design goals by a factor of 3x. Detection height (fire command) requirements were set at a nominal height of 30 in. with a tolerance of 6 in. MIR target closing rates were increased to meet the 260 ft/s requirements. Circuits were added to block the low velocity targets (<15 ft/s). Since electrical power would come from a small battery, low power operation was desired. Initial fuze power requirements were set at a total current of 50 mA with a design goal of using less than 30 mA. Another requirement was for turn-on time to be less than 100 ms (design goal <75 ms). If the current drain on the battery is limited to 3.8 mA, the turn–on time is 80 ms. If higher current drain is allowed during turn–on, the time it is reduced to 30 ms.

The anti-jamming features were not funded and would need to be included before MIR could be implemented as a small munition proximity fuze sensor (see Fig. 2). However, the MIR technology is simple and lends itself to inexpensive microchip production.

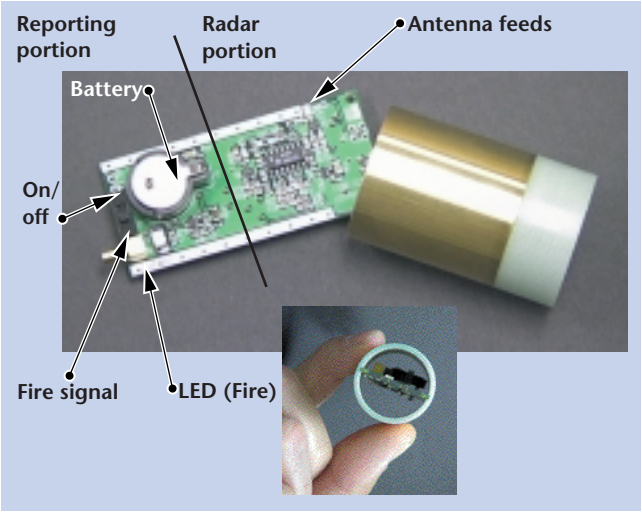

Figure 1. The proximity fuze, containing circuits and functions in addition to the radar sensor.

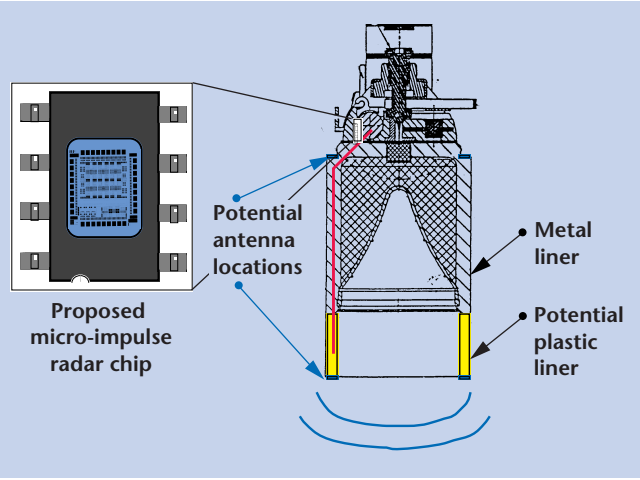

Figure 2. The MIR fuze sensor, with potential for being designed into a modified XM-80 liner.

Advanced Target Discrimination for National Ballistic Missile Defense

L. C. Ng, R. M. Greenman

One of the critical problems in building a robust ballistic missile defense system is the ability to discriminate between decoys and real targets prior to endgame. This problem is complicated by at least four factors: 1) a large number of objects may be within the sensor field-of-view; 2) the decoy signatures are designed specifically to emulate the real target; 3) a target (re-entry vehicle, or RV) may be enveloped inside a decoy balloon; and 4) the problem must be solved within a given time constraint. These combined factors create an extremely challenging target discrimination problem. This work investigated the merits and efficacy of several discrimination algorithms and the means to address one of the most difficult advanced countermeasures—the enveloped RV.

With the nation's interest in building a National Missile Defense system, it becomes obvious that a robust target/decoy discrimination capability is needed to address potential advanced countermeasures.

Target/decoy discrimination technology is based on analyzing a set of actively and/or passively observed feature vectors derived from the target and decoy characteristics. Typically, discriminating features might be related to parameters such as an object's distinct spin dynamics, thermal intensity, radar cross-section, surface reflectance, and emissivity. A data fusion algorithm based on either a Dempster-Shafer (D-S) or a classical Bayesian formulation may be used to produce a target probability likelihood rank list. The object with the highest rank will then be taken as the real target.

During this past year, we addressed the comparative performance of D-S- and Bayesian-based fusion algorithms using a traditional set of feature vectors. We found that the implementation choices between D-S and Bayesian classifiers must be weighted over a set of technical compromises. For example, D-S requires less *a priori* knowledge about the object class, but takes a longer time to converge since additional knowledge must be gleaned from more real-time measurements. D-S does not require *a priori* knowledge of the exact number of objects to be classified, but will require additional computations and more complex logic to resolve additional hypotheses.

In the coming year, we will address one of the most difficult discrimination problems—the discrimination of an enveloped RV—based on a kinematic sweeper concept (see figure). In the vacuum of space, all objects, regardless of their weight, move at the same velocity. Decoy balloons by necessity must be light-weight. A small, high-explosive source would be detonated at the vicinity of the threat cloud to create an expanding gas bubble. The dynamic interaction of the gas bubble with the threat cloud would cause lighter objects to sweep away at a faster speed than the RV. Observing the resulting kinematic motions would provide favorable measurements to identify the real target. The measured dynamic motions thus form an additional set of observations that can be added to the existing feature vector. Again a D-S- or a Bayesian-formulated data fusion algorithm may be used to determine the effectiveness, timeliness, and robustness of the approach.

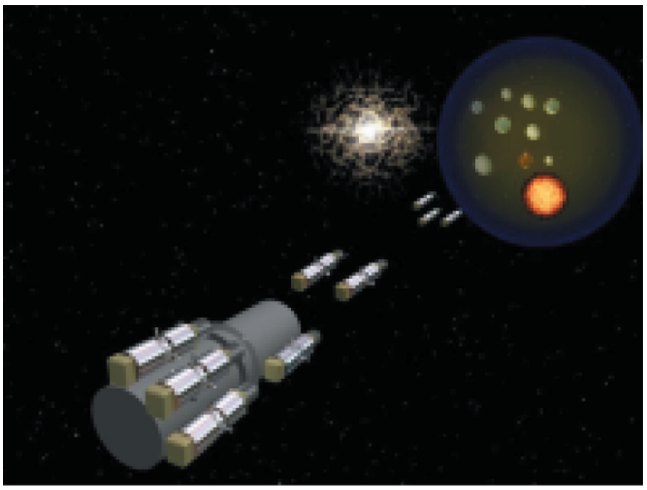

Kinematic sweeper concept: the threat cloud is perturbed with an expanding gas bubble created by the detonation of a compact high-explosive source.

Low-Power Wireless Modem ASIC

C. McConaghy, C. Chien,* I. Elgorria*

Low-power wireless sensors require that all the subsystem components be small in size and low in power. One of the key components for direct sequence spread spectrum (DSSS) radio frequency systems is the modulator/demodulator (modem), which we had previously developed based on field programmable gate arrays (FPGA). In this year's work the modem is implemented as an application-specific integrated circuit (ASIC), resulting in a significant decrease in power and size.

Wireless microsensors work has shown a need for low power and small size electronics. Spread spectrum wireless communication has been used to improve reliability and security in these sensors. The spreading and de-spreading functions are performed by digital logic in the modem. In our previous work, custom designed modems were implemented using FPGAs. Although the FPGA approach allowed rapid development of the modem algorithms, ultimate performance is achieved by an ASIC implementation. The following table compares power and size for the FPGA and ASIC designs.

FY98	FY99	FY00
XC4062XL FPGA	XCS20XL FPGA	0.35-µm CMOS ASIC
35 mm x 35 mm	14 mm x 14 mm	2 mm x 2 mm
250 mW	50 mW	6 mW

The 3.3-V ASIC design has the same functionality as the previous FPGA design, including programmable symbol rates of 8 to 90 kb/s with a 1 MHz chip rate. These designs were experimentally verified in two wireless sensor design iterations. Using 1-mW 900-MHz DSSS RF links, these modules were able to communicate with other modules located around a building.

In both the ASIC and FPGA designs the digital logic is written in a high level language called VHDL. The VHDL is then compiled with the proper library for the desired implementation. After design, the ASIC was fabricated by a foundry in a standard 0.35-μm CMOS process.

The chips have returned from the foundry and are in evaluation. Initial evaluation indicates that the measured power drain is 3.3 mW receive and 6 mW transmit, as predicted. Lock-on of data packets has been observed and testing under various noise conditions remains to be completed.

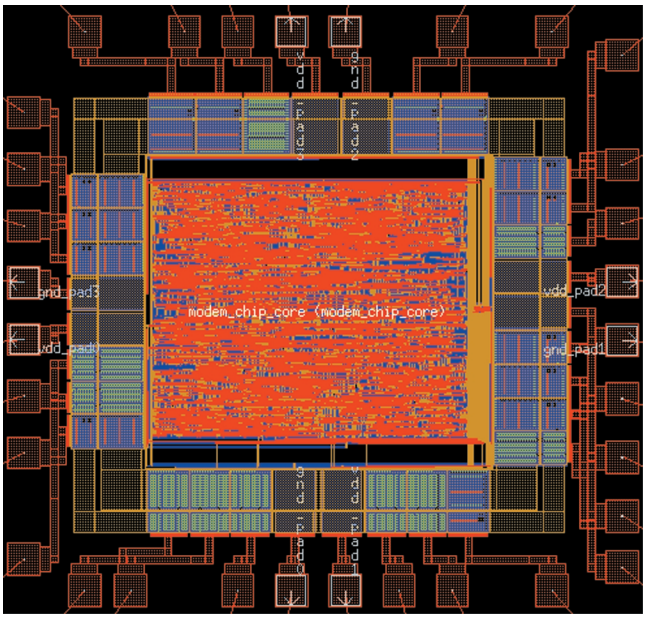

Layout of the spread spectrum modem ASIC in 0.35-µm CMOS.

* University of California Los Angeles

Wireless Microaccelerometer Sensor

C. McConaghy, S. Swierkowski, J. Trevino

National security and environmental monitoring needs exist for intelligent networks of small-sized, low-power sensors, with many sensor nodes practically possible. Wireless and MEMS (Microelectromechanical System) technologies enable us to demonstrate a prototype network module. We have developed a MEMS accelerometer with a 10-µg sensitivity in the 1 Hz to 10 Hz range. This is useful for monitoring ground signatures in national security applications as well as movement in large structures such as bridges and buildings. In addition, this sensor is easily incorporated in a wireless node because of its small size (15 mm x 15 mm x 3 mm) and low current (2 ma) drain.

We have demonstrated a small wireless sensor system module with a spread spectrum transceiver, signal processor, controller, MEMS sensor and battery in a system package of less than 2 in. x 2 in. x 1 in.

The heart of any accelerometer is the proof mass and spring combination. The resonant frequency determines the bandwidth and the sensitivity of the accelerometer. Present surface machined sensors typically have resonant frequencies above 1 kHz and a concomitant low sensitivity at low frequencies, in large part because of the small proof mass. We have built a low resonant frequency device with much greater sensitivity using bulk wafer machining for a full wafer thickness (380 µm) proof mass (16 mm^2).

The key component is the 380-µm wafer-thick silicon proof mass (see figure). Our eight very sensitive springs (tethers) were each 3 mm long by 50 µm wide by as thin as 5 µm. The device resonance was 118 Hz and the mass was capacitively detected to a precision of 0.1 nm.

This device was tested with a PZT positioning stage that applied known accelerations at low frequencies. The device sensitivity (27 µV/µg) is reasonably flat, as expected, in the target signature range. The lowest amplitude tests were limited by the electronics noise floor and at 1 Hz, a 10-µg signal was clearly visible.

The silicon part is bonded between two glass capacitor electrode plates to complete the 10-µg MEMS accelerometer sensor, which is 15 mm x 15 mm x 3 mm.

Field tests with real signature sources remain to be done. New spin-off devices with fiber optic sensing and smaller designs for defense systems testing are underway.

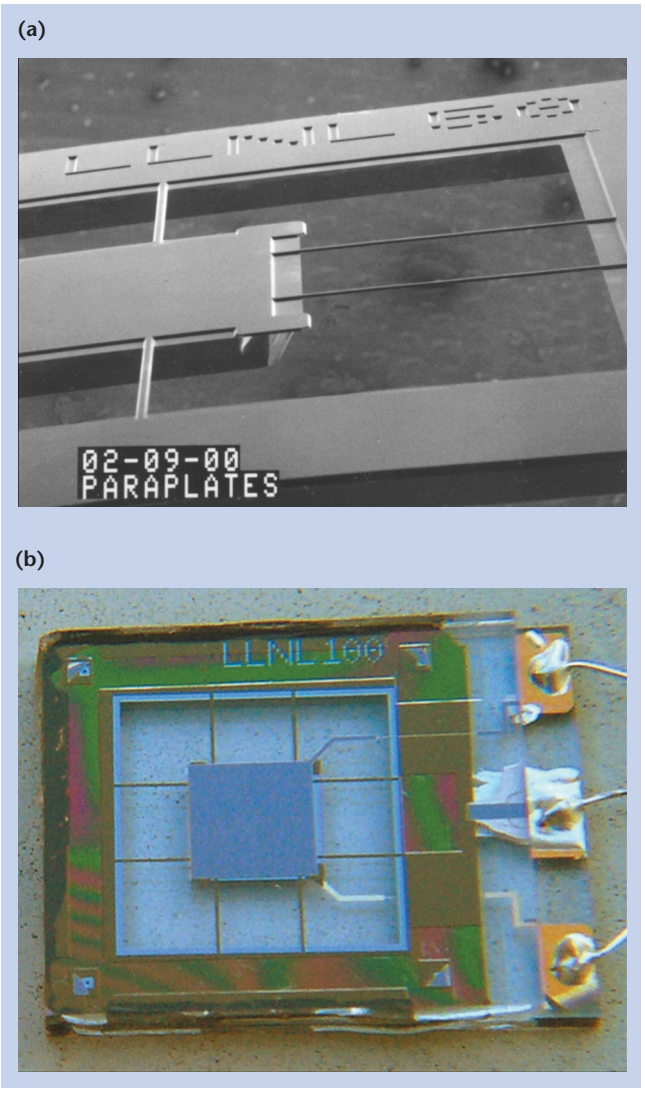

Key component of the accelerometer: 380-µm wafer-thick silicon proof mass, with 4 of the 8 tethers, shown in (a). This part is bonded between two glass capacitor electrode plates (b) to complete the 15-mm-x-15-mm-x-3mm MEMS sensor.

Sensor-Driven Estimation of Chemical, Biological and Nuclear Agent Dispersal

D. Harris

As part of our tech-base technology initiatives, a strategic initiative (SI) proposal was identified as a new opportunity for NARAC and Engineering tech-base at LLNL. The opportunity entails shifting NARAC's current operations from open-loop projection of future plume distributions to closed-loop estimation of past, present, and future plume distributions. The loop can be closed with real-time data fed back from dense networks of sensors in the theater to NARAC's models. The proposed system is an instance of a more general paradigm emerging in the physical sciences: complex numerical models for physical processes developed originally to explain experimental observations statically are embedded in real-time, sensor-driven systems that dynamically estimate parameters of interest. This paradigm represents the maturing of scientific models into operational systems.

NARAC currently has sophisticated dispersion models for predicting patterns of mean plume concentration given a source, but no systematic capability to invert for source locations and characteristics given plume observations. We proposed to develop an inversion capability by establishing the modeling, estimation, and communication framework to exploit data first from networks of pre-deployed sensors at cooperating sites, then from next-generation networks of rapidly-deployed, mobile sensors. The significance of networks of mobile sensors is that the condition of poorly constrained inverse problems may be improved by judicious placement of sensors to acquire, surround, and track an evolving plume. We envisioned a project-deploy-correct cycle, in which NARAC forecasts guide sensor placement in real time, and network data is fed back to update the models. The cycle may repeat from initial detection until final plume dilution.

The main applications of interest are: 1) treatment and protection of civilian and military populations in scenarios of chemical, biological, and radiological attack; 2) accidental industrial release of toxins; 3) accidental release of radionuclides from cooperating DOE and DoD facilities; and 4) bomb damage assessment and minimization of collateral civilian exposure in strikes against WMD facilities.

Tech-base opportunities arise in support of these applications: 1) application of basic atmospheric dispersion science to practical inverse problems; 2) advanced dispersion models that integrate empirically-derived statistics of turbulent concentration fluctuations; 3) efficient backward-time (reciprocal) and parallel implementations for these models to meet stringent real-time requirements; 4) meteorological data assimilation and wind field ensemble technology (available from collaborators); 5) an integrating statistical estimation and forecasting framework to invert agent concentration and meteorological data for source characteristics and plume concentration history; 6) adaptation of robust military communication technologies (JBREWS) to assure that field data can be communicated to NARAC under rapid-deployment conditions; and 7) integration of miniaturized, fast-response biological and chemical agent sensors under separate development into an operational forecast and inversion system.

The expected results of the proposed initiative was a set of field-validated technologies that would radically expand NARAC's operational capabilities: 1) codes to estimate rapidly source location and characteristics from real-time concentration observations; 2) codes to estimate past plume concentration and dosage in space and time; 3) codes to forecast plume concentration and dosage in an ensemble of wind fields; and 4) a communication framework for integrating these models with current and next generation theater meteorological and concentration sensors.

The success of this initiative would provide NARAC with new capabilities to retain and expand its current customer base for radiological releases, and enable LLNL to pursue new opportunities in environmental hazard mitigation, and civilian and military CBN attack scenarios.

The technologies to be developed under this initiative have natural marketing outlets through existing LLNL NAI programs.

Implementation of Inertial Sensors in Distributed Networks

C. Lee, R. R. Leach, Jr., T. Woehrle

Distributed wireless sensor networks made up of hundreds to thousands of individual sensor nodes can be deployed in locations or on structures in severe, inaccessible, remote environments. Measurements such as acceleration, gathered from these networks, can be used to collect information such as ground vehicle motion; to monitor the state/health of a structure or mechanical system; or to validate large-scale computational simulation models. A key step in creating a distributed sensor network is the selection of appropriate sensors for the given application. This project develops a test capability for evaluating accelerometer sensor packages for implementation in distributed networks.

The primary goal of this project is to evaluate acceleration sensors that will be used in distributed networks. Two requirements for sensor packages are that the overall package be as small as possible and that the sensors be sensitive enough to measure motion in a near DC-level frequency range. Consequently, capacitive-type micromachined accelerometers are chosen for their miniature size and frequency sensitivity. There is a trade-off, however, between small size and signal-to-noise ratio. Accelerometers with small inertial proof masses have trouble differentiating signals from background noise. This is especially true at low excitation frequencies.

Using an air-bearing vibration shaker table, we are evaluating a series of off-the-shelf commercial capacitive accelerometers. Their measurement sensitivities are being compared to larger, heavier seismic-sensitive accelerometers (see figure). Tests will also be performed on custom-made, lab-fabricated accelerometers. Pre-recorded ground motion vibration measurements from field tests will be input to the shaker table. Thus, we can determine how well the capacitive, micro-machined accelerometers can measure actual seismic data.

In future work, the shaker table will be used as a platform for controlled testing of algorithms for system identification and modeling updating, to validate simulation models of structural and mechanical systems. A system identification algorithm can take accelerations measurements made on a structure and estimate the physical characteristics that represent that system. These characteristics can then be compared to those predicted by a computational simulation model. A model-updating algorithm would then be used to modify the simulation model to better reflect the actual measurements.

Acceleration measurements taken on an aluminum tower fixed to the shaker table (see figure) will be used to study system identification and finite element model updating techniques. Furthermore, the tower can be modified by removing reinforcement struts to mimic localized damage. The system identification procedure will then be used to specify the location of the damage.

(a)

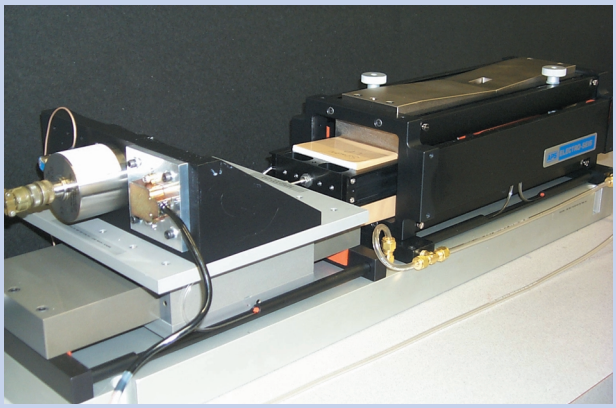

(b)

Experimental setups for (a) sensitivity measurements, and (b) finite element model updating algorithms.

Microtechnology and Microdevices

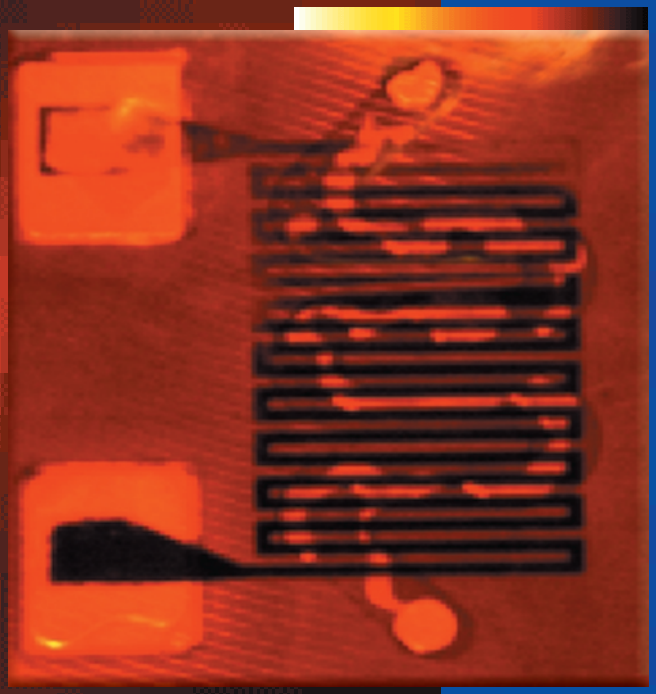

6

Thermomechanical Characterization of Nickel-Titanium-Copper Shape Memory Alloy Films

K. P. Seward, P. B. Ramsey, P. Krulevitch

We have developed a novel characterization method for modeling the thermomechanical behavior of shape memory alloy (SMA) films. This automated test has been tailored to characterize films for use in microelectromechanical system (MEMS) actuators. The shape memory effect in NiTiCu is seen in the solid-state phase transformation from an easily deformable low-temperature (martensite) state to a "shape remembering" high-temperature (austenite) state. The accurate determination of engineering properties for these films necessitates measurements of both stress and strain in microfabricated test structures over the full range of desired deformation.

SMA films are an attractive solution in MEMS systems because they provide the highest work output per unit volume of any microactuator alternatives. Our results move us one step closer to a comprehensive SMA characterization tool to allow effective and optimal design of MEMS that take full advantage of actuation properties.

Our testing method provides data based on the resistive heating of the films rather than ambient heating; thus, constant current conditions are imposed on the films in a room temperature environment. Varying the strain and measuring the stress on the films under these conditions allows the plotting of characteristic curves and the derivation of constitutive relations for use in the design of new actuators.

Because SMA films behave differently than bulk materials and vary in mechanical properties with distinct fabrication methods, a simple technique to provide all necessary mechanical data is beneficial. The automated test we have developed is non-destructive, and provides a comprehensive range of thermomechanical and electromechanical information with simultaneous determination of stress-strain behavior and material resistivity of both phases, recoverable stress and strain against a load, actuation fatigue behavior, response and cycling times, and power requirements for actuation of fixed-fixed NiTiCu ribbons.

The figure shows a photograph of a test chip: a NiTiCu ribbon with two 2-mm gauge sections is suspended by a Si frame and electrical contact pads are patterned to allow resistive heating. Unlike traditional mini-tensile testing schemes in which strips of SMA film are totally or partially freed from the substrate and then strained, our tests use out-of-plane stretching without detachment from the substrate. Freestanding fixed-fixed NiTiCu ribbons were patterned on the same wafer as 1-cm-square unpatterned (blank) chips used in curvature measurements, and test chips with a blank pattern and a window etched beneath in the Si, forming a NiTiCu membrane for use in pressurized diaphragm measurements.

We have generated a mathematical model and characterization data for uniaxial tensile tests, bimorph curvature tests, and diaphragm bulge tests. With this comprehensive testing, the design of SMA microactuators is greatly simplified. Accurate material property measurements enable design by the simple determination of the characteristic equations for the device in question and correlation of those equations with the stress-strain curves found by testing ligaments with the same composition and fabrication methods. With the stress-strain curves from these tests, analytic solutions to the design problems associated with SMA films are ascertained.

An instrument like this can be used in-line for device qualification, to allow for quality control during a MEMS manufacturing process by checking one or several devices per wafer for forces, deflections, power requirements, and calibration errors all at the same time and in just a few seconds.

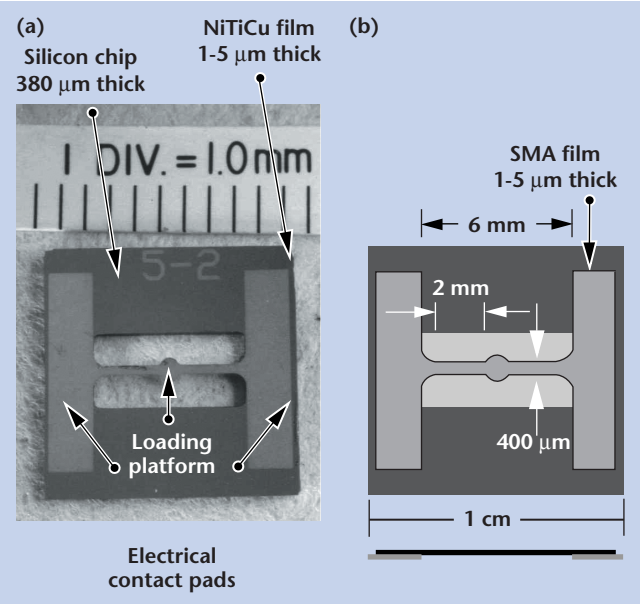

Photograph of test chip (a), with detail (b).

Micro-Bellows and Related Structures

A. F. Bernhardt

A bellows provides flexible separation between interior and exterior volumes. It is like a flexible membrane but with much higher displacement and much greater latitude in material composition. Bellows are available as components on the macroscale level but not on the microscale level and certainly not fabricated *in situ*. In some actuator applications, arrays of micro-bellows are needed and *in-situ* fabrication is advantageous or, perhaps, essential.

We have designed a process for fabricating a bellows *using a single lithography step*. This is possible because of our unique capability of depositing and exposing photoresist on 3-D surfaces. Our laser exposure tool permits exposure of the rings on the inside of a cylindrical hole, provided the diameter of the hole is bigger than its depth. Fabrication issues include control of the curvature and depth of the folds of the bellows to prevent weak spots. Depending on the application, a variety of displacements, sizes, spring constants, wall strengths and materials may be desirable.

The basic fabrication strategy was validated. We fabricated a nickel micro-bellows in holes in a copper sheet. The sheet was masked with electroplated photoresist and nickel was electroplated onto the sides of the hole and onto the top of the sheet. The copper was then etched selectively in basic copper chloride solution, leaving the nickel attached to the sheet only at the top.

The application of the micro-bellows to a micro-internal-combustion generator has been explored and deemed unworkable due to unfavorable heat transfer scaling which reduces engine efficiency.

Remote Hydrogen Sensor

D. R. Ciarlo

Preliminary results have demonstrated the feasibility of a novel remote hydrogen sensor. The sensor makes use of a bi-morph structure consisting of a 1.4-µm-thick palladium film on a 200-µm-thick strip of glass. In the presence of hydrogen, a stress is chemically induced in the palladium film, causing the glass to bend. This bending is measured remotely, with either optics or radiography.

The remote detection of hydrogen generated inside a closed container is an important problem in scientific, industrial, and military apparatus. Hydrogen is a by-product of the deterioration of organic components and it needs to be detected at levels of a few ppm and above. This problem can be readily solved if a tube can be inserted to periodically extract gas for analysis. However, such openings are not always permitted.

The hydrogen sensor under development in this proposal can detect hydrogen inside a closed container without physical access or, at worst, with the use of non-electrical fiber optics.

The operating principle for this sensor relies on the behavior of a bi-morph structure. One element of the bi-morph reacts with hydrogen, while the other element does not. The reaction causes a chemically-induced strain, which bows the bi-morph structure, similar to the behavior of a temperature-activated bi-morph. The sensitivity of the sensor is determined by the selection of materials and by the size and shape of the elements. We used palladium for the reactive component since palladium is known to readily absorb hydrogen to form palladium hydride.

One way to remotely read out this sensor is to use radiography. The resolution of radiography in a high contrast environment is 10 to 20 µm. If the contrast is low, as it would be when looking through other material, the resolution is only 75 to 100 µm. This resolution can be improved by using high-contrast beads and/or by using a set of bi-morphs, attached at their ends so that gaps are measured.

During FY00 we performed experiments to test the feasibility of this sensor on bi-morphs shown in the figure. We used type 0211 borosilicate glass for the unreactive element of the bi-morph. This glass was 200 µm thick, 0.5 cm wide, and 4 cm long. For the reactive metal we used 1.4-µm-thick palladium films. Following the deposition, the palladium film was clearly in a state of tensile stress, as seen from the direction of bow in the glass substrate. The radius of curvature for the bow was 0.85 m, as measured with a laser scanner. The bi-morph was then placed in a 4% hydrogen-in-nitrogen atmosphere at room temperature for one hour. Following this treatment the film was clearly in a state of compressive stress, as determined from the direction of bow in the glass substrate. The radius of curvature of the glass substrate was 1.18 m.

The stress in a thin film on a much thicker substrate can be calculated from:

$$\sigma = \left(\frac{1}{6RT}\right)\frac{EH^2}{(1-\nu)}$$

where σ = stress in the thin film (MPa); n = Poisson's ratio for glass, 0.17; E = Young's Modulus for glass, 50 x 10^3 MPa; H = substrate thickness (m); R = radius of curvature; and T = film thickness.

The calculated tensile stress in the palladium film after deposition was 337 MPa, tensile. Following the one-hour treatment in 4% hydrogen, the stress in the palladium film was 243 MPa, compressive. The center of the glass strip before and after hydrogen treatment moved a total of 370 µm.

The above experiments demonstrate the feasibility of this remote hydrogen sensor. Further experiments are needed to optimize the shape of the sensor and to calibrate its response.

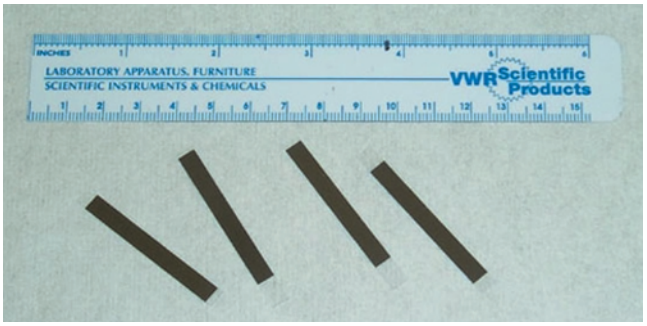

Palladium-glass bi-morph strips for the measurement of hydrogen.

Microfabricated Deformable Mirrors for Adaptive Optics Applications

J. A. Folta, J. Yu, S. S. Olivier, P. Krulevitch, W. D. Cowan

Adaptive optics (AO) technology is critical for many current and developing applications at LLNL. In particular, most large laser systems, including those being developed for Inertial Confinement Fusion and Laser Isotope Separation, require AO to correct for internal aberrations. In addition, AO can provide capability for both high-resolution imaging and beam propagation through the atmosphere. Requirements for laser systems, imaging and propagation applications are currently driving wavefront control technology toward increased spatial and temporal frequency capacity, as well as reduced system costs.

Using microelectromechanical systems (MEMS) fabrication techniques, the cost of AO can be reduced by a factor of 1000 from that of standard deformable mirror (DM) technology. Proper design and coating of the MEM DM arrays extend the operation of these devices to high average and peak power conditions. Taken together, the advantages of MEM DM technology have the potential to revolutionize the field of adaptive optics.

In FY99, we designed a high-stroke actuator. MEM DMs based on this actuator can offer vertical strokes up to tens of microns with kHz response time. In FY00 we developed an approach to improve the mirror surface quality and optical fill-factor of existing MEM DM prototypes.

The two most critical issues limiting the application of current prototype MEM DMs are surface quality (flatness), and fill factor. *There are currently no available devices that meet minimum requirements for LLNL AO applications.* The target surface figure for our transferred mirror arrays is 50 nm peak-to-valley curvature across 200-μm-square mirror pixels. Our goal is to accelerate MEM DM development in collaboration with external groups to produce a working device for evaluation in the LLNL advanced AO test-bed. The most advanced devices in terms of quality, reliability and availability are from the Air Force Research Laboratory (AFRL). A typical device is a 12-x-12 array of micro-actuators with a 203-µm period, providing up to 0.7 µm vertical stroke.

We developed a method to improve surface quality by performing post-processing on AFRL devices by adding a flat mirror surface to the actuator array. For bonding we use an Au-to-Au compression technique developed at UC Berkeley.

A multilayer stack serves as our mirror surface. Experimental data show we can accurately tune the stress of this multilayer during and post deposition, allowing us to precisely control the mirror flatness. Fabrication challenges included electroplating uniform arrays of high-aspect ratio Au bumps for the bonding process. We deposited a uniform array of 11-μm tall Au bumps, electroplated onto a continuous 1.38-μm-thick mirror surface. We then developed a photolithographic patterning and etch process to pixelate the mirror surface, resulting in a 12-x-12 mirror array with a 94% fill factor. We then successfully bonded the mirrors to Au-coated Si wafers. Pull tests performed on the bonded mirrors yielded bond tensile strength on the order of 100 MPa. The bond also endured greater than 6 h of hydrofluoric acid release bath without failure. We are currently working on the release process.

Our Au-to-Au compression bonding technique shows great promise for transferring high-quality, flat, mirror structures to foundry-fabricated arrays of micro-actuators. Such devices will find broad application for compact, inexpensive AO systems.

High Voltage Photovoltaic Arrays

G. Cooper, J. D. Morse

The objective of this project was to take the high-voltage isolation technique developed in FY99 and apply it to a full high-voltage photovoltaic series array of diodes and demonstrate monolithic integration of such an array up to 1200 V. Another important guiding principle is to keep the process compatible with commercial processes as much as possible.

The primary difference between the photovoltaic device and the other devices with which we had experience was the extreme topography on the wafer surface that was required to electrically isolate the diodes from each other (Fig. 1). Compensating for the deep topography has been driving most of the effort this year.

As can be seen in Fig. 2, the profile of the trench sidewall is not flat. Portions of the epitaxial structure protrude from the wall, a result of differences in solubility of the various epitaxial layers in the wet etching solutions used to etch the trench. The protrusions make coverage of the wall with a continuous film of metal very difficult. Our standard process for depositing and patterning metal films on GaAs devices, the lift-off technique did not work in this case.

Two other techniques warranted further exploration: electroplated metal and sputtered metal. We explored the techniques in parallel until it became clear that electroplated metal would require much more development than sputtering, and we were making good progress on the sputter technique. The sputter technique blankets the entire wafer with the metal layers. Places where the metal is not supposed to be in contact with the GaAs are covered with a SiO_2 layer prior to metal deposition. The deposited metal film is patterned by applying a protective, photo-patterned polymer and then chemically etching the metal away in the exposed areas. Much effort was spent on the deposition and patterning of the protective polymer, extreme topography once again causing difficulties. We adapted an electroplated photoresist process to our process and have been using it to pattern interconnect metal on real device structures.

We then uncovered a problem with the effectiveness of the electrical barrier layer, involving current injection and transport in our semi-insulating GaAs substrates. Because of the layout of the photovoltaic array, the maximum voltage difference between any two adjacent structures was 200 V, the limit to which we had tested our isolation layers. However, it was possible for current to be injected into the substrate from more remote structures at higher voltages. We were able to fill in this void in our experimental data and resolved the leakage current question to our satisfaction.

The existing design is probably not the most efficient in terms of converting light into electrons. We plan to investigate the limits of array designs to achieve maximum compactness without sacrificing functionality. It is hoped that this process will eventually be transferred to a commercial manufacturer to supply the needs of the DoD and DOE communities.

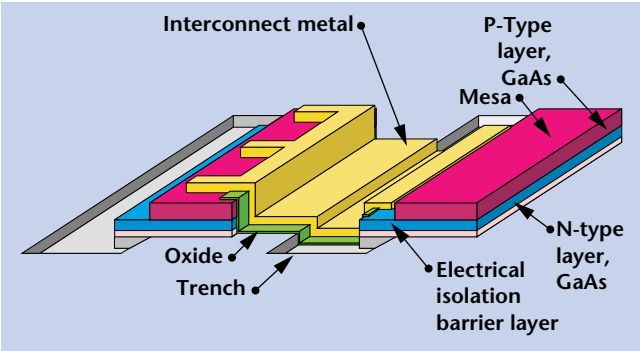

Figure 1. Idealized structure of photodiodes and the interconnect between them.

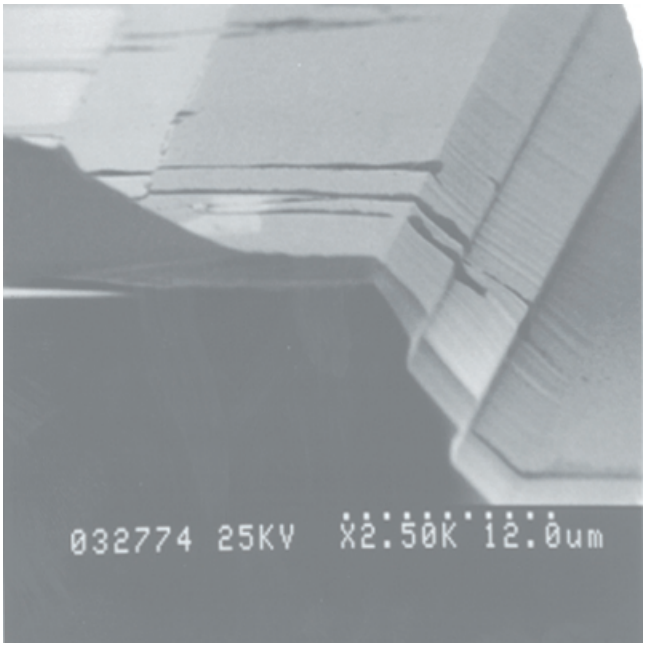

Figure 2. Scanning electron micrograph of trench sidewall.

Chambered Capsule Coatings

A. F. Jankowski, J. P. Hayes, J. D. Morse

The sputter-deposition of coatings onto polymer capsules is accomplished using a chambered substrate platform as opposed to a conventional, open bounce pan configuration. Metals are sputter-deposited through an aperture onto a 1- to 2-mm diameter hollow polymer sphere within a chamber that is two to three times the size of the capsule diameter. The uniformity of the coating thickness can depend upon the method by which the capsules are moved within each chamber. Two methods are assessed to produce a random bounce of the capsules within each chamber, the first by ultrasonic vibration and the second by pulsed-gas levitation.

The fabrication of targets for inertial confinement fusion can require the production of ablative coatings that are deposited on a mandrel, usually consisting of a thin-walled polymer shell. In typical deposition processes, the coating is applied as the capsule, *i.e.*, the substrate mandrel, bounces in a pan. Difficulties arise with capsule motion, often producing clusters, null modes, or runaway modes.

Our method represents a significant improvement in controlling capsule motion, providing both an improved sample yield and greater uniformity of samples as qualified by surface finish.

In our approach, each capsule is individually chambered within a volume about two to three times the size of the mandrel diameter. The capsules are coated by sputter deposition through an aperture into the chamber. The capsules are polymer shells 1 to 2 mm in diameter and 10 to 15 μm thick, composed of a polyimid or polystyrene of a density 2.0 g/cm^{3}. The sputter deposition process uses a coating system that features an array of planar magnetron sources, each with a 3.3-cm-diameter target. Up to 1 kWh of coating is applied to the capsules in some instances. For a 150-μm-thick coating, the total weight increases to 1.3 to 4.6 mg per coated capsule.

The substrates can be configured in two ways, each providing random motion of a capsule within its own chamber. The ultrasonic vibration configuration uses a piezoelectric driven at high frequency to create a surface wave in the base plate that moves up and down to displace the capsule. An Al coating is applied to 1-mm-diameter capsules. In pulsed-gas levitation, the capsule is displaced by oscillating a partial flow of the working gas directly beneath the capsule. The diameter of the pulsed-gas inlet tube is 70 to 80% of the capsule diameter. A Ni coating is applied to 2-mm-diameter capsules. In each case, the capsule chamber is cube shaped with a lateral dimension 30 to 40% larger than the capsule diameter.

The capsule coatings are characterized for continuity, uniformity, thickness, and morphology using both methods. The coated capsules are fractured for evaluation in cross-section.

We have demonstrated that uniform coatings can be produced using a chambered substrate platform. Potential advantages of the chambered approach versus an open-pan configuration include improved sample yield, accommodation of varying sample size, and reduced surface roughness. For applications that involve the deposition of toxic materials, the chambered approach minimizes the generation of an aqueous toxic waste stream.

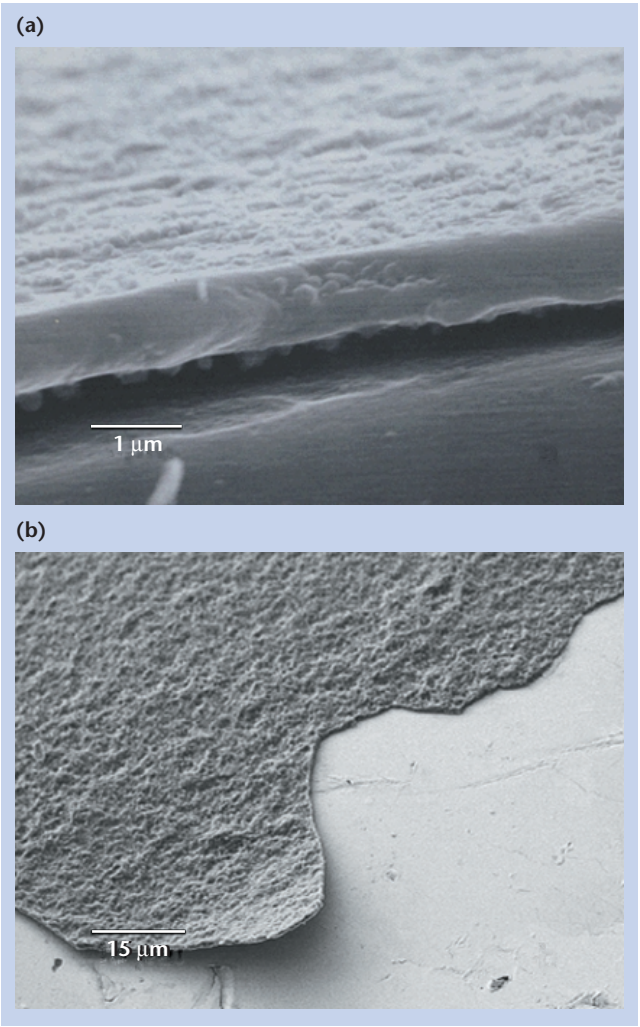

Scanning electron micrographs of a cross-sectioned (a) Al-coated, 1-mm-diameter capsule, and (b) Ni-coated, 2-mm-diameter capsule.

Highly Parallel Microfabricated Biochemical Microliter-Scale Processor

R. Miles, K. Bettencourt, S. Nasarabadi, J. Hamilton

Biological terrorism is a threat to the security of the United States. New tools are needed to detect and analyze the environment surrounding the suspected release of biological pathogens. Typical tests for biological particles can take hours to perform in laboratory conditions; tests needed to determine the type and extent of an attack must be re-engineered to take only minutes in field conditions.

Sample preparation is the most time-intensive and costly part of conducting biological tests. The objective of this work is to reduce these costs through the development of automated integrated sample preparation and performance of the assay.

The polymerase chain reaction (PCR) assay was used as the test vehicle for this work. PCR assays are used to identify specific parts of the DNA molecule that are unique to a given organism. Pathogens such as anthrax or plague can be identified using PCR. The steps required to process the sample for PCR include fractionation of the biological particle of interest from the rest of the fluid in which it is suspended, lysing of the organism, separation of the DNA from other cellular material, mixing the DNA with the PCR reagents, and PCR amplification.

The apparatus shown in Fig. 1 illustrates the initial device used to demonstrate the PCR sample preparation and amplification functions. The device consists of electrodes patterned on a glass wafer. A thin sheet of wax is used to define the channels and act as a spacer between the top and bottom glass wafers. All pumps and valves are external to the device. Using this configuration, many plates can be stacked to permit highly parallel testing where many assays are conducted simultaneously. The channels can be small, which allows for use of small aliquots of expensive reagents.

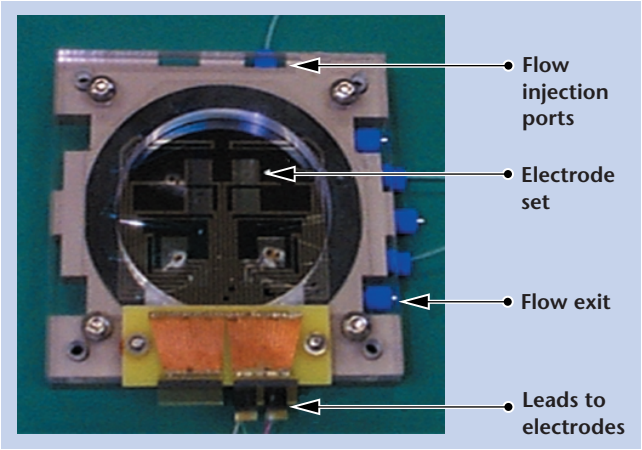

Figure 1. Device for performing PCR sample preparation and amplification.

Dielectrophoretic (DEP) trapping is used to selectively trap species of interest. DEP trapping is achieved when a nonlinear electric field gradient is generated using the electrodes patterned on the glass. An electric dipole is generated within the particle which then moves toward the areas of high field gradient near the channel walls. Selective trapping of DNA, *Erwinia herbicola (E.h.), Bacillus globigii (B.g.)*, and polystyrene beads has been observed. By trapping particles such as *E.h.*, a model for plague, and *B.g.*, a model for anthrax, larger quantities of sample can be concentrated, thus increasing the overall sensitivity of the assay.

A captured sample of *E.h.* was lysed by introducing lysing solution into the channel. The DNA was captured on a set of electrodes downstream using the DEP force. Reagent was introduced. Thin film electric heaters patterned on the glass were used to heat and cool the DNA to achieve amplification.

Further work was done to replace the glass/wax structure with a structure comprised of thin layers of polyimide such that the cost of the device would be low enough to consider it disposable. Such a heater/channel device is shown in Fig. 2. This is particularly useful to avoid sample-to-sample contamination or to deal with long-term fouling of the device.

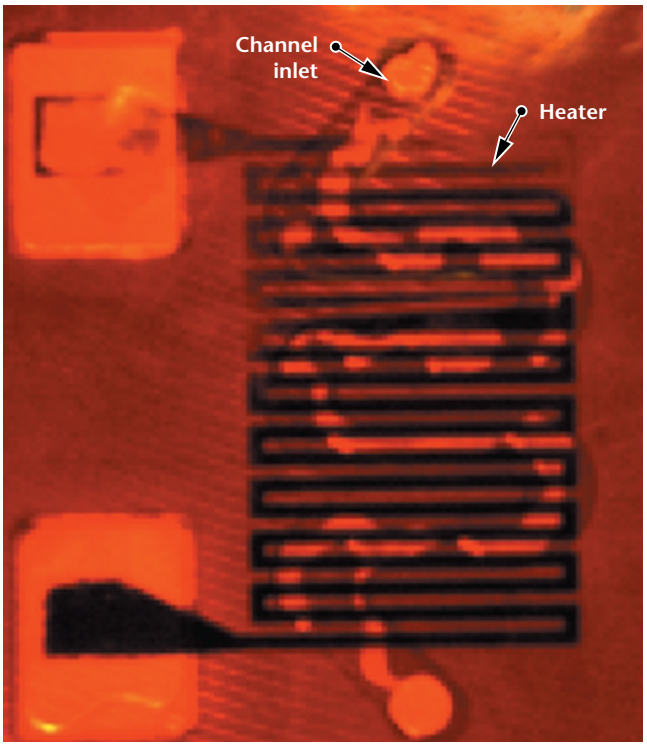

Figure 2. Polyimide PCR amplification chamber.

Nondestructive Characterization

Sonic IR for Nondestructive Evaluation

W. O. Miller

LLNL has supported reduction-to-practice methods of nondestructive evaluation (NDE). Infrared methods have been part of that effort for many years, primarily using flash heating and passive imaging. Sonic IR shows promise as a new IR NDE technique that can detect flaws, such as tightly closed cracks, that are difficult to detect with other methods. We have evaluated Sonic IR on several materials and flaw types, and the results are presented here for aluminum oxide, carbon composites, glass, and steel.

Sonic IR works by dynamically exciting the part being tested with an acoustic probe in physical contact with the part. Resulting differential motion across a crack face creates heat by friction, and a traditional IR camera images the temperature rise at the crack. The LLNL tests were done with a rented ThermoSoniX system from Indigo Systems Corp. (Fig. 1).

We found that the method and equipment used for this study were effective in most circumstances but not in others. Some tests showed excellent indications of damage, while other tests failed to show any damage where damage was known. Several parts shattered during testing. The response was found to be modestly sensitive to the contact location of the acoustic probe and also sensitive to the type of support used for the test objects in one case.

The main effort was to see if Sonic IR could detect small cracks in aluminum oxide, a dense, stiff ceramic. Three types of aluminum oxide coupons with flaws were made. Notched beam and Vickers-indented coupons produced detectable thermal images. The inability to detect flaws in surface ground coupons may be due to both inadequate spatial and temporal resolution of the IR system, and a poor match of input forcing between the acoustic probe and the aluminum oxide parts. Additional effort to resolve this is underway.

Tests were made on carbon composite tensile specimens that had been fatigued to failure. The Sonic IR images of the damage areas were clear, and in excellent agreement with ultrasonic images. The contact location of the acoustic probe was found to have a modest effect on the image quality.

Tests were made on a large carbon composite tile that had been improperly fabricated. The thermal images were found to vary markedly with the support method (Fig. 2).

Tests on a slab of laser glass that had spallation pits from laser-induced damage showed weak thermal images at the spall sites, where the glass had fractured. Tests on heavy steel plates showed thermal images at the impact zones.

A thorough knowledge of this method will require understanding how the energy transfer from probe to part to support takes place, and how the part dynamically responds, particularly the response at the flaw.

The equations governing Sonic IR suggest that the forced dynamic response of the part being excited depends on both the input forcing, and the natural response of the system. The results of this study suggest that changes to these parameters will make a significant impact on the production of a thermal signature. Certainly the input frequency has an effect on the response. It would be interesting to consider broadband input or a frequency sweep input to obtain a wider range of response.

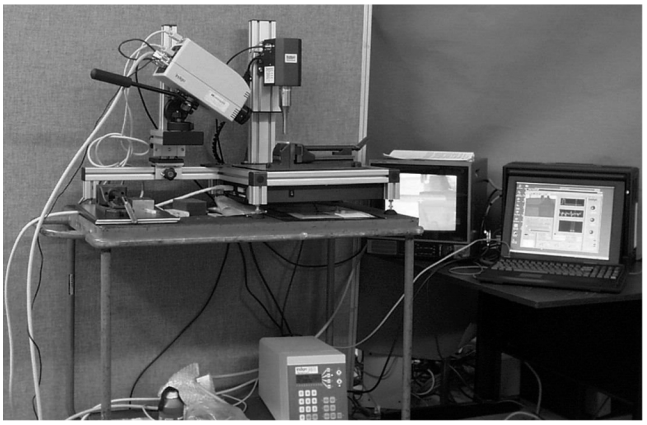

Figure 1. Photograph of the ThermoSoniX system showing IR camera, acoustic probe, test stand, PC, and monitor.

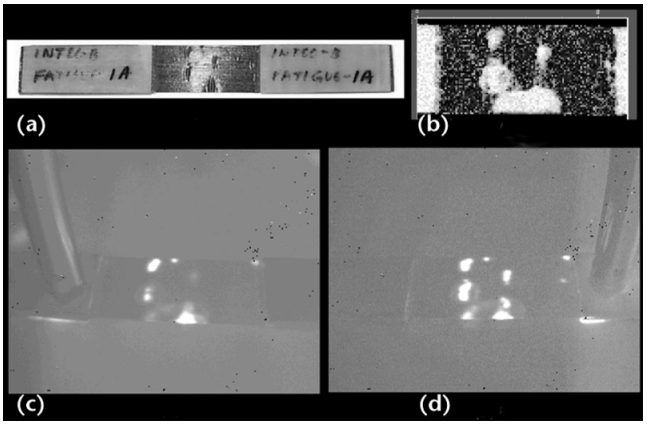

Figure 2. Sample test results for carbon composite tensile specimen: (a) photograph of specimen; (b) ultrasonic image of damage; (c) Sonic IR image, probe at left grip; (d) Sonic IR image, probe at right grip.

Superresolution of Buried Objects in Layered Media by Near-Field Electromagnetic Imaging

S. K. Lehman, D. Chambers

Tomographic imaging is a collection of techniques to reconstruct images of the unknown internal structure of an object from fields transmitted through and/or reflected from it. In non-invasive wave probing of layered media in near-field conditions, few outside of optical microscopists have taken advantage of the evanescent part of the scattered field to enhance resolution. We have developed an imaging technique to be used in near-field environments that achieves resolution beyond the diffraction limit, or equivalently "superresolution," by including the evanescent part of the field backscattered from buried objects.

In this work we dealt principally with diffraction tomography to determine non-invasively the location and nature of objects buried in a layered medium within the near-field of the radiation (see figure). The advantage of the diffraction tomography method is that the inverse to the forward problem is easier to solve and implement than in the full-wave method. The disadvantage is that the simple scattering approximation limits its range of applications.

We performed an extensive study on forward scattering and showed it consists of a two-step process: a convolution in the spectral domain between the scattering object and the total field, followed by a propagation away from the source. The convolution results in the conversion of evanescent field information into propagating fields. Through a small example using two point scatterers, we showed improved resolution when evanescent field information is incorporated into the reconstruction.

We performed finite-difference time-domain simulations of two phantoms: two 1.5-cm-diameter poles separated by 10 cm, and an eight-pole phantom with varying separations. We also collected real wide-band microwave data on two aluminum poles separated by 10 cm, and on a buried aluminum resolution phantom.

We reconstructed the simulated and real data using both our new extended resolution algorithm and a classical low-pass algorithm. We developed contrast and resolution figures of merit to compare the two reconstructions, and demonstrated that our algorithm achieves higher resolution and improved contrast over the classical method, even in cases where the forward scattering model (that is, the Born approximation) is not valid.

Our inversion algorithm is based on a generalized Fourier transform which allows for complex frequency variables. Future work must include a formalization of this transform and the development of a closure relation.

The reconstruction algorithm makes use of a wavenumber cutoff based on an estimate of when signal information falls below the noise floor within the evanescent region. Techniques can be developed that choose this wavenumber cutoff automatically.

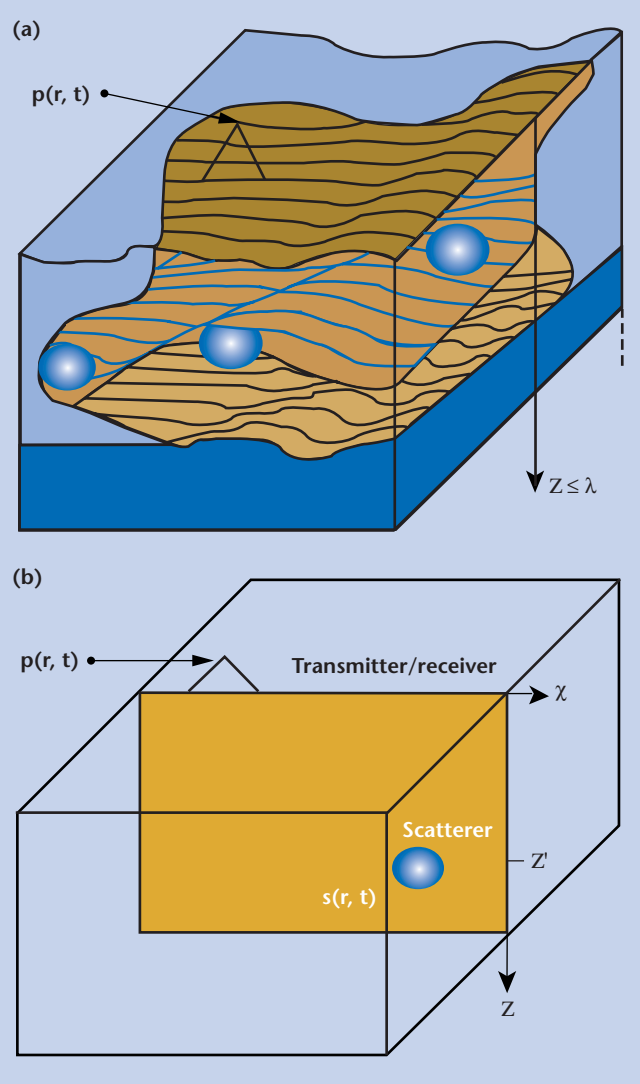

(a) Problem scenario: to determine non-invasively the location and nature of objects buried in a layered medium and residing within the near-field of the radiation. (b) Two-dimensional simplification: a scattering object is buried in medium. A transmitter/receiver launches a pulse, p, into the medium and records the echo from the scatterer.

Development of True-3D

G. P. Roberson, R. L. Perry, E. P. Goodwin

Imaging requirements in nondestructive evaluation (NDE) have become more demanding in recent years. Advances in NDE detector systems are yielding larger and more revealing data sets and the computers that process this data are less expensive and far more powerful. These factors are opening the door for new and more complicated algorithms, and place our existing algorithms in a constant state of change. In the past, it was necessary to develop our own image-processing algorithms, including the most basic components. However, today there are commercial products that provide a development program that includes fundamental tools for image processing coupled with tools for developing graphical user interfaces (GUI). We are using such a package to develop a new image-processing program called True-3D.

True-3D was developed to simplify volume image processing, providing a GUI for simple parameter entry and, where possible, interactive tools with immediate graphical feedback for process optimization. The program is a series of interface windows where the first level is a foundation containing common image-processing tools such as file readers and converters, filters, color-table manipulators, and various types of viewers. Specific and complex image-processing algorithms can be linked to the first interface level and may contain as many interface windows as necessary to perform the parameter setup. We have developed the True-3D foundation and incorporated interfaces for three complex algorithms including image reconstruction, segmentation/extraction, and volume rendering.

True-3D was developed using a rapid-prototyping language called Interactive Data Language (IDL). IDL is an array-oriented language with numerous mathematical analysis and graphical display capabilities. True-3D includes a GUI with typical functions such as pull down menus, sliders, buttons and many other interactive interfaces. In some cases, the interactive interface is linked to a display window that allows the operator to adjust a parameter and observe the results for optimization.

We have incorporated three complex algorithms in True-3D that contain a portion of code written in the C language and "wrapped" within an IDL application. We use IDL to develop the GUI that sets up and calls the external C portion of the algorithm. The computational-intensive portion of the algorithm is written in C and runs much faster than it would if implemented in IDL alone.

In the coming year, we intend to distribute the C portion of the code on a clustered computer system for parallel computation. It would be very expensive to distribute an IDL application over a large cluster. In this scenario, IDL would operate on only one computer, the controller, and the C portion of the algorithm would be distributed over the cluster.

The figure shows an example of the two GUI windows within True-3D used to set up the rendering algorithm, based on Cell-Tracer, a program developed at LLNL. There are several windows that are not shown that are accessed prior to this point and used for retrieving, filtering, and understanding the data. The two windows shown in the figure are used to set up parameters such as the location of the eye and light source, background color, and interactive adjustment of transfer functions for color and opacity. The result of the transfer function adjustment on the data is observed in the GUI window prior to rendering. The program creates a set of rendered images, each representing a frame of a movie at different angles around the volume data set.

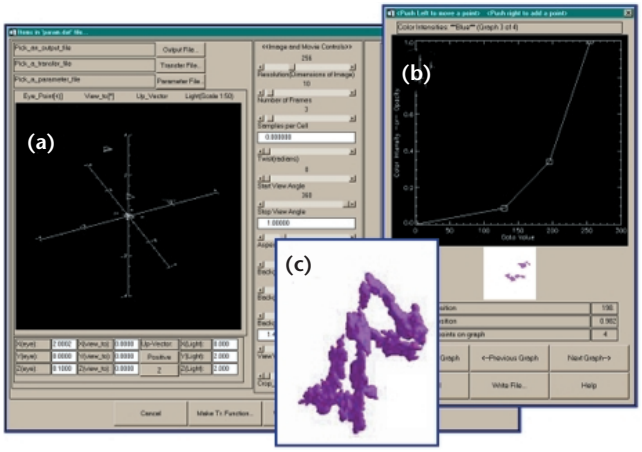

True-3D GUI used to set up the rendering algorithm: (a) interface for adjusting parameters associated with the eye and light positions, background color, number of rendered frames to generate, size of each frame, and others; (b) interface used to interactively adjust the color and opacity transfer functions; and (c) a single frame of the rendered results.

Rapid, High-Resolution Ultrasound Tomography

J. Kallman, E. Ashby, D. R. Ciarlo, G. Thomas

Transmission ultrasound imaging at LLNL is performed by passing ultrasound through an object of interest and mechanically scanning a point sensor to determine the sound field transmitted. This process is slow, typically taking 20 min per acquired field. We have produced a sensor that acquires the acoustic field over the 2-D sensor aperture in 20 s. This, and anticipated further increases in speed make feasible new uses for transmission ultrasound in nondestructive evaluation and medical imaging. This sensor technology will make possible near real time inspection of parts as they come off assembly lines, as well as rapid transmission ultrasound tomography for breast cancer screening. Laboratory uses for this technology include rapid inspection of composites and ceramics, both of which are absorbing materials, and thus present difficulties for reflection ultrasound.

The objective of this project is to speed the acquisition of transmission ultrasound data for tomography through the use of a new kind of acoustic sensor. The Optically Parallel Ultrasound Sensor (OPUS) images an acoustic pressure wave over an entire surface by converting sound pressure into an optical modulation.

The key to this conversion is evanescent field coupling. When light encounters the interface between a slow medium (high index of refraction) and a fast one (lower index of refraction), light is both reflected and transmitted. The transmitted light is refracted according to Snell's Law: $n_1\sin(\theta_1) = n_2\sin(\theta_2)$, where n_1 and n_2 are the slow and fast media indexes respectively, θ_1 is the angle of incidence, and θ_2 is the angle of refraction. As θ_1 approaches the critical angle θ_c (where $n_1\sin(\theta_c)/n_2 = 1$), θ_2 approaches 90°, and the light that is transmitted decreases.

Beyond the critical angle, all the light is reflected (total internal reflection (TIR)). There is, however, an evanescent field that extends beyond the slow medium and into the fast one. If another piece of slow medium intercepts this field, some of the light tunnels across the gap and is transmitted, with a corresponding decrease in the reflection from the original TIR interface. The amount of light transmitted is sensitively dependent on the gap size (by the time the gap is approximately 1 wavelength, the evanescent field has dropped to almost zero).

We exploit this phenomenon by suspending a flexible membrane over the TIR surface and exposing the opposite surface of the membrane to an acoustic medium. An acoustic wave hitting the membrane will cause it to deflect, changing the gap between the membrane and the TIR surface, and causing a change in the reflection. By illuminating the TIR surface with a strobe light and observing it with a video camera, we can observe and record the membrane deflections.

LLNL's computational modeling expertise was used to design both the optical and mechanical aspects of OPUS, and its microfabrication capabilities were crucial to the generation of the membrane and its supports.

In FY00 we built robust, low tension membranes that produced sensors that can survive indefinitely. We upgraded our camera to speed data acquisition by a factor of 100. We acquired multiple views of a 2.5-D phantom and performed diffraction tomographic reconstructions using these data.

In FY01 we plan to increase the size of the sensor aperture, increase the signal to noise ratio of the data acquisition, and do tomographic imaging of larger objects.

A patent for this technology was issued in FY00.

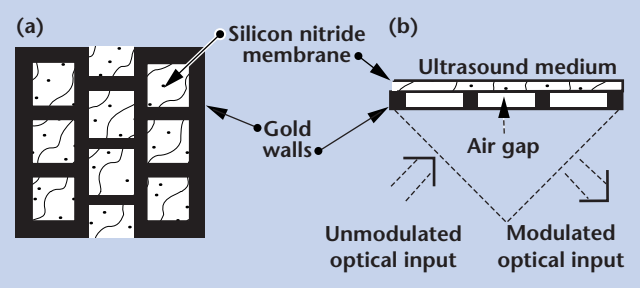

(a) Top and (b) side views of the optically parallel ultrasound sensor. The silicon nitride membrane is 100 nm thick and stands on gold walls 200 nm high.

Aircraft Buried Wiring Inspection

K. Dolan, R. Druce, P. Durbin, M. Hoffman, T. Rosenbury

Feasibility studies were conducted to determine the applicability of LLNL-developed nondestructive evaluation and electrical characterization methods to the problems of aging wiring in aircraft.

Aging aircraft wiring may fail without warning. Diagnostics are needed both as a part of repair troubleshooting to identify and locate failed wires and connectors, and as preventative maintenance to detect system anomalies that may become failures. In addition, a fundamental understanding is needed of insulation and connector aging and wear. An effort was made to match LLNL technologies to this problem and to perform preliminary investigations of wire harness sets provided by commercial aviation.

Micropower Impulse Radar (MIR) was identified as a wideband fault detector that could operate on both powered and unpowered aircraft cables and circuits. MIR technology is based on emission and detection of very low-amplitude and short-voltage impulses, and has high sensitivity for accurate detection of reflections from boundaries between different materials. The operator could measure wire breaks and disconnects, and detect problems with dielectric insulation and shield integrity, *e.g.*, abrasions and breaks. MIR offers advantages over currently used time domain reflectivity that include: 1) lower power input; 2) higher sensitivity; 3) diagnostics without breaking circuit connections (*e.g.*, as a built-in diagnostic tool); and 4) accurate fault location by use of an auxiliary "sniffer". These methods were demonstrated on cables provided by the aviation industry (see figure).

Partial Discharge Analysis is a nondestructive technique for diagnosing wire and cable insulation. A feasibility study used electromagnetic field modeling to estimate the wave impedance of wire bundles going through enclosures of various sizes, providing information useful for circuit modeling. The advantages of this method are that it is sensitive to changes in the insulation, and provides a unique signature of the wiring system.

Pulsed Thermal Inertia (PTI) infrared imaging is a sensitive method for imaging time-resolved temperature changes by measuring resistance of materials to temperature change. PTI was used on cable bundles with pulsed thermal sources to image hidden damage in cable terminations. This technique is probably not applicable since it is difficult to interpret and access is needed to the wire or connector.

Aging Wiring Studies was proposed as future work to address insulation integrity in aged wiring by characterizing both new and used samples of insulation for flaws, change of stabilizer or molecular weight, presence of contaminants from the use environment, and change in dielectric characteristics. The ultimate goal would be to develop simple tools to test electrical wiring in place, to identify unusual accidental damage, verify service life estimates, and confirm the adequacy of maintenance and repair activities.

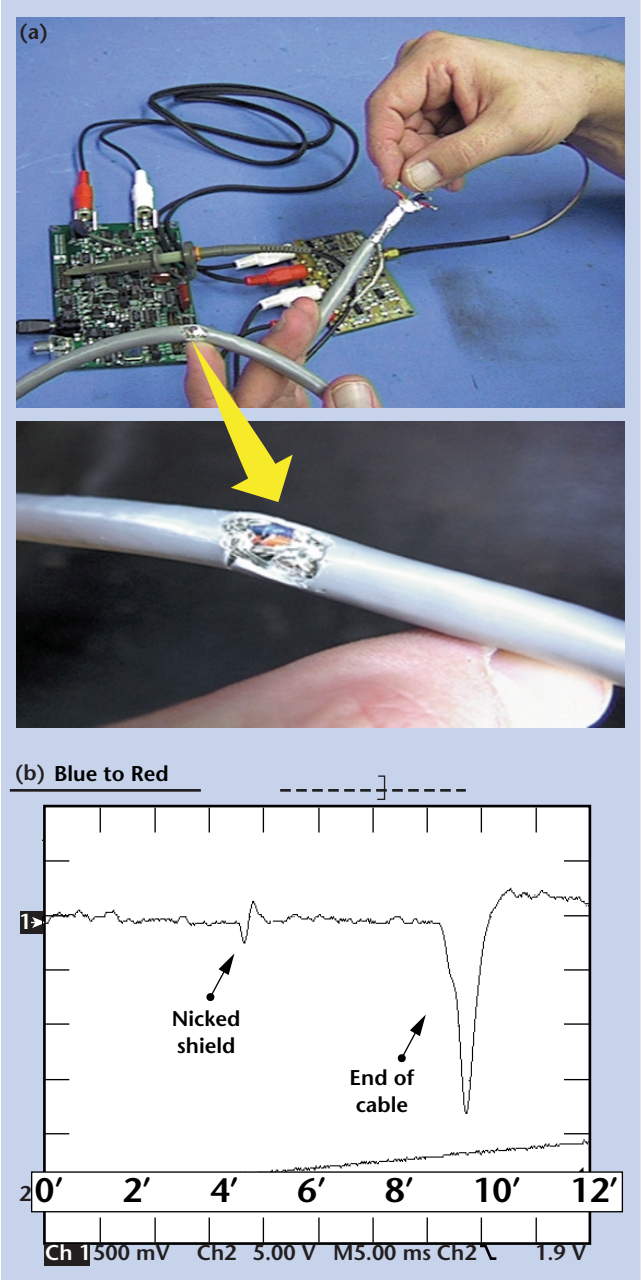

(a) Photograph and (b) plot of MIR demonstration system with measured cable fault signal. The plot shows signal indications for damaged cable shield (nicked shield) and cable open (end of cable).

Mid-to-Long-Wave Raman Converter for LIDAR

M. Bowers, D. Johnson, L. Little

We have developed a mid-to-long wave Raman converter that can turn a mid-wave LIDAR (Light Detection and Ranging) into a dual-band LIDAR without significant additional hardware or complexity. The converter, which uses state-of-the-art methods and parts, is designed to achieve greater than 30% quantum efficiency (QE) from the telecommunications (1530 nm to 1560 nm) to the long-wave (7.5 mm to 9.6 mm) bands.

Neither mid-wave LIDAR nor long-wave LIDAR is capable of detecting all of the chemicals that may be of interest from Hazmat spills, chemical weapon releases, or the production of weapons of mass destruction.

A new Raman frequency converter system has recently been developed that allows low-power CW diode signals to be frequency-converted in the visible spectrum with high efficiency (on the order of 80%). The far IR poses additional problems that need to be addressed in this project, including IR coatings with the required reflectivity, multiple Stokes shifts, coatings that can selectively favor the wavelengths of interest while attenuating unwanted wavelengths, and proper formatting of the cell geometry for the pump pulse. New developments in high-finesse cells has opened the door for applications such as LIDAR, where the peak powers are not extremely high. Another enabling technology is the ability to combine multiple gases into a single Raman cell and work with multiple Stokes shifts from each of the various gases.

The first phase of the project was to design and model the long-wave Raman converter using a numerical model to simulate the expected results for various cell configurations. We found CH_4 to be the best choice as a frequency-shifter gas to reach the long-wave IR.

All of our selected wavelengths will be able to be generated by the next generation LLNL LIDAR system.

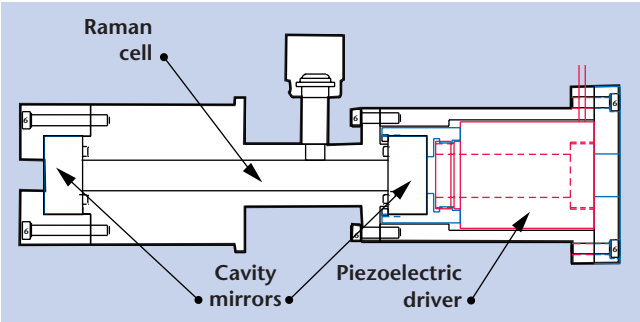

Figure 1. A CAD drawing of the Raman cell.

Today, however, only the 1.52 to 1.56 µm and the 3.4 to 3.6 µm bands are available. For the optimal prototype demonstration, we chose the 1.5 µm band pumping the $D_2 + N_2$ gas-filled cell.

The Raman cell (Fig. 1) has been designed with safety and performance in mind. The stainless steel high pressure cell has an active length of 10 cm. The Integrated Safety Worksheet, the Engineering Safety Note, and an addendum to the Operational Safety Procedure have been completed. A high pressure manifold has been designed to allow evacuation and filling of the Raman cell to pressures of 15 atm, well above the expected working pressure of 5 to 10 atm. The major components have been ordered and received.

To couple light into the Raman cell for pumping, the source light must be at a resonant frequency of the Raman cell. This is difficult when the finesse is high (57 for this design at the pump wavelength), and the free spectral range is short (1.5 GHz). An active method must be used to continuously keep the pump frequency and the resonant frequency to within a fraction of the cell passband of each other. We have modified the commonly-used Pound-Drever-Hall method to achieve this purpose (Fig. 2).

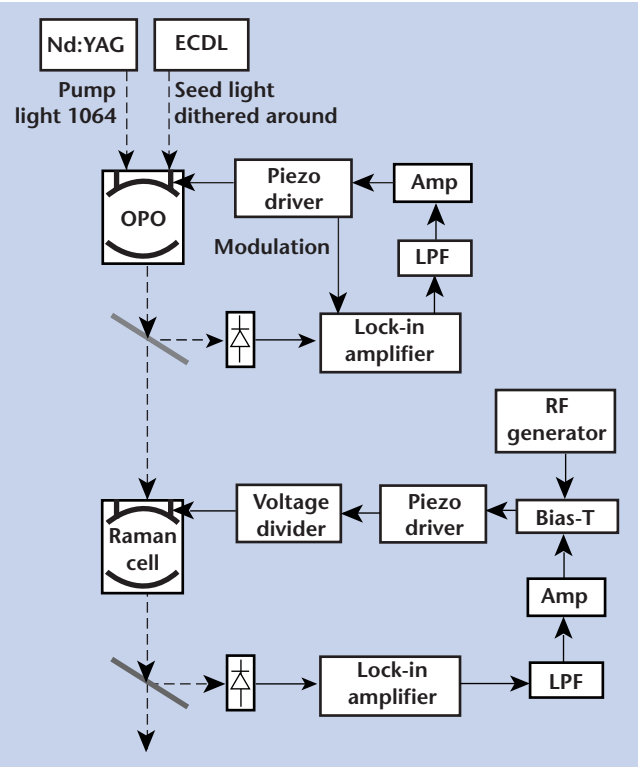

Figure 2. Proposed frequency-locking setup for the full system.

Ultrasonic Phased Arrays

G. Thomas, R. Huber

Ultrasonic phased arrays offer advantages over single element transducers in several areas. For one, the arrays can be used to focus energy at various locations in a volume simply by changing the signals being sent to the transmitters, whereas for single elements, the focus is fixed. Focusing acoustic energy at the location of interest in a part greatly improves the imaging and characterization capability of an acoustic NDE system. Improved nondestructive characterization will lead to higher confidence in materials and structures important to LLNL. The focusing can be dynamic and therefore very fast. In addition, the array system will allow acoustic energy to be directed into complex shapes. Also, arrays reduce the need to scan since a larger portion of the part being investigated can be insonified, compared with a single element. This can lead to significant savings in the time required to evaluate large materials and structures.

For this project, an ultrasound array system was obtained for NDE applications. The system was designed and built by R/D Tech for LLNL, based on input from members of this project. The system consists of a 64-element piezoelectric array and 16 individual pulser-receivers. Figure 1 is a photograph of the 64-element array. A PC is used to control the system. The array elements have a center frequency of 5 MHz. The 16 pulser-receivers can be used to access any contiguous section of the first 16 elements of the 64-element array. A planned upgrade to the system will allow access to 32 elements of the array. Further upgrades could allow access to all 64 elements of the array at the same time. Having multiple pulser-receivers allows different signals to be sent to the elements being addressed. This has advantages over standard phased-array type equipment that can alter the phase of the signals being sent to the transducers, but cannot alter the signals themselves.

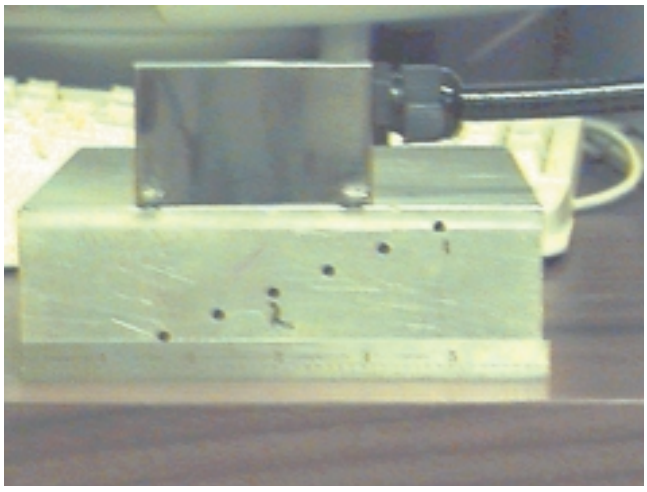

Figure 1. Photograph of transducer array.

Figure 2 shows a comparison of the dynamic focusing capability of this array system versus a fixed focus single element transducer. The array can focus acoustic energy to one location in the material, as indicated by the red lines in the figure. Then, simply by changing the signals being sent to the array elements, the array can then focus at a completely different location in the material, as indicated by the blue lines in the figure. A unique feature of the system is that it can be used for time-reversal applications. This feature stems from the fact that the system has individual pulser-receivers. This allows focusing of acoustic energy through a volume that may be anisotropic. The time-reversal feature has a user-friendly graphical user interface for a PC.

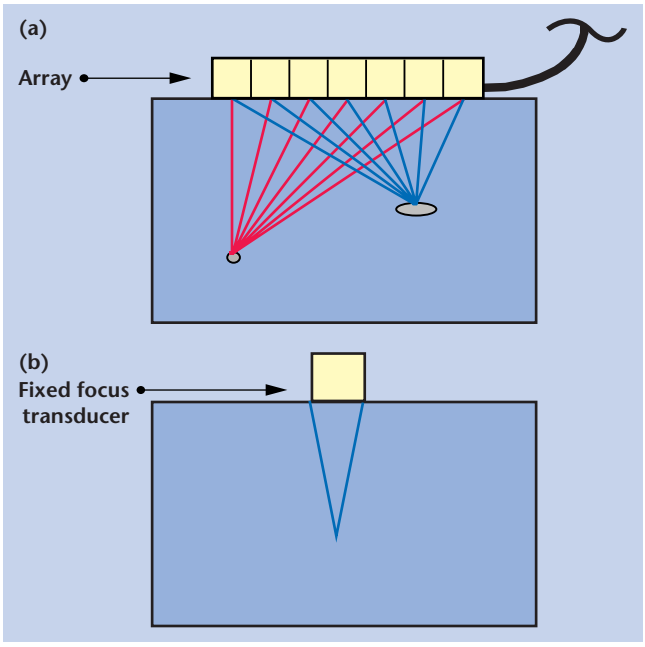

Figure 2. Comparision of (a) array and (b) fixed-focus transducer.

Development of a Multi-Layer Guided Wave Inspection Technique

M. Quarry, D. Chinn, T. Hay

This study investigates the inspection of a particular layer of a multi-layer structure using ultrasonic guided waves. Techniques based on Lamb waves have been developed for the inspection of plate structures and are well understood. Guided waves also exist in multi-layered plates. Energy distributions vary across the thickness of a multi-layer structure depending on the mode and frequency. Hence, a potential way to inspect the bottom layer of a structure is to find modes with sufficient energy in the bottom layer. We have used guided waves for crack detection in a four-layer, tungsten-epoxy-steel-alumina structure.

Our objective was to inspect the bottom layer of a structure (Fig. 1) with access limited to the top surface. Guided waves with significant energy in a given layer can penetrate into and propagate in hidden layers. Any particular layer can be inspected by exciting a guided wave mode in the multi-layer that has sufficient energy in the layer of interest. Pulse-echo and through-transmission techniques provide valuable information about the mechanical integrity of structure.

We used phase velocity dispersion curves to supply the physical characteristics required for modes to exist in the structure, and group velocity dispersion curves to describe the speed at which each mode propagates and enables the localization of flaws in the structure.

Each point on the dispersion has a unique displacement pattern across the thickness of the structure. As a result, each mode has different properties as it propagates in the structure. Some modes have a lot of energy in the bottom layer, while some have very little. Inspecting the bottom layer requires a mode to have at least a sufficient amount of energy in that layer. Modes with these characteristics must be found and excited to develop a successful inspection technique.

To control and excite guided waves, we used variable-angle beam probes with a longitudinal wave transducer with a Plexiglas wedge material. Modes were searched by sweeping the angle of incidence and frequency. The searching of modes identifies the best mode candidates for the particular inspection application.

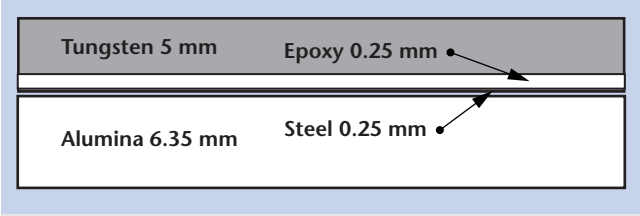

Figure 1. The structure of a four-layer specimen. Materials are pressed together.

Two four-layer specimens (one with no flaws, the other with a crack in the alumina layer) were tested in pulse-echo and through-transmission setups (Fig. 2). Pulse-echo setups are useful when a flaw such as a crack creates a strong reflection. Through-transmission setups generally have greater sensitivity when flaws have a long length along the propagation direction. The pulse-echo setup is likely more sensitive for detecting cracks.

Placing a sensor on the bottom of the structure, we were able to confirm that energy propagated in the bottom layer, which establishes a basis for inspecting the structure for damage. Our theoretical computations support the hypothesis that the mode must have sufficient energy in the layer of concern for flaw detection. The concepts for inspecting multi-layer structures pursued in this work may also be applied to a variety of multi-layer structures. The success of this study demonstrates proof-of-principle for using the technique on other layered structures.

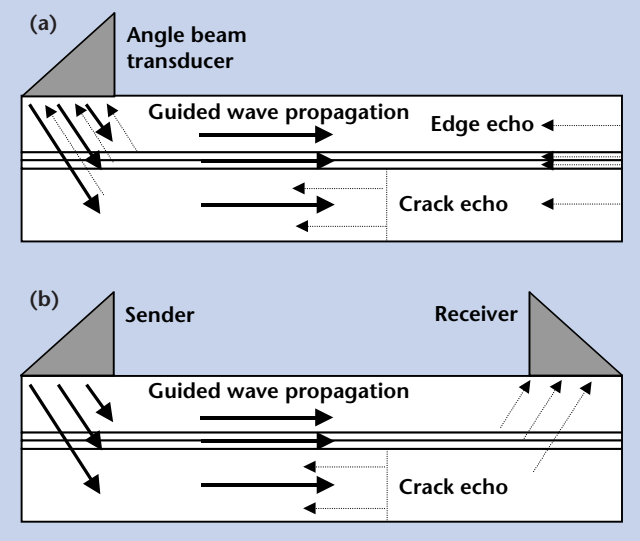

Figure 2. (a) Guided wave pulse-echo setup, and (b) through-transmission setup. In the pulse-echo concept, ultrasonic energy is coupled into the top layer, then penetrates subsequent layers. Modes are reflected at the edge of the plate and at the crack in the bottom layer. In the through-transmission concept, amplitude and time of arrival are changed by the presence of flaws.

Near Nanoscale X-Ray Computed Tomography

K. Dolan, J. J. Haskins, D. Haupt, C. Logan, D. Schneberk

Requirements for components of computed tomography systems are considered that would allow sub-micrometer x-ray spatial resolution. With present and near term technology, we conclude spatial resolution in the sub-micrometer range is obtainable, but that x-ray optics will be required.

The objective of this project is to evaluate the properties of scintillators, cameras and x-ray sources needed to do sub-micrometer x-ray imaging for computed tomography, and to define areas where advances are needed.

Sub-micrometer computed tomography has applications such as NIF target as-built dimensional characterization, micromechanical device characterization, and material damage and material property studies. This technology provides internal dimensioning, material density and discontinuity distributions at small scale lengths without disturbing or destroying samples, so that use functions of the samples can be studied after characterization. The results are true 3-D characterizations of internal features, discontinuities, and material distributions that lend themselves to modeling and validation studies.

Small scale x-ray imaging requires artifact free, high-fidelity and high-efficiency imaging media, large image recording arrays with high bit depth (greater than 2k x 2k at 14 bits), low-loss and distortion-free light propagating media (high-quality, low-f-number lenses), and intense x-ray sources (synchrotrons or conventional sources with x-ray optics). We have performed some experiments with synchrotron sources and others with conventional x-ray sources (without x-ray optics).

Requirements for scintillator materials are that they have a reasonably high effective atomic number (greater than 50); have high efficiency for converting x-ray energy to light (>10^4 photons/MeV-g); emit in the 450- to 650-nm wavelength to be compatible with silicon chip sensitivity; have short decay times (<100 ns) and no afterglow, to allow high x-ray flux, high tolerance to radiation dose (no darkening); be non-hygroscopic (as protected by transparent coating when applicable); and provide flaw-free fabrications with dimensions that are at least 25 mm x 25 mm x 0.5 to 1 mm thick.

All scintillator and luminescent materials examined microscopically to date have shown fabrication flaws, observed as both point flaws and line flaws that result in artifacts in recorded images (see figure). Image processing can be used to remove some artifact indications, while dithering the scintillator during data acquisition has potential for averaging out artifact indications from scintillator flaws.

Scintillator materials that bear further investigation are $CdWO_4$, CsI(Tl), LYSO, and BGO. Luminescent glasses, such as LKH-5 will continue to provide imaging capability at conventional x-ray tube dose rates, but are probably not appropriate for use with higher intensity sources due to afterglow and radiation damage effects. A potential new technology that provides promise of thin, flaw-free single crystal scintillators is vacuum coated $CdWO_4$ thin films on glass substrates.

The brightest x-ray sources will be needed. We have demonstrated that the Stanford Synchrotron Radiation Laboratory (SSRL) beam line 10-2 provides sufficient intensity to obtain x-ray images at 2-μm pixel size in about 15 s. This provides a resolution of approximately 250 lp/mm. A gain of a factor of 10 in beam intensity can be realized by moving to the Advanced Light Source (ALS) at LBL.

If a scintillator can hold 500 lp/mm, the pixel size could be reduced to 1μm. To obtain spatial resolution beyond this would appear to require x-ray optics and projection magnification.

Applications of the present technology have included computed tomography characterization for spallation studies, Omega-3 glass damage studies, foam characteristics, small sample explosive characteristics, and damage growth as a function of load of cast Mg samples.

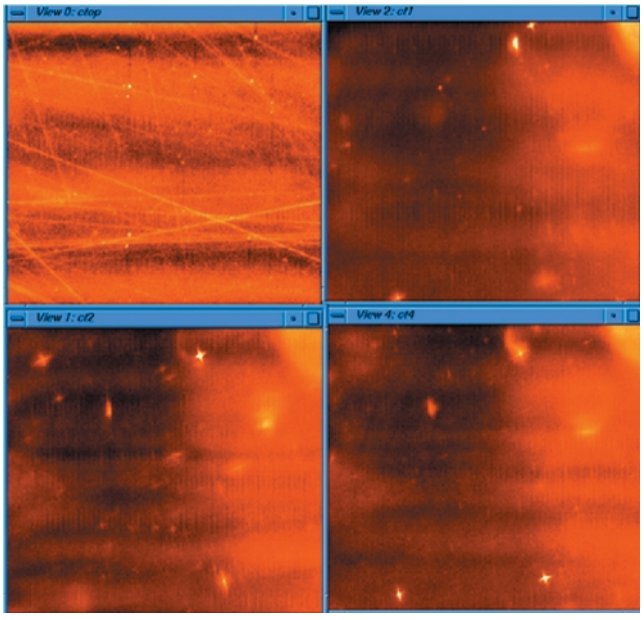

Scintillator material flaws as imaged with a CCD camera on the surface (upper left), and at various depths in material.

Powder Flow and Die-Filling Studies Using Computed Tomography and Ultrasonic Testing

J. J. Haskins, P. Martin

Nondestructive Evaluation Characterization at LLNL has been involved in a collaborative effort with General Motors Corporation to enhance powder metal processing capabilities. Powder metallurgy, an important, emerging processing methodology, is a near net shape process. LLNL has the expertise to enhance the capabilities of the powder metal industry from powder handling and consolidation, to densification and final inspection of the finished components. Our goal is to develop a fully functional center capable of processing powder metals on site. The net gain to the DOE and the powder metal industry will be cost and energy savings, with the increased deployment of powder metallurgical components.

Technically the goal is to demonstrate our diagnostic capabilities on pressed and sintered parts. GM has supplied ring gears and connecting rods. Initial work has involved the ring gears, approximately 5 3/4 in. OD by 4 3/4 in. ID and 1 1/8 in. high. Each gear has 90 teeth on the ID, running at approximately 20° (see figure). The features of concern lie at the root of the teeth and in layers along the sides of the teeth. These layers can be detected using metallography, but success depends on chance and the number of sections polished. Much of the current focus is on improving the sensitivity of the CT scan and on better ways to evaluate the large data sets obtained. The initial data obtained showed anomalies close to the gear teeth as expected. Later data showed anomalies at other locations and in other orientations.

We carried out ultrasonic testing (UT) of pressed, sintered powder specimens, using an A-scan (raw amplitude versus time-of-flight data), a B-scan (comparable to a radiographic CT slice), and a C-scan (maximum value of the signal as a function of position).

Based on our initial round of data from ultrasonic testing, we have concluded that there are discontinuities present in the component, that these discontinuities can be located and sized, and that the discontinuities do not appear to occur at any characteristic depth or location.

To build upon these results, and to enhance the capabilities for inspection of powder metallurgical components, the following action items have been proposed for continuation of this technology base work: 1) regions of the ring gear containing discontinuities will be sectioned; 2) these sections will be inspected using CT; 3) some discontinuity-free regions of the ring gear will be used to fabricate calibration standards (with flat bottomed holes); 4) UT and CT data will be compared, and potentially complementary capabilities will be identified; and 5) UT inspection of connecting rods supplied by GM will be evaluated.

As a result of the work performed so far, GM has signed a contract with LLNL to continue this work, and we have been invited to make a presentation at the annual meeting of the Center for Powder Metal Technology.

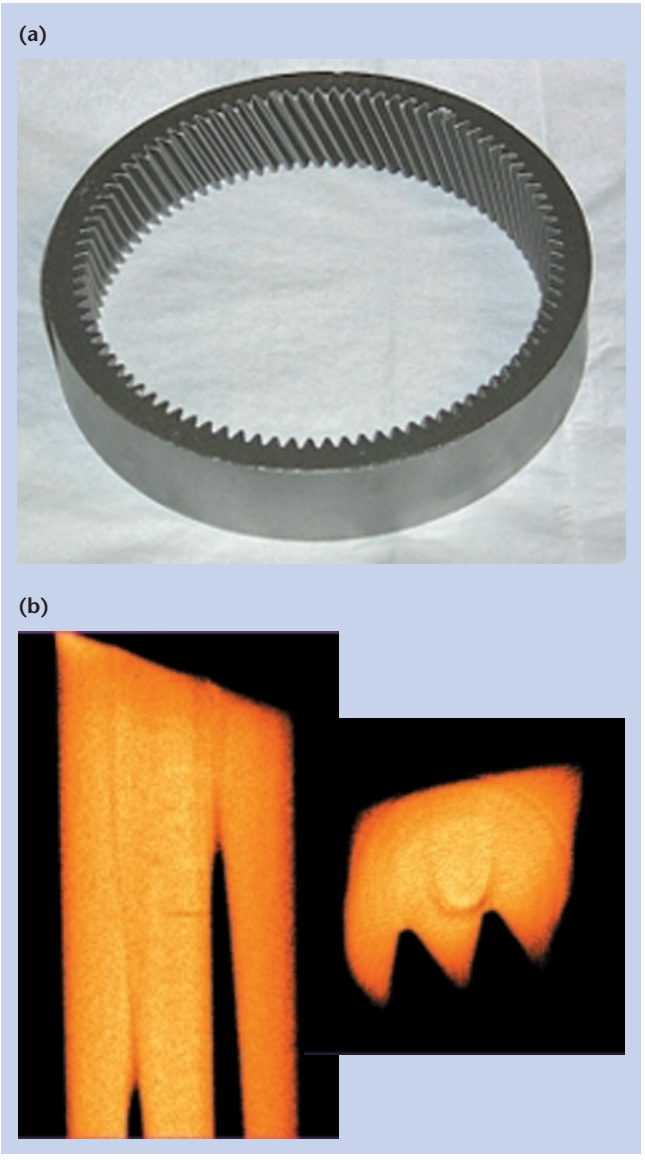

(a) Photograph of ring gear; (b) Y and Z slices through ring gear sample with prominent defect region.

Selected Engineering Publications

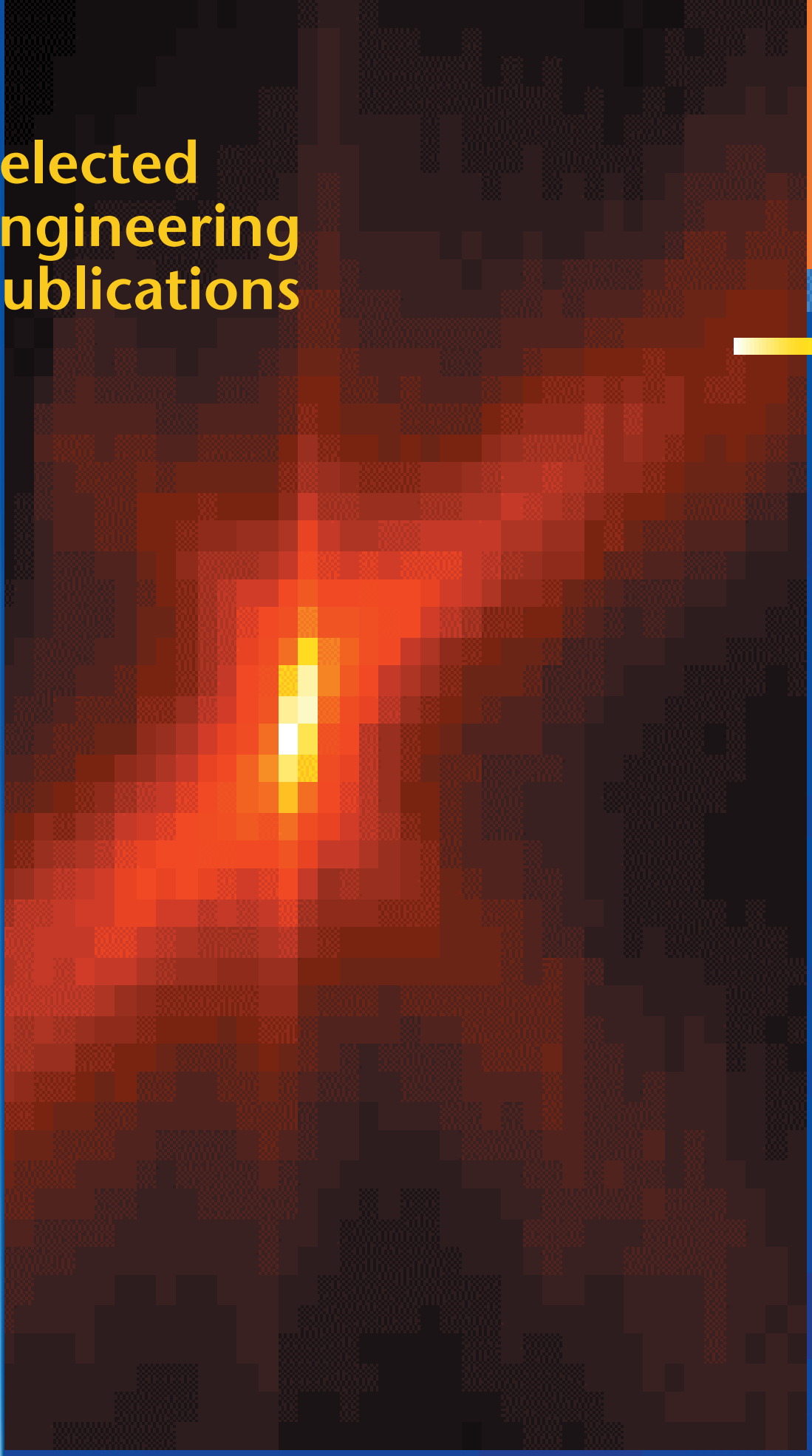

Berryman, J., L. Barcka, and G. Papanicolaou (2000), "Time reversal acoustics for multiple targets," *J. Acoust. Soc. Amer.* (UCRL-140465).

Buettner, H. M., W. Labiak, and A. Spiridon (2000), "Remote instrumentation and safeguards monitoring for the Star project," Nuclear Plant Instrumentation, Control and Human-Machine Interface Technologies Meeting, American Nuclear Society, Nov. 13–16.

Buettner, H. M., E. Didwall, F. Followill, D. McCallen, and R. Morey (2000), "GPR characterization of underground facilities at NTS," *Proc. of the Unattended MASINT Sensor and Geophysical Conf.,* Quantico, Virginia, Nov. 7–8.

Burke, G. J., and D. J. Steich (2000), "Numerical modeling of shielding by a wire mesh box," 16th Annual Review of Progress in *Applied Computational Electromagnetics*, pp. 452–459, Monterey, California, March 20–24.

Candy, J., and D. Chambers (2000), "The role of the time reversal processor in acoustic signal processing," *J. Acoust. Soc. Amer.* (UCRL-JC-141160).

Candy, J., D. Chambers, R. Huber, and G. Thomas (1999), "Matched-field imaging of laser generated ultrasound for nondestructive evaluation," *J. Acoust. Soc. Amer.* (UCRL-133397).

Candy, J., D. Chambers, R. Huber, and G. Thomas (2000), "Ultrasonic matched-field imaging for nondestructive evaluation," Ocean Imaging Conf. (UCRL-136369).

Candy, J., (2000), "The role of the time reversal in signal processing," C.A.S.I.S. Workshop at LLNL (UCRL-VG-141331).

Caporaso, G., and J. McCarrick (2000), "Ion-Hose instability in long pulse induction accelerators," *Proc. of the 20th Int. LINAC Conf.,* pp. 500–02, Monterey, California, Aug. 21–25.

Chambers, D., and A. Gautesen (2000), "Multiple eigenvalues of the time reversal operator for a single hard scatterer," *J. Acoust. Soc. Amer.* (UCRL-139914).

Chambers, D., and A. Gautesen (2000), "Time reversal for a single spherical scatterer," *J. Acoust. Soc. Amer.* (UCRL-JC-141165).

Chen, Y.-J., D. Ho, J. McCarrick, A. C. Paul, B. Poole, S. Sampayan, L. Wang, and J. Weir (2000), "Physics design of the ETA-II/Snowtron double pulse target experiments," *Proc. of the 20th Int. LINAC Conf.,* pp. 482–4, Monterey, California, Aug. 21–25.

Conrad, D. C. (2000), "Underground explosions are music to their ears," *Science and Technology Review,* pp. 4–11, July/Aug. (UCRL-52000-00-7/8).

Conrad, D. C., P. Egan, and the LLNL/BN SCE Team (2000), presented by Ray Heinle, "U1a vessel experiments: OBOE and beyond," JOWOG 32 PDT, Aldermaston, England, Nov 29–Dec. 1.

Cooperstein, G., W. DeHope, *et al*. (2000), "Progress in rod pinch electron beam diodes as intense x-ray radiographic sources," 13th Int. Conf. on High-Power Particle Beams (BEAMS 2000), Nagaoka, Japan, Jun. 25–30.

Cunningham, C. T., and R. S. Roberts (2001), "An adaptive path planning algorithm for cooperating unmanned air vehicles," *Proc. of the IEEE Int. Conf. on Robotics and Automation*, Seoul, Korea, May (UCRL-JC-140415).

Dudley, D. G., H.-Y. Pao, and D. A. Hill (2000), "Introduction to special issue," *IEEE Transactions on Antenna and Propagations,* **48**, No. 9, Sept.

Eppler, W. G., D. W. Paglieroni, M. Petersen, and M. J. Louie (2000), "Fast normalized cross-correlation of complex gradients for autoregistration of multi-source imagery," ASPRS DC 2000 Conf., May 22–27.

Falabella, S., Y.-J. Chen, T. Houck, J. McCarrick, S. Sampayan, and J. Weir (2000), "Effect of backscattered electrons on electron beam focus," *Proc. of the 20th Int. LINAC Conf.,* pp. 458–60, Monterey, California, Aug. 21–25.

Ge, J., D. Ciarlo, P. Kuzmenko, B. Macintosh, C. Alcock, and K. Cook (2000), "Etched silicon gratings for NGST," *Next Generation Space Telescope Science and Technology*, ASP Conf. Series, **207**, p. 457.

Ge, J., D. Ciarlo, P. Kuzmenko, C. Alcock, B. Macintosh, R. Angel, N. Woolf, M. Lloyd-Hart, R. Q. Fugate, and J. Najita (2000), "Adaptive optics high resolution spectroscopy: present status and future direction," *Proc. Imaging the Universe in Three Dimensions,* ASP Conf., **195**, p. 568.

Ge, J., J. P. Lloyd, D. Gavel, B. Macintosh, C. E. Max, D. Ciarlo, P. Kuzmenko, and J. R. Graham (2000), "High spectral and spatial resolution spectroscopy of YSOs with a silicon prism and adaptive optics," BAAS, **197**, p. 5201.

Guethlein, G., T. Houck, J. McCarrick, and S. Sampayan (2000), "Faraday cup measurements of ions backstreaming into an electron beam impinging on a plasma plume," *Proc. of the 20th Int. LINAC Conf.,* pp.467–9, Monterey, California, Aug. 21–25.

Handler, F.A., and L. C. Ng (2000), "Signal detection and feature extraction for target/decoy discrimination from IFT-1A flight experimental data: a technical response to Dr. Ted Postal's allegations (U)," published as a POET document.

Holzrichter, J. F., and L. C Ng (2000), "Speech articulator and user gesture measurements using micropower, interferometric EM-sensors," IEEE-Instrumentation and Measurement Technology Conf. (IMTC), Budapest, Hungary, May 21–23 (UCRL-JC-140496).

Huber, R., J. Candy, D. Chambers, and G. Thomas (1999), "Processing of laser-based ultrasound for matched-field imaging," Quantitative NDE Conf. (UCRL-134055).

Le Sage, G. P., S. G. Anderson, T. E. Cowan, J. K. Crane, T. Ditmire, and J. B. Rosenzweig (2000), "RF photoinjector development for a short-pulse, hard x-ray Thomson scattering source," AIP Conf. Proc. for the Advanced Accelerator Conf., Santa Fe, New Mexico, (UCRL-JC-140148).

McCarrick, J. (2000), "The effect of asymmetric plasma plumes on the transport of high-current electron beams," *Proc. of the 20th Int. LINAC Conf*, pp. 461–3, Monterey, California, Aug. 21–25.

Merrill, R. D., *et al.* (2001), "Material transfer system in support of the plutonium immobilization program," *Proc. of the American Nuclear Society Ninth Topical Int. Meeting on Robotics and Remote Systems*, Seattle, Washington, March 4–8.

Merrill, R. D., *et al.* (2001), "Remote equipment development for the plutonium ceramification test facility at LLNL," *Proc. of the American Nuclear Society Ninth Topical Int. Meeting on Robotics and Remote Systems*, Seattle, Washington, March 4–8.

Ng, L. C., G. C. Burnett, J. F. Holzrichter, and T. J. Gable (2000), "Denoising of human speech using combined acoustic and EM sensor signal processing," IEEE ICASSP-2000, Istanbul, Turkey, Jun. 6 (UCRL-JC-136631).

Paglieroni, D. W., and R. S. Roberts (2000), "Optimal segmentation strategy for compact representation of hyperspectral image cubes," *Proc. ASPRS DC 2000 Conf.*, May 22–27.

Pao, H.-Y. (2000), "In memoriam of James R. Wait," Guest Editor, *IEEE Transactions on Antenna and Propagations*, Special Issue, **48**, No. 9, Sept.

Pao, H.-Y., and J. R. Wait (2000), "Electromagnetic induction and surface impedance in a half-space from an overhead moving current system, *IEEE Transactions on Antenna and Propagations*, **48**, No. 9, Sept.

Poole, B. R., Y. J. Chen, A. C. Paul, and L.-F. Wang (2000), "Particle simulation of DARHT-II downstream transport," *Proc. of the 20th Int. LINAC Conf.*, Monterey, California, August 21–25.

Puso, M. A, and T. A. Laursen (2000), "A method for 3D contact surface smoothing," *Int. J. for Numerical Methods*.

Puso, M. A. (2000), "An energy and momentum conserving algorithm for rigid-flexible body dynamics," *Int. J. for Numerical Methods*.

Richardson, R., S. Sampayan, and J. Wier (2000), "Elliptical x-ray spot measurement," *Proc. of the 20th Int. LINAC Conf.*, Monterey, California, August 21–25.

Roberts, R. S. (2000), "Characterization of hyperspectral data using a genetic algorithm, IEEE Thirty-Fourth Asilomar Conf. on Signal, Systems and Computers, Pacific Grove, California, Oct. 29–Nov. 1.

Sampayan, S., G. Caporaso, Y.-J. Chen, S. Falabella, D. Ho, T. Houck, E. Lauer, J. McCarrick, R. Richardson, D. Sanders, and J. Weir (2000), "Beam-target interaction experiments for Bremsstrahlung convertor applications," *Proc. of the 20th Int. LINAC Conf.*, pp. 464–6, Monterey, California, Aug. 21–25.

Tomascik-Cheeseman, L. M., R. Raja, L. M. Kegelmeyer, S. L. Mabery, B. J. Marsh, F. Marchetti, J. Nath, and A. J. Wyrobek (2000), "Parallel expression analyses of DNA repair genes in adult mouse tissues using cDNA microarrays," *Proc. of the Environmental Mutagen Society*, New Orleans, Louisiana, in *Environmental and Molecular Mutagenesis*, **35**, No. 31, p. 61, April.

Wang, L., G. J. Caporaso, and E. G. Cook, "Modeling of an inductive adder kicker pulser for DARHT-2," *Proc. of the 20th Int. LINAC Conf.*, Monterey, California, August 21–25.

Wang, L., S. M. Lund, and B. R. Poole (2000), "Dipole septum magnet in the fast kicker system for multi-axis advanced radiography," *Proc. of the 20th Int. LINAC Conf.*, Monterey, California, August 21–25.

Author Index

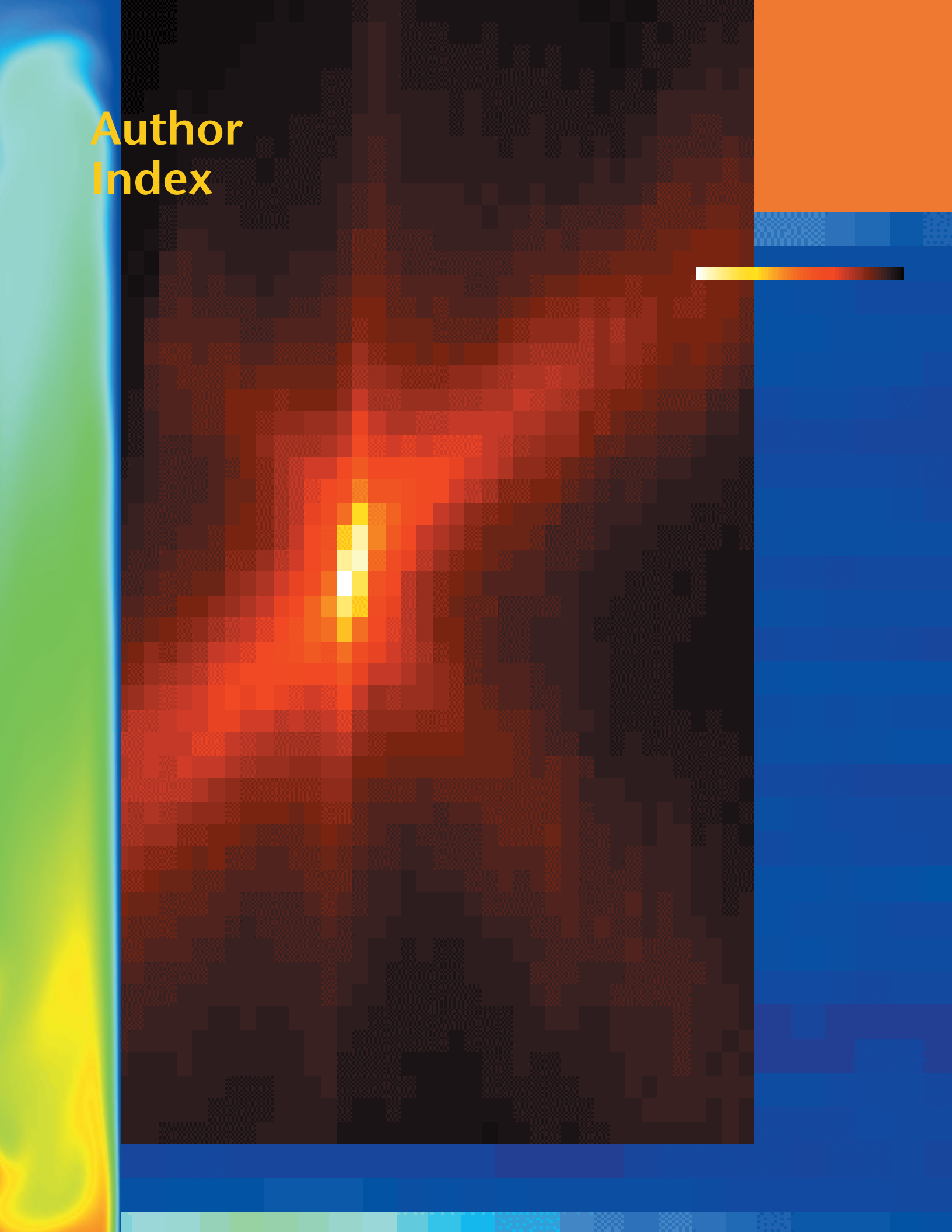

Manuscript Date September 2001
Distribution Category UC-42

Work performed under the auspices of the U.S. Department of Energy by the University of California, Lawrence Livermore National Laboratory under Contract W–7405–Eng–48.
ENG-01-0004b-AD

Engineering Directorate
Lawrence Livermore National Laboratory
University of California
P.O. Box 808, L-124
Livermore, California 94551

http://www-eng.llnl.gov/